HOLOGRAPHIC HEADS-UP DISPLAY FOR NAVAL AVIATION TRAINING

Alfred H. Rodemann, et al

Naval Training Equipment Center
Orlando, Florida

May 1975

Unclassified

SECURITY CLASSIFICATION OF THIS PAGE (When Data Entered)

REPORT DOCUMENTATION PAGE

READ INSTRUCTIONS BEFORE COMPLETING FORM

1. REPORT NUMBER: IH-229
2. GOVT ACCESSION NO.
3. RECIPIENT'S CATALOG NUMBER

4. TITLE (and Subtitle): HOLOGRAPHIC HEADS-UP DISPLAY FOR NAVAL AVIATION TRAINING

5. TYPE OF REPORT & PERIOD COVERED: Final Report, July 72 to December 74

6. PERFORMING ORG. REPORT NUMBER: IH-229

7. AUTHOR(s): Alfred H. Rodemann, Denis R. Breglia, Windell N. Mohon

8. CONTRACT OR GRANT NUMBER(s)

9. PERFORMING ORGANIZATION NAME AND ADDRESS: Physical Sciences Laboratory, Naval Training Equipment Center, Orlando, Florida 32813

10. PROGRAM ELEMENT, PROJECT, TASK AREA & WORK UNIT NUMBERS: Project 3713-03

11. CONTROLLING OFFICE NAME AND ADDRESS: Department of the Navy, Naval Training Equipment Center, Orlando, Florida

12. REPORT DATE: May 1975

13. NUMBER OF PAGES: 165

14. MONITORING AGENCY NAME & ADDRESS (if different from Controlling Office)

15. SECURITY CLASS. (of this report): Unclassified

15a. DECLASSIFICATION/DOWNGRADING SCHEDULE

16. DISTRIBUTION STATEMENT (of this Report)

Approved for public release; distribution unlimited.

17. DISTRIBUTION STATEMENT (of the abstract entered in Block 20, if different from Report)

Government Rights in Data Statement: Reproduction of this publication in whole or in part is permitted for any purpose of the United States Government.

18. SUPPLEMENTARY NOTES

19. KEY WORDS (Continue on reverse side if necessary and identify by block number)

Displays
Holography
Dicromated gelatins
Optics

20. ABSTRACT (Continue on reverse side if necessary and identify by block number)

This report summarizes the results of an effort to apply the technology of high efficiency holographic lens design and fabrication to the specific case of a heads-up display system for use in visual simulators for aviation training. Design methods are developed. Materials research is described. Holographic lens elements are evaluated.

DD FORM 1 JAN 73 1473 EDITION OF 1 NOV 65 IS OBSOLETE S/N 0102-014-6601

PRICES SUBJECT TO CHANGE

Unclassified

SECURITY CLASSIFICATION OF THIS PAGE (When Data Entered)

TABLE OF CONTENTS

LIST OF ILLUSTRATIONS

LIST OF TABLES

SECTION I

INTRODUCTION

The application of holographic technology to the production of gratings having imaging characteristics similar to ordinary reflective and refractive optical elements has been previously proposed[1,2*]. The technology in terms of uniform, highly efficient, wide angle, low aberration and easily produced off-axis holographic lenses is relatively new and still requires much analysis and experiment. This report summarizes the results of an effort to apply the technology to a specific case; a multi-channel, heads-up, virtual image display for a visual simulation system. This effort included investigations of recording media, analysis of image aberrations, analysis of effects of recording medium distortion, description of recording geometry, and design considerations. Chronologically, the effort was devoted to literature search, recording system design and fabrication, investigation of various recording materials, design and evaluation of holographic lenses, optimization of recording techniques, production of a display lens, and test and measurement of the display lens.

The theory of diffraction from a stratified grating has been studied previously[3,4,5,6,7]. Holograms may be divided into several types; thin or thick, transmission or reflection, absorption or phase. The maximum theoretical efficiencies of the various types of holograms assuming sinusoidally structured gratings can be calculated[6]. The various maximum diffraction efficiencies are listed in Table 1.

TABLE 1. MAXIMUM DIFFRACTION EFFICIENCIES OF SINUSOIDAL HOLOGRAPHIC GRATINGS

Medium	Utilization	Grating	Maximum Diffraction Efficiency
Thin	Transmission	Phase	33.9%
		Absorption	6.25%
	Reflection	Phase	33.9%
		Absorption	6.25%
Thick	Transmission	Phase	100%
		Absorption	3.7%
	Reflection	Phase	100%
		Absorption	7.2%

*Superscripts refer to reference numbers

In Table 1 the medium is defined as thin or thick depending on the value of Q.[2]

$$Q = \frac{2\pi\lambda d}{n_0 \Lambda^2} \qquad (1)$$

Where λ = wavelength of recording light
d = thickness of recording material
n_0 = index of recording medium
Λ = grating period

for $Q >> 1$ the grating is thick.

Reflection and transmission holograms are defined by whether the diffracted beam exits the medium on the same side of the grating or on the opposite side of the grating, as the incident beam, respectively. The recording and reconstruction of plane wave transmission and reflection holograms are illustrated in Figure 1. Figure 1 also demonstrates that the fringes are parallel to the emulsion surface for the reflection case and perpendicular for the transmission case.

The difference between phase and absorption gratings is in terms of how the light incident on the processed grating is modulated. In a phase grating the phase of the light wave is modulated while the amplitude is not. This leads to the theoretically high diffraction efficiencies attainable with phase recording media. Absorption gratings modulate the amplitude of the incident light by absorbing portions of it and so lowering the overall light available in the diffracted beam.

Diffraction efficiencies are defined as η where;

$$\eta = \frac{ID}{IO} \qquad (2)$$

Where ID = diffracted intensity
IO = incident intensity available.

The qualification "available" on IO indicates that reflection and scatterings losses are not considered. Based on the above analysis highly efficient holographic lenses should be either thick phase transmission or thick phase reflection type.

The choice for the particular application at hand was narrowed to thick phase transmission holograms by the following considerations: (1) Previous experiments with reflection holograms indicated that due to their inherent requirement for recording higher spatial frequencies experimental set-ups had to be more mechanically stable; and (2) Previous results demonstrated large ambient humidity effects due to the fringes being parallel to the recording medium surface and so susceptible to humidity induced shrinking or swelling.

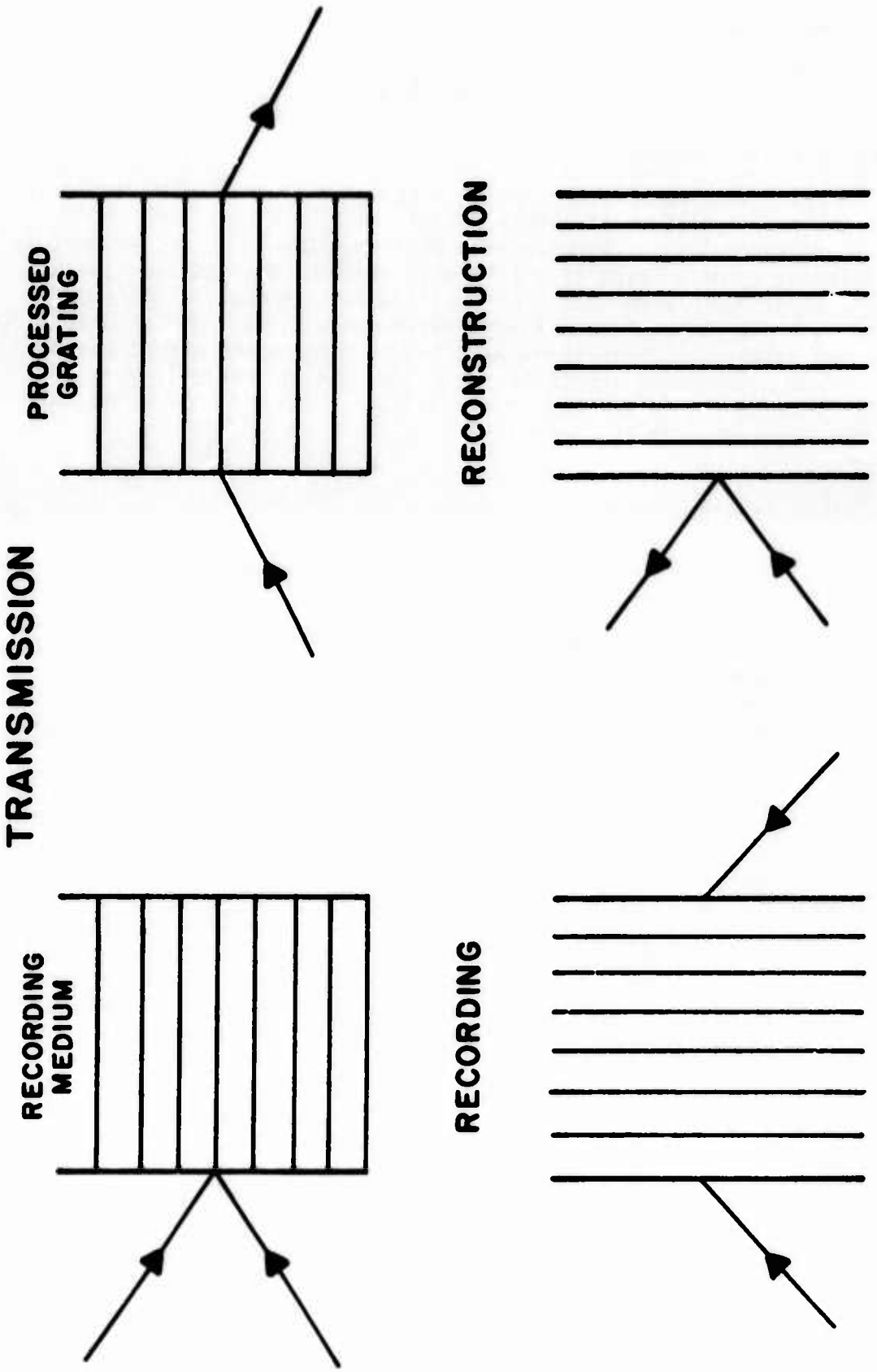

FIGURE 1 - Recorded and Reconstructed Rays for Transmission and Reflection

SECTION II

THEORETICAL ANALYSIS

A. HOLOGRAPHIC RECORDING

The basic requirements for making a hologram are: (1) two mutually coherent intersecting wavefronts of light; and (2) a recording medium capable of recording the interference pattern. The first requirement is satisfied by using a laser of sufficient coherence to generate the two wavefronts or beams such that high contrast interference fringes can be formed over the range of path length differences encountered in the hologram recording geometry. Where large path length differences are required a laser of long coherence length is required. The coherence length of "L" of the laser can be calculated from equations 3 and 4 if the wavelength or frequency bandwidth is known.[8]

$$L = \frac{\lambda^2}{\Delta\lambda} \tag{3}$$

$$L = \frac{c}{\Delta\nu} \tag{4}$$

where

L = coherence length
λ = wavelength
$\Delta\lambda$ = wavelength bandwidth
c = speed of light
$\Delta\nu$ = frequency bandwidth.

An alternate way of determining coherence length is to experimentally determine by interferometry the maximum path length difference allowable to still have relatively high contrast fringes. In practice the experimental method is used since it not only determines coherence length but also tests platform stability since the fringes can be observed and any vibration or long term motions can be visually monitored. Platform stability is another requirement if coherence is to be maintained while the recording medium is being exposed. Any changes in path length differences during exposure will cause fringe shifting and corresponding loss of fringe contrast in the processed hologram. Therefore changes in path length due to mechanical flexing or vibration of the platform (including optics, mounts and plate holder) and changes in the air path induced by changing thermal gradients or air velocity must be minimized. The methods used to achieve required coherence and stability are discussed in Section III A.

The requirements on the recording material are that power density thresholds, wavelength sensitivity, and resolution capability be compatible with the laser and hologram recording system used. The theoretical aspects of holograms may be found in many texts[9],[55],[56] and are not repeated here.

B. PHASE RECORDING MATERIALS

The materials available for recording thick phase transmission holograms include bleached photographic emulsions, dichromated gelatins, photo polymers, photo-chromics as well as many more exotic materials

such as; $LiNbO_3$:Fe, $Sr_{0.75}Ba_{0.25}Nb_2O_6$, and $BaTiO_3$.[3] The basic properties of these materials as applied to the production of holographic gratings are outlined below.

1. BLEACHED SILVER HALIDE

The requirement for extremely high resolution capability (in excess of 1000 l/mm) limits the choice of commercial photographic emulsions available for holographic applications. Photographic emulsions[11,12] consist of minute crystals of silver halide imbedded in a colloid (usually gelatin). When exposed and developed, these crystals or grains are usually developed completely, thus the size of the developed silver grains is initially determined by the size of the crystals from which they are formed, and the emulsion behaves as if the crystals are the photo sensitive units. This means that high resolution photographic emulsions must have extremely small grain or crystal size. Small grain size also implies low scattering and corresponding high resolution. The problem with producing emulsions with small grain size is that crystals tend to clump and small crystals require low densities of silver halide in the gelatin if they are not to clump. This explains why high resolution emulsions tend to have low photographic speed or low sensitivity. The low scattering within such an emulsion (usually called a Lippman emulsion) is of the Rayleigh type and inversely proportional to the fourth power of the wavelength.[12] This means that if maximum resolution is to be obtained exposure with light toward the blue end of the spectrum should be avoided. Spectral sensitivities with various sensitizing dyes allow the use of these emulsions throughout the visible spectrum.

To utilize photographic emulsions as phase holograms the metallic silver image must be removed or changed so that it is transparent.[13] This process is known as bleaching and can be accomplished in several ways.[14] If proper developing and fixing techniques have been followed the holographic grating consists of areas of metallic silver suspended in the gelatin. The object of the bleaching is to remove the metallic silver or convert it into a transparent silver compound. Removal of the silver converts the hologram into a relief image which behaves as a thin phase hologram. Conversion into a transparent compound of higher index of refraction than the gelatin results in a thick phase hologram. The potassium ferricyanide bleaching processes are an example of the latter while the cupric halide bleach process is an example of the relief image type. Relief image gratings do have volume or thick hologram properties also due to the different index of refraction of hard and soft gelatin.

Holograms of high diffraction efficiency have been made using the silver conversion type bleaches. The three problems generally associated with this process are (1) printout effect: tendency for the processed hologram to darken on subsequent exposure to light due to photolytic decomposition of the silver compound. (2) haze or scattering on the processed holograms and (3) permanent degradation of diffraction efficiency upon exposure to high humidity.

There are several techniques for stabilizing processed holograms against subsequent darkening. These include replacement of the ferrocyanide, chloride, and bromide ions by iodide,[15] removal of sensitizers by an acid permanganate bath or chemical or thermal hardening of the gelatin,[16] conversion to a dichromated gelatin hologram,[2,17] and desensitization of AgBr holograms by the use of certain organic dyes.[18]

Attempts to minimize scattering in the processed hologram include; a successive darkening bath which restores original density with some loss of diffraction efficiency but with less noise;[19] stress relieving and alcohol drying procedures;[20] potassium permanganate desensitization of cupric bromide bleached plate;[21] and bleaching with bromine vapor.[22] None of these procedures produce high diffraction efficiencies and low noise simultaneously.

Humidity problem[23] solutions have been approached by several methods most of these involve dehydration followed by hardening either chemically or with heat. The dehydration can be accomplished with a variety of solvents. Reduction of flare light[24] is treated by Lamberts.[25]

2. PHOTOPOLYMERS

Several types of photopolymers have been studied.[26,30] The most successful of these has been that described by Booth.[29,30] The material is applied as a coating on a substrate and consists of three parts: a photo-polymerizable monomer, an initiator system, and a polymeric binder.

The recording of a hologram takes place in three stages: initial exposure, diffusion period, and post exposure. During the initial exposure, light polymerizes part of the monomer. During the diffusion period monomer concentration gradients give rise to the diffusion of the smaller monomer molecules from regions of high concentration. The post exposure consists of exposure of the material to uniform intensity until the remaining monomer is polymerized. The net result is that regions initially exposed to high light intensities have greater concentrations of polymer and higher index of refraction. In references 28, 29 and 30, the initiator in the material used is sensitive primarily to ultraviolet radiation centered at 360 nm. But with the addition of dye sensitizers, the initiator can also be sensitive to visible light centered at 475 nm. The hypothetical model assumes no surface relief contribution to diffraction efficiency and this was experimentally verified. Experiments also indicate low response to low spatial frequency. Spatial frequencies should exceed 350 l/mm.[30] The resolution obtained with this photopolymer exceed 3500 l/mm with a 50 percent fall-off in diffraction efficiency at 3000 l/mm. Diffraction efficiencies of 100 percent have been obtained. Due to the relative large thickness of the grating the acceptance angle is smaller than that for bleached silver halides or dichromates.

3. DICHROMATED GELATINS

The use of dichromated gelatin emulsions as a recording medium for holograms has been studied from several standpoints. Shankoff[31,32] first demonstrated that good quality holograms can be recorded on dichromated gelatin and since then several papers have been published on the subject.[2,33,38] Gelatin films can be prepared and sensitized by utilizing commercial emulsions or by coating your own gelatin layers on a suitable substrate.[1,34,37]

The mechanism for formation of high efficiency gratings is explained by Curran and Shankoff.[35] This may be summarized as follows; The gelatin is sensitized in a solution of ammonium dichromate. Upon exposure, the areas receiving light are hardened and made relatively insoluble. Processing involves washing the plate in water and drying it fairly rapidly. The strain caused by the rapid dehydration causes the gel to tear or crack at the boundaries between the hardened and unhardened areas. These cracks make the resultant processed gelatin have onion-like layers whose boundaries are regions of air or low refractive index. These boundaries then cause the high diffraction observed. The observed high diffraction efficiency has also been explained by assuming gelatin of changing refractive index.[2] Problems noted with the use of dichromated gelatins include low sensitivity, tendency to be opaque, and sensitivity of the processed plate to humidity.

A characteristics of dichromates which is discussed in Reference 35 indicates that there is a tradeoff between high diffraction efficiency and angular bandwidth. For the display application considered in this report fairly large (15° - 20°) bandwidths were required which implies diffraction efficiencies of 50% to 60%.

The low, orthochromatic sensitivity can be overcome by using the bleach dichromate technique[17] or the bleach contact print technique.[2] The overall swelling of the processed plate similar to those effects found in silver-halide holography[39] can be remedied using the heat processing technique of Meyerhofer.[2]

4. Exotic Materials

The mechanism for formation of interference patterns in materials such as lithium niobate, strontium-barium niobate, and barium titanate is a light induced refractive index change. Since these materials were not readily available in the size and quantity required for experimentation they were not studied extensively. In general, the refractive index changes are small and therefore the thickness must be large. As stated previously large thicknesses imply small acceptance angles. This leads to elements with small fields of view.

B. RECORDED PATTERN

A geometric derivation of the fringe spacing due to the interference of two plane waves of coherent light is given below. In Figure 2 the lines

labeled P are wavefronts corresponding to loci of equiphase within the two beams. The lines labeled N are normal to the wavefront and correspond to the direction of propagation or the ray direction. The lines labeled F are fringes. The fringes connect the intersection of equiphase front intersections. As the wavefronts propagate in the direction of N the point of intersection moves from O to E along fringe line, producing a bright fringe. The line labeled d corresponds to the physical distance between two adjacent bright fringes. "λ" is the wavelength or distance between two successive equiphase wavefronts.

Using Figure 2, the fringe spacing d can be derived. By inspection, the fringe F bisects rhombus $\overline{AODE}$ and also by definition $\sphericalangle N_1OP_1 = \sphericalangle N_2OP_2 = \pi/2$. Using these relations it is found that $\sphericalangle P_2OP_1 = \pi - \phi$ where ϕ is the interference angle ($\phi = \sphericalangle N_1ON_2$). Similarly $\sphericalangle FOP_1$ is found to be $(\pi/2 - \phi/2)$. By inspection $\sphericalangle AOB = \sphericalangle P_2OP_1 = \pi - \phi$ and $\sphericalangle AOC = \sphericalangle FOP_1 = (\pi/2 - \phi/2)$. Using the definition of sine and cosine on the triangles AOB and AOC it is found that:

$$d/\overline{AO} = \sin \sphericalangle AOC \tag{5}$$

$$\lambda/\overline{AO} = \sin \sphericalangle AOB \tag{6}$$

Solving for d leads to:

$$d = \lambda \frac{\sin \sphericalangle AOC}{\sin \sphericalangle AOB} \tag{7}$$

$$d = \lambda \frac{\sin (\pi/2 - \phi/2)}{\sin (\pi - \phi)} \tag{8}$$

$$d = \lambda \frac{\cos (\phi/2)}{\sin \phi} \tag{9}$$

By definition: $\sin \phi = 2\sin(\phi/2)\cos(\phi/2)$ (10)

Therefore: $d = \frac{\lambda}{2\sin(\phi/2)}$. (11)

If the fringes are formed in a medium then $\lambda = \lambda o/n$ where n = index of refraction in the medium and $\lambda°$ is the wavelength in vacuum. Fringe spacing as a function of interference angle is plotted in figure 3.

D. PATTERN FORMATION IN RECORDING MEDIUM

The spacing and inclination of recorded fringes may be deduced from the incident interfering beam angles and the refraction of each beam at the surface of the recording medium. The resultant fringe spacings and inclination are physically changed by the processing procedure. This change can be accounted for by an overall swelling of the recording medium which results in a net thickness change of approximately 20%.

In figure 4, the two incident interfering beams are labeled B_1 and B_2 having incident angles θ_{B1} and θ_{B2} respectively with respect to the recording medium normal N. Snell's law requires that:

$$\theta'_{B1} = \sin^{-1} (\sin \theta_{B1}/n) \tag{12}$$

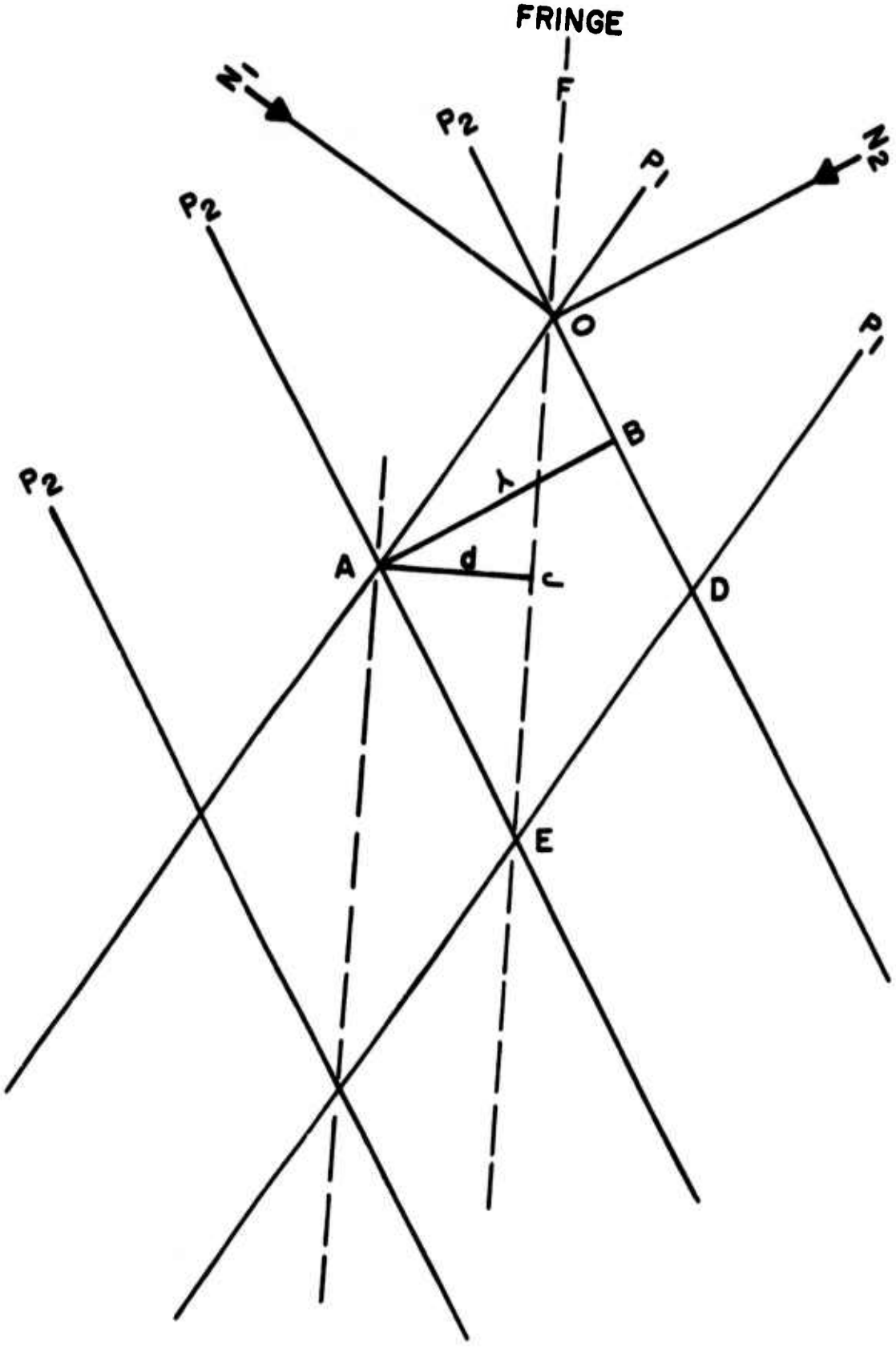

Figure 2. Fringes and Wavefronts

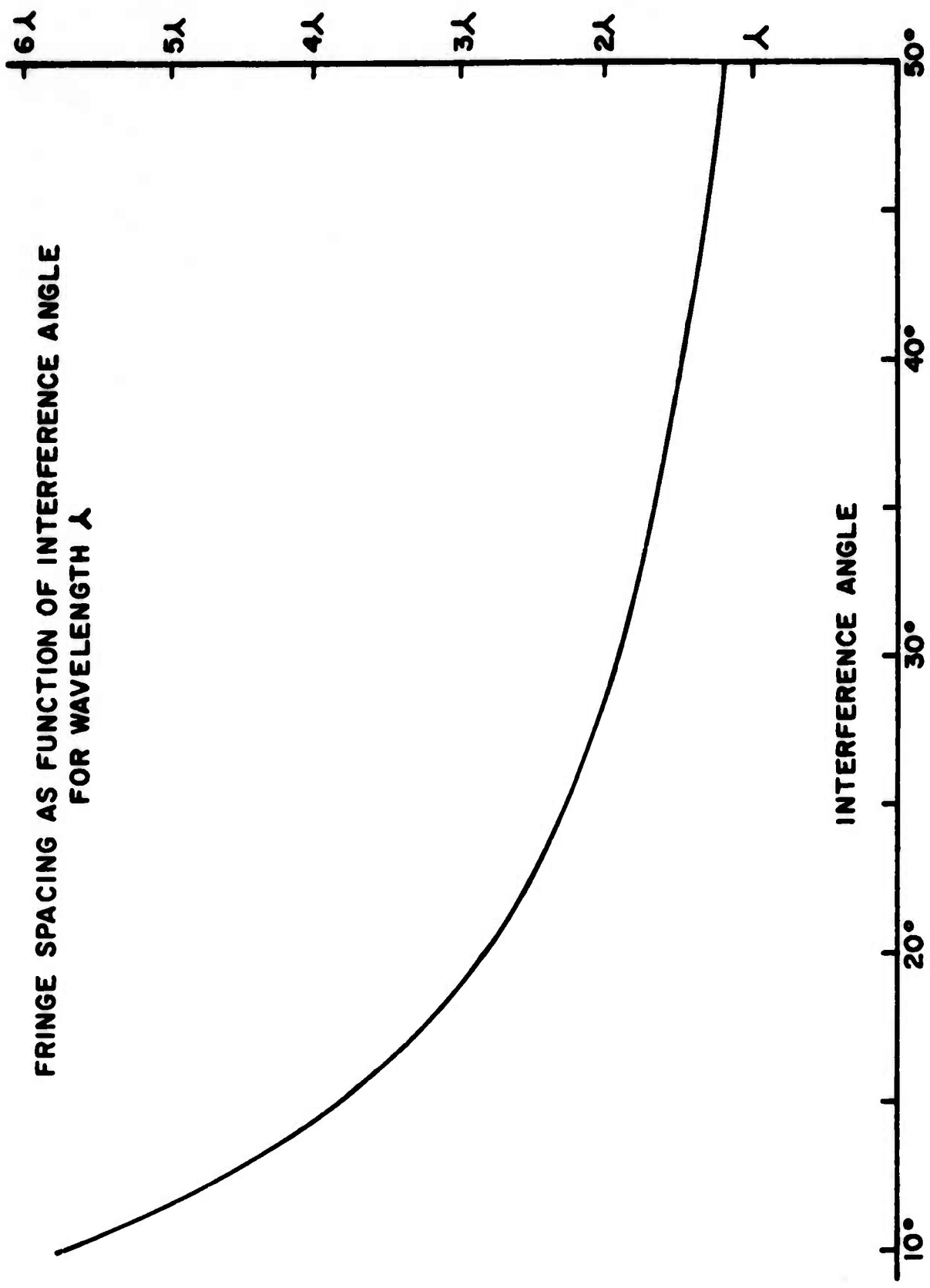

Figure 3. Fringe Spacing vs. Interference Angle

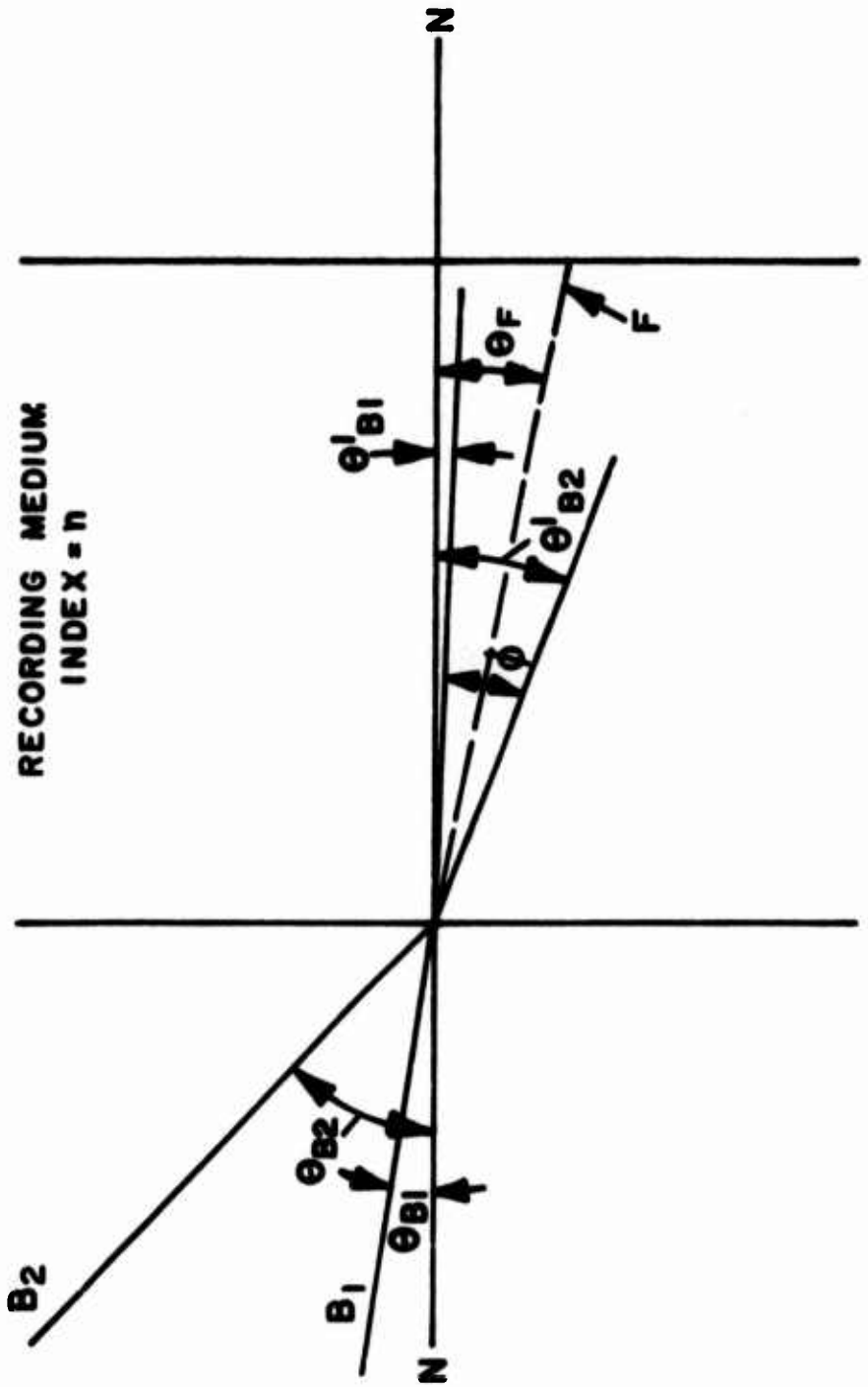

Figure 4. Interference Angles in Recording Medium

$$\theta'_{B2} = \sin^{-1}(\sin\theta_{B2}/n). \quad (13)$$

The angle of interference ϕ is, by inspection:

$$\phi = \theta'_{B2} - \theta'_{B1}. \quad (14)$$

The previous section's results indicate that the fringe spacing is:

$$d = \frac{\lambda}{2\sin(\phi/2)}. \quad (15)$$

The fringe inclination is found by noting that the fringe bisects ϕ.

By inspection the fringe inclination angle is found to be:

$$\theta_F = \frac{1}{2}\phi + \theta'_{B1}. \quad (16)$$

Substituting the value found for ϕ an alternate expression is:

$$\theta_F = \frac{1}{2}(\theta'_{B2} + \theta'_{B1}). \quad (17)$$

1. EFFECT OF SWELLING

The effect of swelling, or having a net thickness change in the processed recording medium relative to the thickness when it is exposed, is to change the fringe inclination and fringe spacing. The relations between initial and final spacings as well as initial and final fringe inclinations are derived below.

Figure 5 depicts the swelling of the recording medium from t_o to t_f. This swelling may be described by a swelling factor "M" such that:

$$M = t_f/t_o. \quad (18)$$

By inspection the angles θ_{FF} and θ_{FO} may be related:

$$\frac{\tan\theta_{FO}}{\tan\theta_{FF}} = \frac{t_f}{t_o} = M. \quad (19)$$

This may be rewritten as:

$$\theta_{FF} = \tan^{-1}(\tan\theta_{FO}/M). \quad (20)$$

Similarly the relation between initial fringe spacing d_o and final fringe spacing d_f may also be derived.

$$\frac{\cos\theta_{FF}}{\cos\theta_{FO}} = \frac{d_f}{d_o} \quad (21)$$

Relating equations 20 and 22 back to the incident beam angles it is found that:

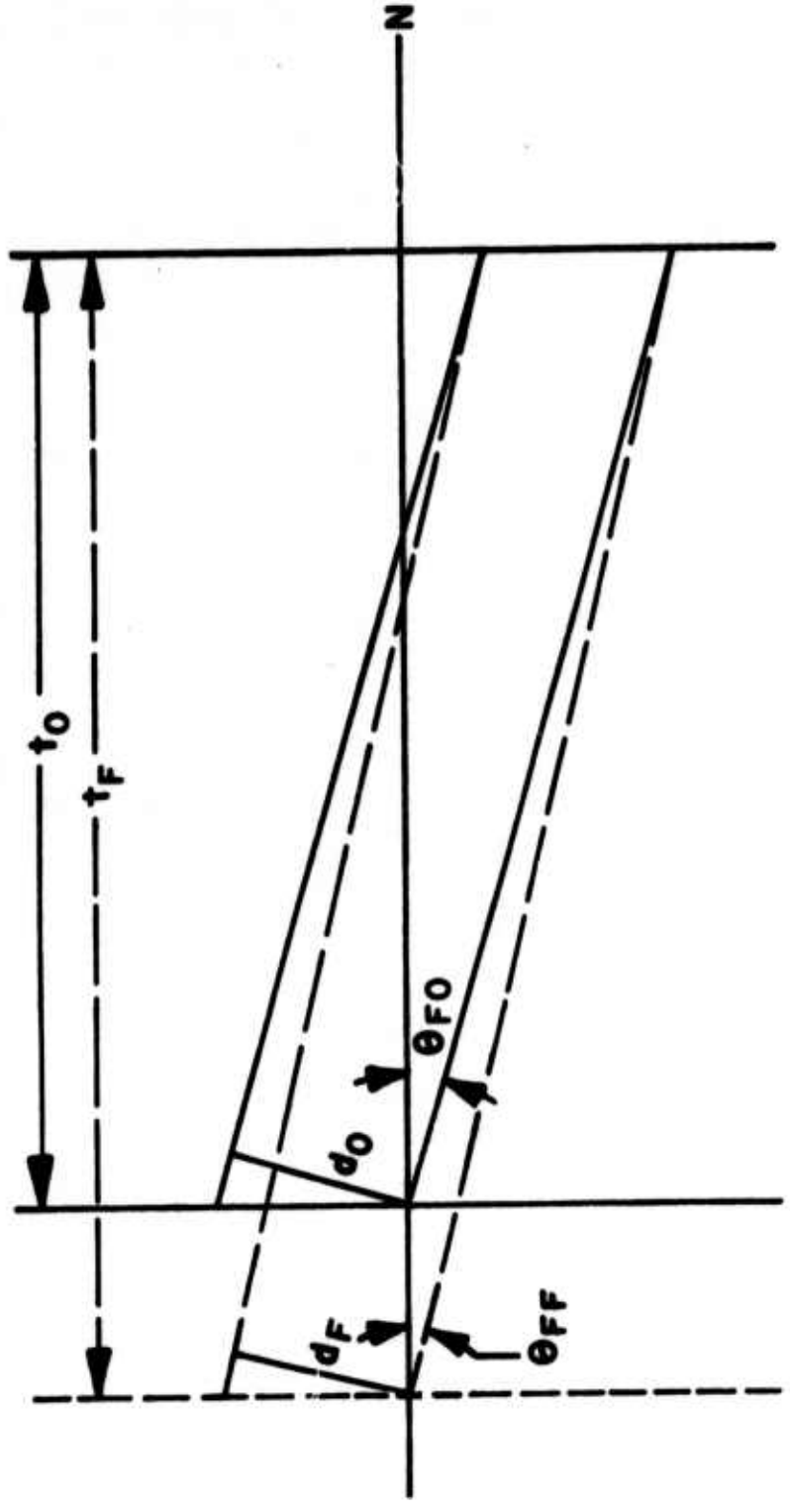

Figure 5. Effect of Swelling on Fringe Inclination

$$\theta_{FF} = \tan^{-1}\left(\frac{\tan\frac{1}{2}[\sin^{-1}(\sin\theta_{B1}/n) + \sin^{-1}(\sin\theta_{B2}/n)]}{M}\right). \quad (23)$$

$$\theta_{FO} = \frac{1}{2}[\sin^{-1}(\sin\theta_{B2}/n) + \sin^{-1}(\sin\theta_{B1}/n)]. \quad (24)$$

$$d_o = \frac{\lambda^o}{2n \sin\frac{1}{2}[\sin^{-1}(\sin\theta_{B2}/n) - \sin^{-1}(\sin\theta_{B2}/n)]}. \quad (25)$$

$$d_f = d_o \frac{\cos\theta_{FF}}{\cos\theta_{FO}}. \quad (26)$$

In this section expressions for the fringe inclination and spacing have been derived as functions of incident beam angles and recording medium swelling.

2. RECORDING PARAMETERS

The incident beam angles on the recording medium are pictured in figure 6. The two incident beams originate from point sources located at distances R_1 and R_2 from the center of the recording plate. The incident angles at the center of the plate are θ_{B10} and θ_{B20} with respect to the plate normal for beams B_1 and B_2 respectively. The relations between the incident angles at the center of the plate and the incident angles at points E_1 and E_2 located at distances of E/2 above and below the plate center are given as:

$$\theta_{B1E1} = \tan^{-1}\left[\tan\theta_{B10} - \frac{E}{2R1\cos\theta_{B10}}\right]. \quad (27)$$

$$\theta_{B1E2} = \tan^{-1}\left[\tan\theta_{B10} + \frac{E}{2R1\cos\theta_{B10}}\right]. \quad (28)$$

$$\theta_{B2E1} = \tan^{-1}\left[\tan\theta_{B20} - \frac{E}{2R2\cos\theta_{B20}}\right]. \quad (29)$$

$$\theta_{B2E2} = \tan^{-1}\left[\tan\theta_{B20} + \frac{E}{2R2\cos\theta_{B20}}\right]. \quad (30)$$

The resultant fringe inclinations and spacing within the recording medium at Points E_1, E_2, and O can then be computed using equation 24.

$$\theta_{FO} = \frac{1}{2}(\theta'_{B20} + \theta'_{B10}) \quad (31)$$

$$\theta_{FE1} = \frac{1}{2}(\theta'_{B2E1} + \theta'_{B1E1}) \quad (32)$$

$$\theta_{FE2} = \frac{1}{2}(\theta'_{B2E2} + \theta'_{B1E2}) \quad (33)$$

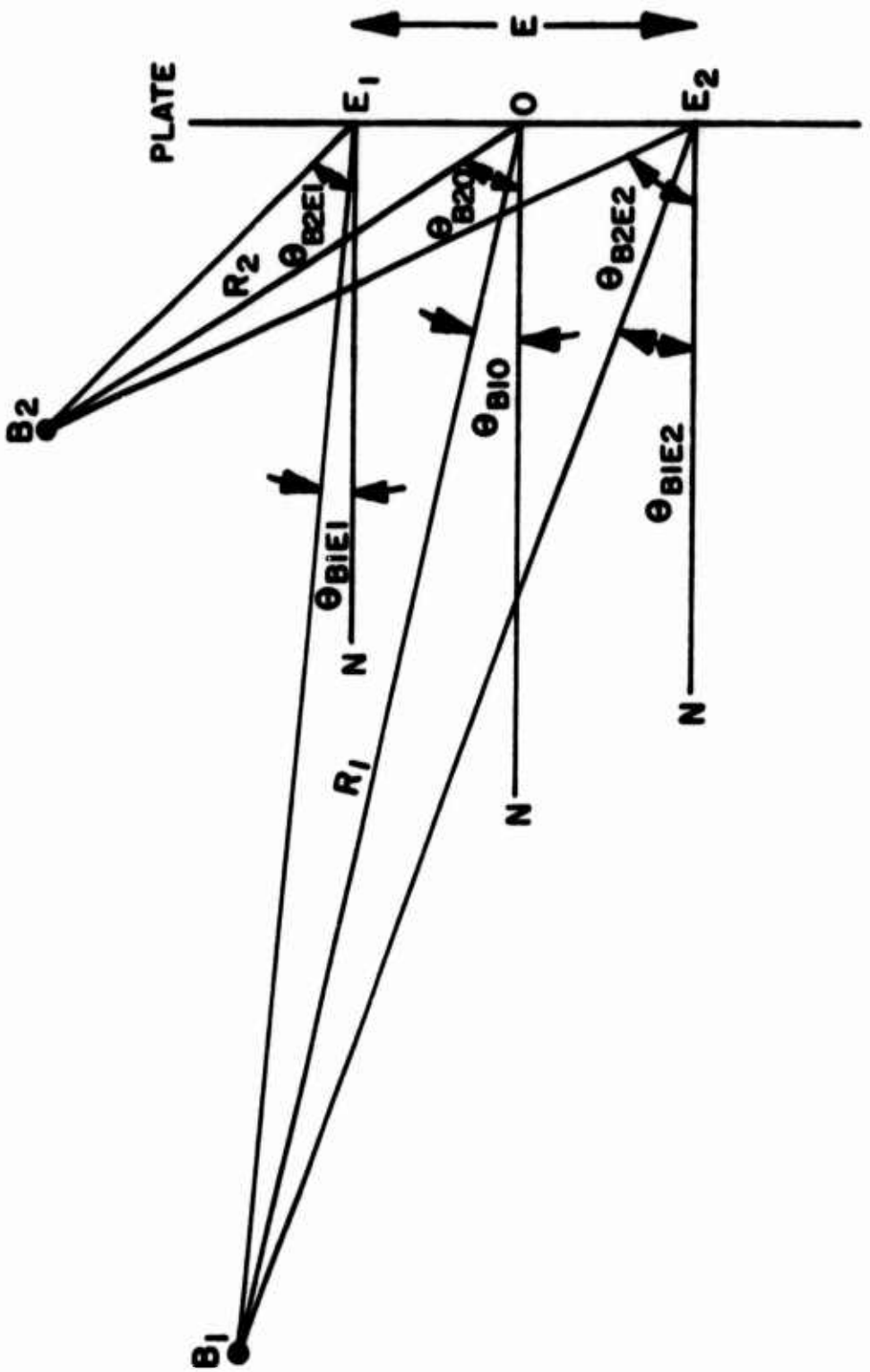

Figure 6. Incident Beam Angles on Recording Plate

Where: $\theta'_X = \sin^{-1}(\sin\theta_X/n)$ (34)

With X = B1O, B2O, B1E1, B1E2, B2E1, B2E2

The fringe inclination and spacing after a swelling M at points E_1, E_2 and O will be:

$$\theta_{FF} = \tan^{-1}(\tan\theta_{FO}/M) \quad (35)$$

$$\theta_{E1} = \tan^{-1}(\tan\theta_{FE1}/M) \quad (36)$$

$$\theta_{E2} = \tan^{-1}(\tan\theta_{FE2}/M) \quad (37)$$

With fringe spacing.

$$d_{FO} = d_O \frac{\cos\theta_{FF}}{\cos\theta_{FO}} \quad (38)$$

$$d_{E1} = d_{E1O} \frac{\cos\theta_{E1}}{\cos\theta_{FE1}} \quad (39)$$

$$d_{E2} = d_{E2O} \frac{\cos\theta_{E2}}{\cos\theta_{F2}} \quad (40)$$

Where d_O, d_{E1O}, and d_{E2O} are the recorded fringe spacing given by:

$$d_O = \frac{\lambda}{2\sin\frac{1}{2}(\theta'_{B2O} - \theta'_{B1O})} \quad (41)$$

$$d_{E1O} = \frac{\lambda}{2\sin\frac{1}{2}(\theta'_{B2O} - \theta'_{B1E1})} \quad (42)$$

And $\lambda = \lambda_o/n$ where n is the index of refraction.

$$d_{E2O} = \frac{\lambda}{2\sin\frac{1}{2}(0'_{B2E2} - \theta'_{B1E2})} \quad (43)$$

By inspection of figure 3 it is obvious that the recorded spatial frequencies are greatest or the fringe spacing smallest at E2. The fringe inclination angle is also greatest at E_2. figure 7 shows the recorded fringe pattern for B1 located at infinity along the normal ($\theta_{B1O} = 0°$; $R_1 = \infty$) with B_2 located at B2 in the figure. The wavelength is greatly exaggerated but the inclination angles are accurate. The net result is that, if there is no swelling or shrinking, a collimated beam incident on the processed plate from the right at 0° angle will be Bragg-diffracted to focus at B2. Bragg diffraction occurs when the plane spacing, angle of incidence, and wavelength are such that the reflected waves from each plane interfere constructively. With swelling, however, the interference fringe inclination angles are changed non-uniformly and the spacings are changed non-uniformly. This situation is illustrated in figure 8. This means that the

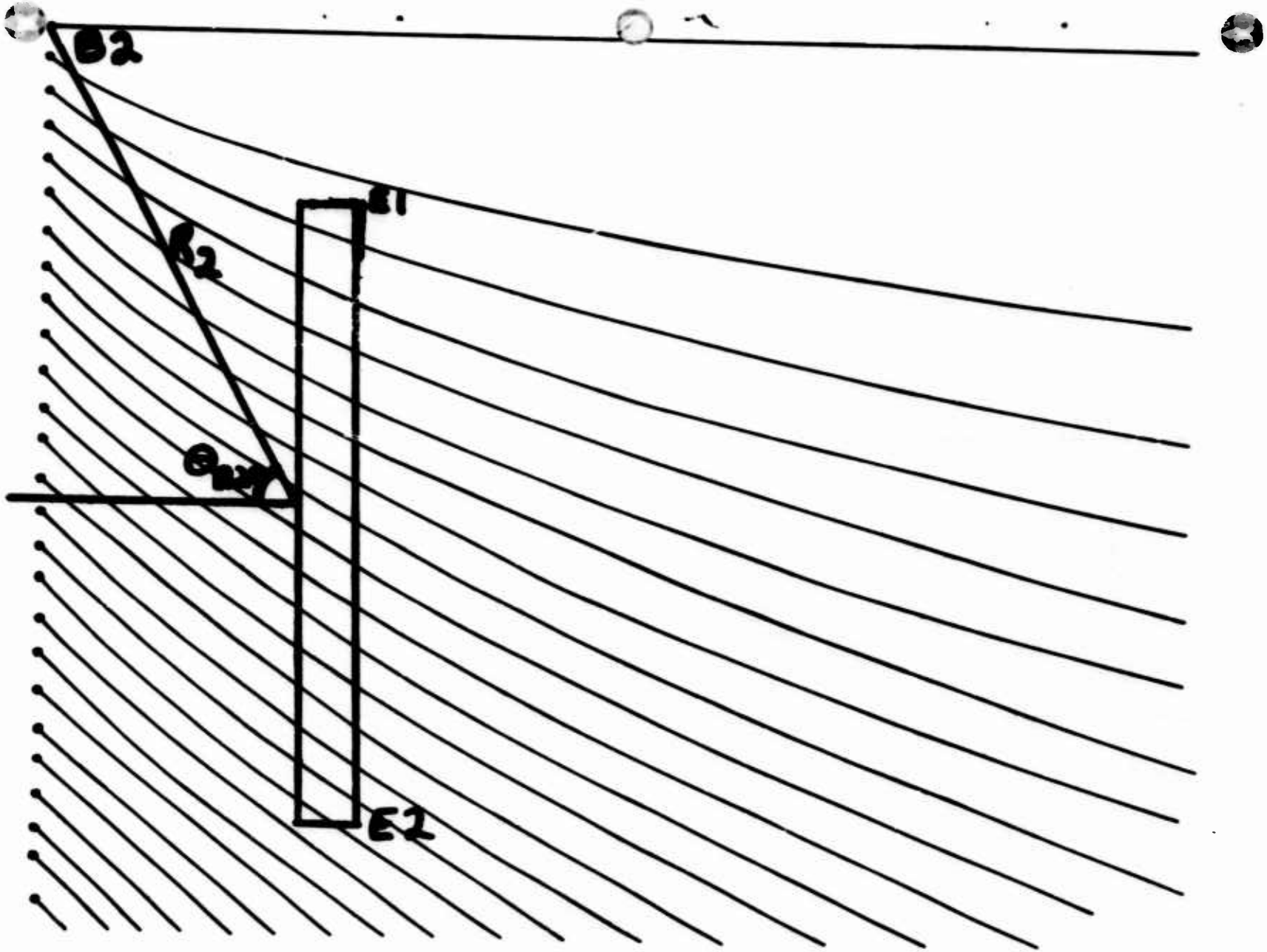

Figure 7. Recorded Fringe Spacings

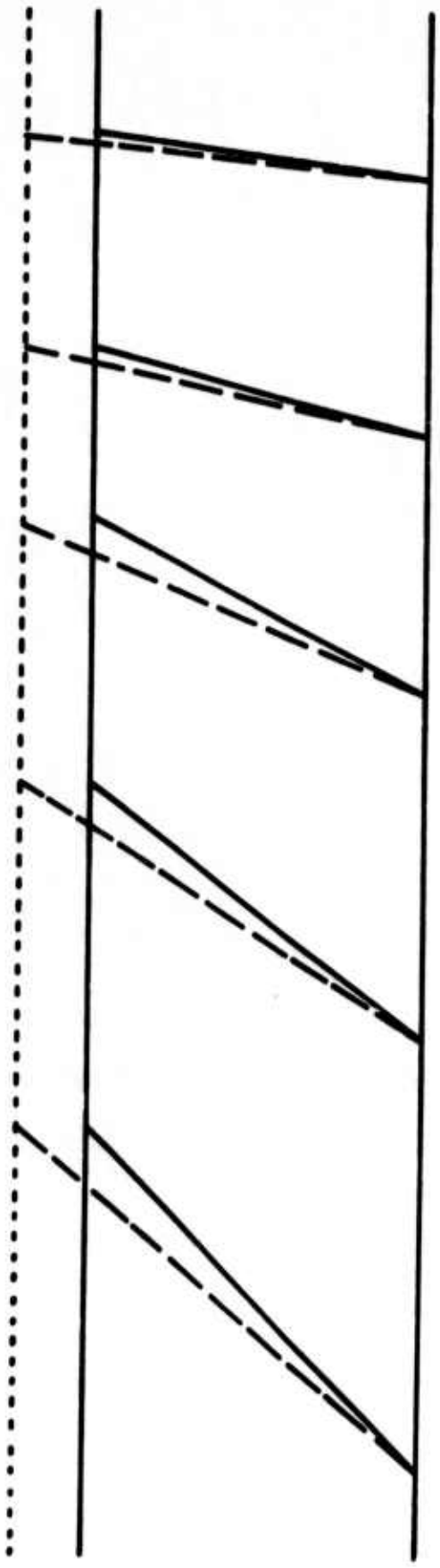

Figure 8. Effect of Swelling on Fringe Inclination Angles

processed plate can no longer Bragg diffract a collimated beam to a focus. The large fringe inclination angles will be changed a larger amount than the small fringe inclination angles.

3. AN EXAMPLE

A representative ray trace for λ° = 488 nanometer light being diffracted by a grating which was recorded with 488 nm light and which swelled 20% during processing is given below:

The initial conditions are chosen to be:

$$R_1 = \infty$$

$$R_2 = 0.5 \text{ meters}$$

$$\theta_{B10} = \theta_{B1F1} = \theta_{B1E2} = 0^\circ$$

$$\theta_{B20} = 30^\circ$$

$$\lambda^\circ = 488 \text{ nm}$$

$$n = 1.5$$

$$E = 0.1 \text{ meters}$$

The angles θ_{B2E1} and θ_{B2E2} can be determined by equations 29 and 30

$$\theta_{B2E1} = 24^\circ\ 48' \qquad (44)$$

$$\theta_{B2E2} = 34^\circ\ 43'$$

Using equation 34 the refracted ray angles are found to be:

$$\theta'_{B1E1} = \theta'_{B10} = \theta'_{B1E2} = 0^\circ$$

$$\theta'_{B2E1} = 16^\circ\ 14'$$

$$\theta'_{B20} = 19^\circ\ 28' \qquad (45)$$

$$\theta'_{B2E2} = 22^\circ\ 19'$$

The fringe inclination angles can now be determined from equations 31, 32, and 33

$$\theta_{FE1} = 8^\circ\ 7'$$

$$\theta_{F0} = 9^\circ\ 44' \qquad (46)$$

$$\theta_{FE2} = 11^\circ\ 9'$$

The resultant fringe angles after a swelling of 20% can be determined from equations 35, 36, and 37 with M = 1.2:

$$\theta_{E1} = 6^\circ\ 47'$$

$$\theta_{FF} = 8^\circ\ 8' \qquad (47)$$

$$\theta_{E2} = 9^\circ\ 20'$$

The "before swelling" fringe spacing determined by the initial interference angles from equations 41, 42, and 43 with $\lambda^\circ = 488$ nm and $n = 1.5$.

$$d_{E10} = 1152 \text{ nm}$$

$$d_0 = 962 \text{ nm} \qquad (48)$$

$$d_{E20} = 841 \text{ nm}$$

After swelling the spacings are determined by equations 38, 39, and 40

$$d_{E1} = 1156\text{nm}$$

$$d_{F0} = 966\text{nm} \qquad (49)$$

$$d_{E2} = 846\text{nm}$$

These data can be used to determine total diffraction angles or the interference angles which initially are required to produce the new fringe spacings. By using equation 14 and inspection:

$$\phi_{E1} = 16^\circ\ 10'$$

$$\phi_0 = 19^\circ\ 22' \qquad (50)$$

$$\phi_{E2} = 22^\circ\ 10'$$

By combining these results with the chosen requirement that Bragg diffraction conditions be maintained at the center of the grating (point 0), a value for required incident angle of a collimated beam to Bragg diffract from the recorded grating can be found;

$$\theta'_{B10} = -1^\circ\ 33' \qquad (51)$$

And by applying Snell's law

$$\theta_{B10} = -2^\circ\ 19' \qquad (52)$$

Assuming that the playback or incident beam is collimated, then:

$$\theta_{B1E1} = \theta_{B1E2} = \theta_{B10} = -2^\circ\ 19' \qquad (53)$$

and

$$\theta'_{B1E1} = \theta'_{B1E2} = \theta'_{B10} = -1° 33' \qquad (54)$$

By raytracing assuming Bragg diffraction at the center of the grating and ordinary diffraction at the points E1 and E2 the diffracted ray directions can be calculated;

$$\theta_{B20} = 27° 19' \qquad \theta'_{B20} = 17° 49'$$

$$\theta_{B2E1} = 22° 14' \qquad \theta'_{B2E1} = 14° 37' \qquad (55)$$

$$\theta_{B2E2} = 31° 33' \qquad \theta'_{B2E2} = 20° 25'$$

These are plotted together with ray directions for M values other than 1.2 in figures 9 and 10. Noted differences have been exaggerated by making E larger than 100 mm.

Experimental measurements of recording beam angles and diffracted beam angles for many gratings processed by the method described in Section III indicate grating swelling of 20% (or M= 1.2). This swelling will be used as a parameter in display lens design considerations. No attempts were made to vary swelling by changing concentration of sensitizing solution as described in reference 1.

As can be seen in figure 11 the swelling causes the blue image point (P_B) or focus to shift away from the optimum or focal point of the unswollen recorded grating (R). At the same time the point becomes aberrated leading to poor image quality. Fortunately illumination by light of longer wavelength tends to shorten the focal length and it is possible to get a fairly good image point (P_Y) in the swollen grating by illuminating with yellow light a grating made with blue light. To demonstrate the difference in focus for an unswollen grating several ray traces are pictured in figure 12.

Figure 12 shows the points reconstructed by a grating made with blue light and reconstructed with blue, yellow, and red light. The blue light is incident at a 0° angle and the exiting angle at the center of the grating is 30°. The other colors are incident at an angle satisfying the Bragg condition at the center and edges. It is apparent that the yellow and red rays focus at a shorter distance from the grating than the blue light. This observation together with the known swelling properties of the recording medium led to the use of yellow light as an illumination source for a grating recorded in blue light. A sample computation is made in the next section to demonstrate this application.

4. ILLUMINATION WITH DIFFERENT WAVELENGTHS

If the processed grating is illuminated with a monochromatic beam of wavelength different from the recording wavelength the ray trace will be different. If the previous example is used and

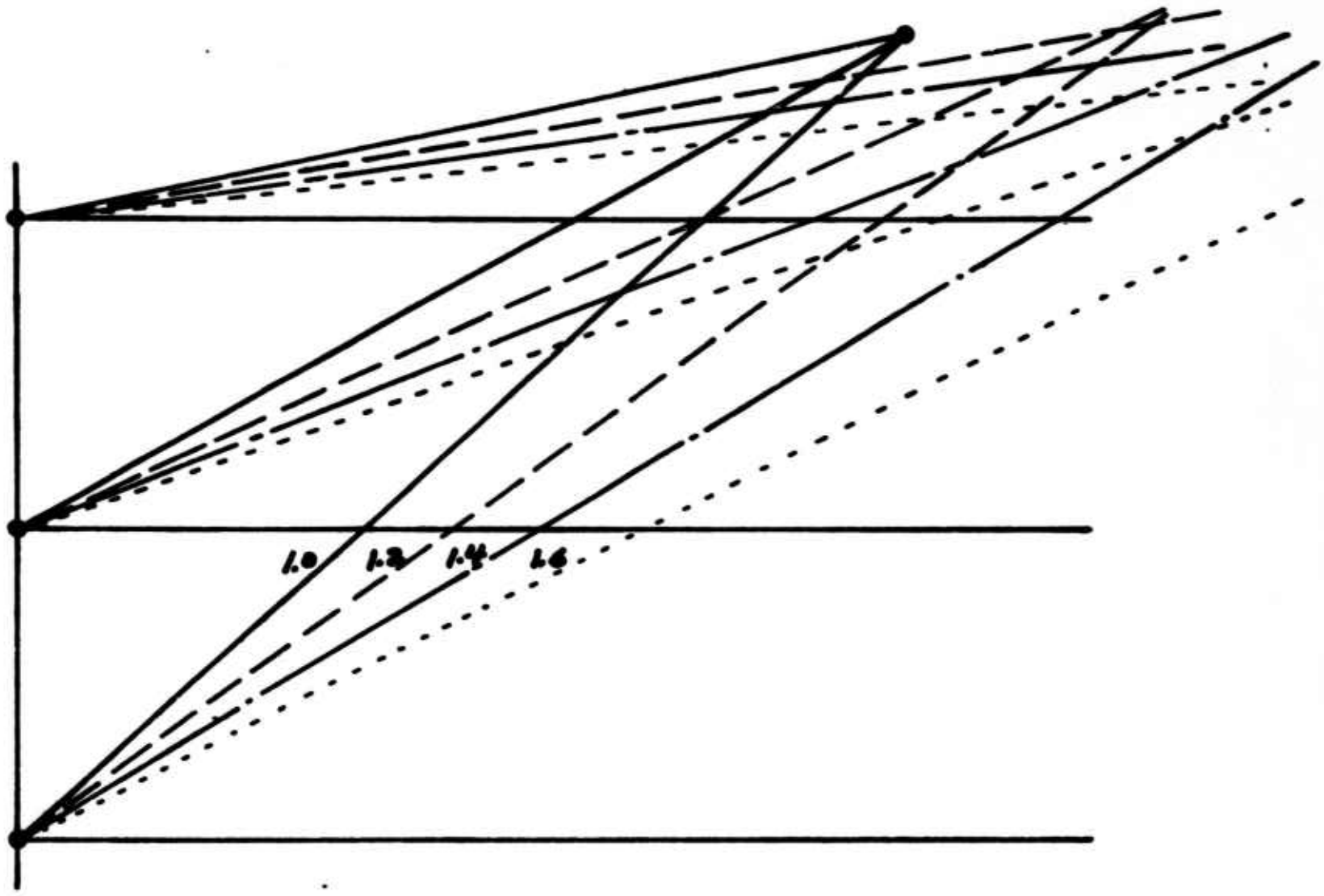

Figure 9. Effect of Swelling on Diffracted Ray Directions for M = 1.0, 1.2, 1.4, 1.6

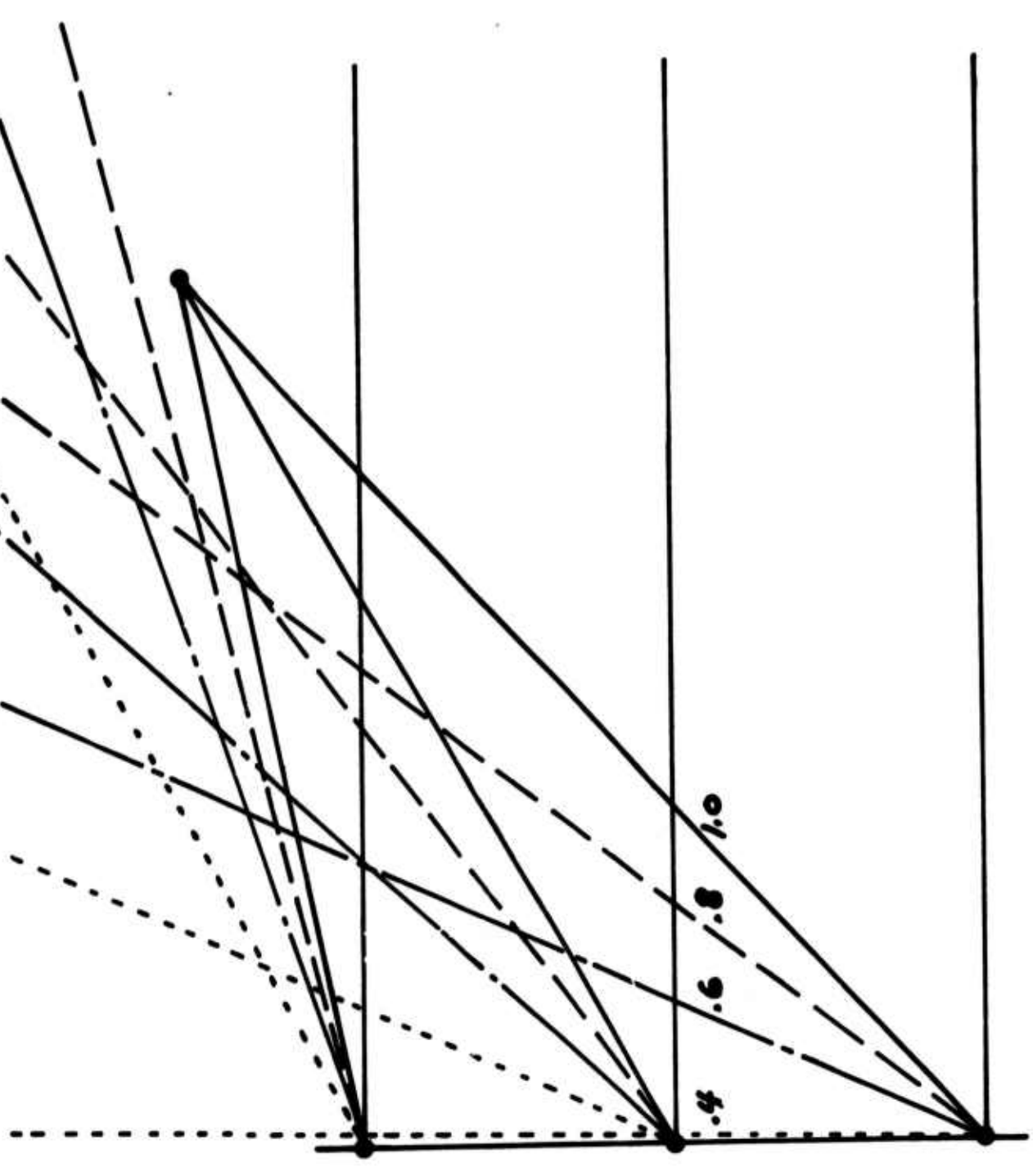

Figure 10. Effect of Swelling on Diffracted Ray Directions for M = 1.0, .8, .6, .4

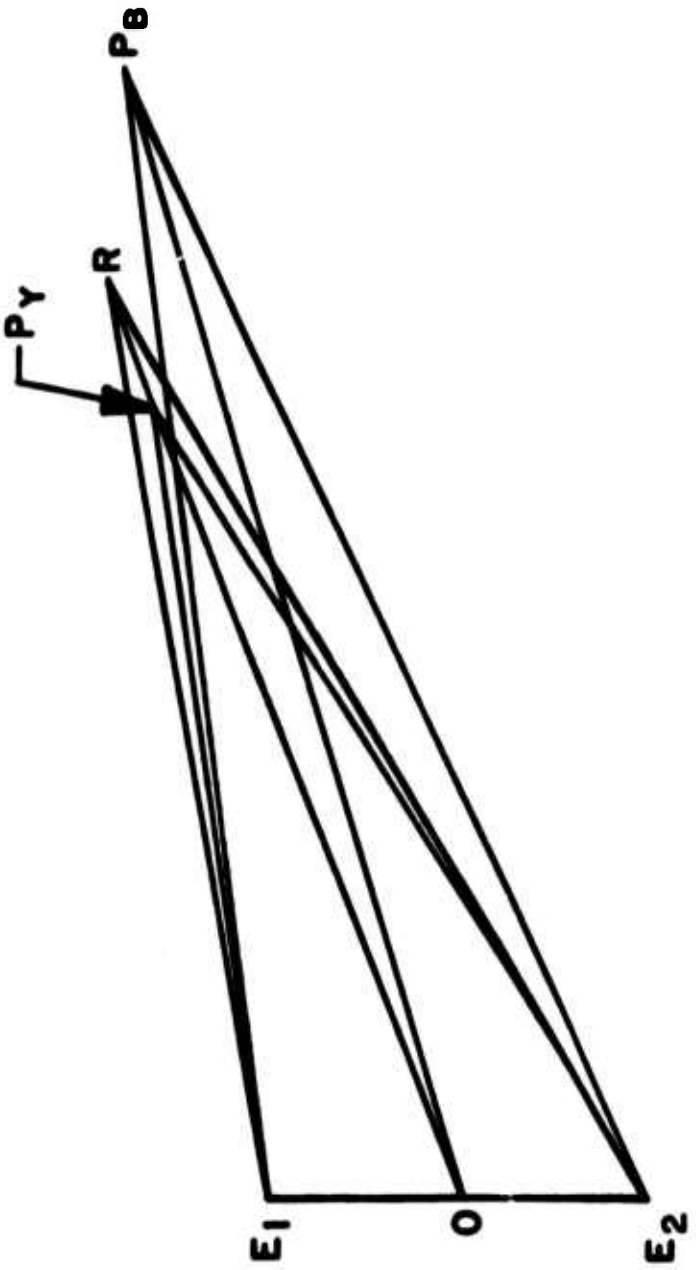

Figure 11. Effect of M = 1.2 with Blue and Yellow Illumination

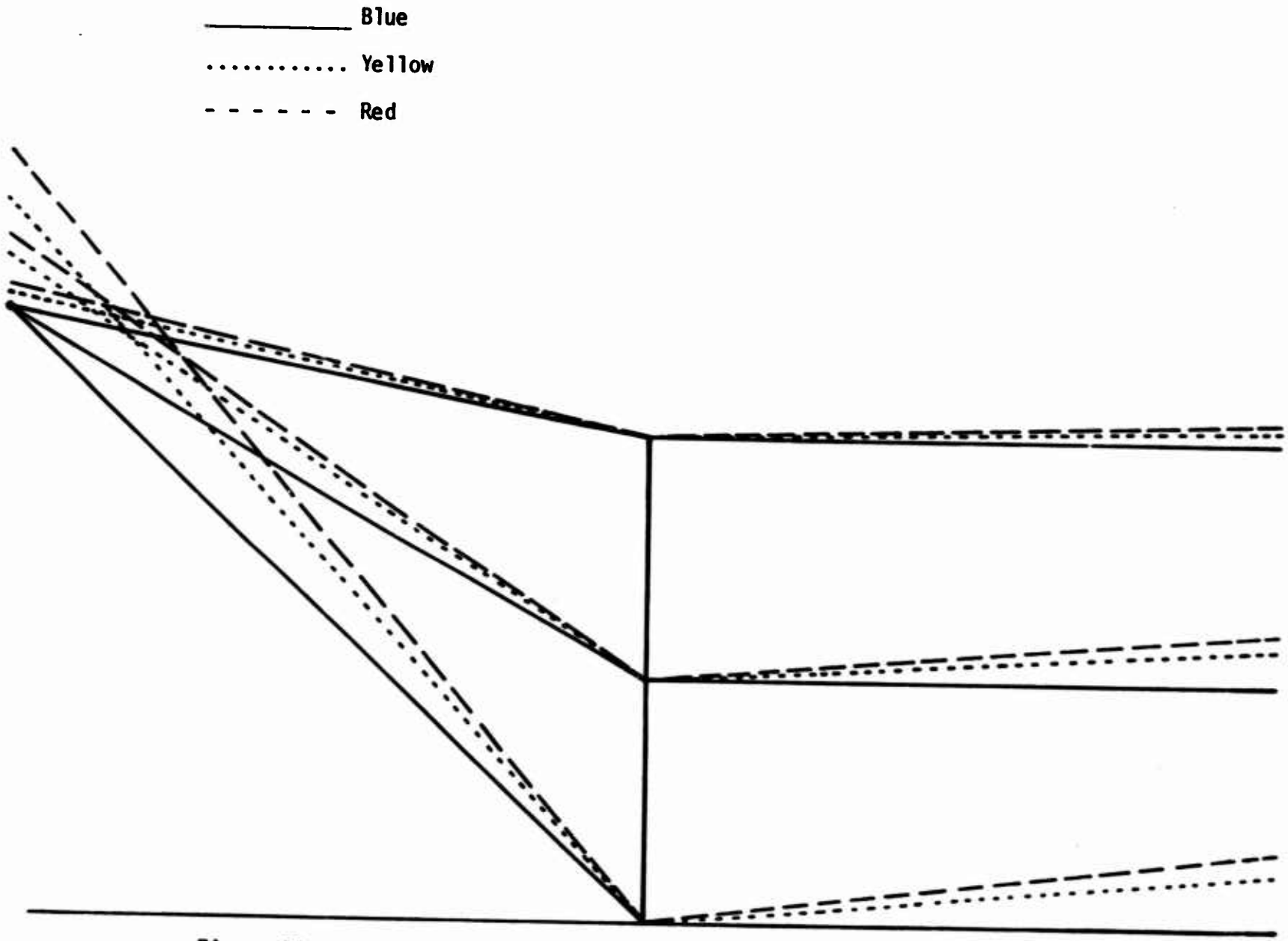

Figure 12. Illumination of Unswollen Grating with Blue, Yellow, and Red Light

Bragg diffraction at the plate center is assumed for incident light of wavelength 568.2nm the incident angle at point 0 can be calculated and then the diffraction angles at the other points on the grating. From the previous section it is known that the fringe spacings and inclination angles in processed gratings are:

$$d_{E1} = 1156\text{nm} \qquad \theta_{E1} = 6^\circ\ 47'$$

$$d_{F0} = 966\text{nm} \qquad \theta_{F0} = 8^\circ\ 8' \qquad (56)$$

$$d_{E2} = 846\text{nm} \qquad \theta_{E2} = 9^\circ\ 20'$$

Bragg diffraction at the 0 point fringe implies a total diffraction angle of

$$\phi_{Y0} = 2\sin^{-1}\frac{\lambda}{2\,d_{F0}} = 22^\circ\ 36' \qquad (57)$$

This means that the incident yellow light must hit the fringe with an incident angle of 11° 18' with respect to the fringe. Since the fringe is inclined at an angle of 8°8', θ'_{YB10} = 8°8 -11°18 = -3°10 and θ_{YB10} can be found from Snell's law to be:

$$\theta_{YB10} = -4^\circ\ 45' \qquad (58)$$

Correspondingly θ_{YB20} and θ'_{YB20} are found to be:

$$\theta'_{YB20} = 19^\circ\ 26' \qquad (59)$$

$$\theta_{YB20} = 29^\circ\ 56'$$

Using $\theta_{YB1E1} = \theta_{YB1E2} = \theta_{YB10}$ and computing ordinary diffraction at points E1 and E2 it is found that:

$$\theta'_{YB2E1} = 15^\circ\ 42'$$

$$\theta'_{YB2E2} = 22^\circ\ 42' \qquad (60)$$

And from Snell's law it can be found that:

$$\theta_{YB2E1} = 23^\circ\ 57'$$

$$\theta_{YB2E2} = 35^\circ\ 22' \qquad (61)$$

The resultant angles may be compared to the original recording parameters in Table 2.

TABLE 2. PLAYBACK ANGLES VS. RECORDING ANGLES

Recording	Playback Blue	Playback Yellow
24° 48	22° 14	23° 57
30°	27° 19	29° 56
34° 43	31° 33	35° 22

These are plotted in an exaggerated fashion in figure 11 to show the original recorded point position and the relative position of the two foci (blue and yellow). It is apparent that to reconstruct the original point position would require illumination with a wavelength between the blue and yellow. However the yellow wavelength is more practical for reasons discussed elsewhere and yellow is used in all evaluations.

The examples and computations demonstrate a diffraction ray tracing technique that can be used to predict the performance of a holographic lens when the exposure parameters are known. Correspondingly if the desired lens parameters are known then exposure parameters can be calculated. The computations also demonstrate several characteristics of holograms made in the described manner. In general, the following statements can be made:

(1) Illumination of a processed (swollen) grating with the blue recording light leads to an aberrated image at a longer focal length.

(2) Illumination with yellow light wavelength leads to a less aberrated image with a shorter focal length.

(3) It may not be possible to choose a recording set up which will Bragg diffract at all points after processing at any wavelength.

E. DESIGN CONSIDERATIONS

1. SYSTEMS CONCEPT

The initial design goal was to demonstrate the feasibility of using a holographically produced, multichannel lens element in a heads-up display for eventual application to visual simulation systems. The original concept which was considered is pictured in figure 13. In this concept it was planned to use CRT screens as inputs, and have channels 1 and 2 incident at approximately 60° and 120° with respect to line of sight with the grating at approximately 45° to the line of sight. As investigations proceeded it was found that even though it is possible to use a broad band object such as a CRT (see section on multi-element lens inputs) it would simplify the system if it were designed for monochromatic light.

The next modification to the original concept was made after consideration was given to imaging properties of the holographic lenses. Theoretical calculations indicated, and experiments verified, that when interference angles were large, corresponding to large diffraction angles, two effects were noted. One, the diffraction efficiencies dropped and two, the aberrations greatly increased for any points a finite distance from the original point used to make the hologram. These characteristics led to the conclusion that the interference angles should be small and should be approximately the same for each channel.

Based on these results the original concept was modified to that in figure 14. In this concept the interference angle for

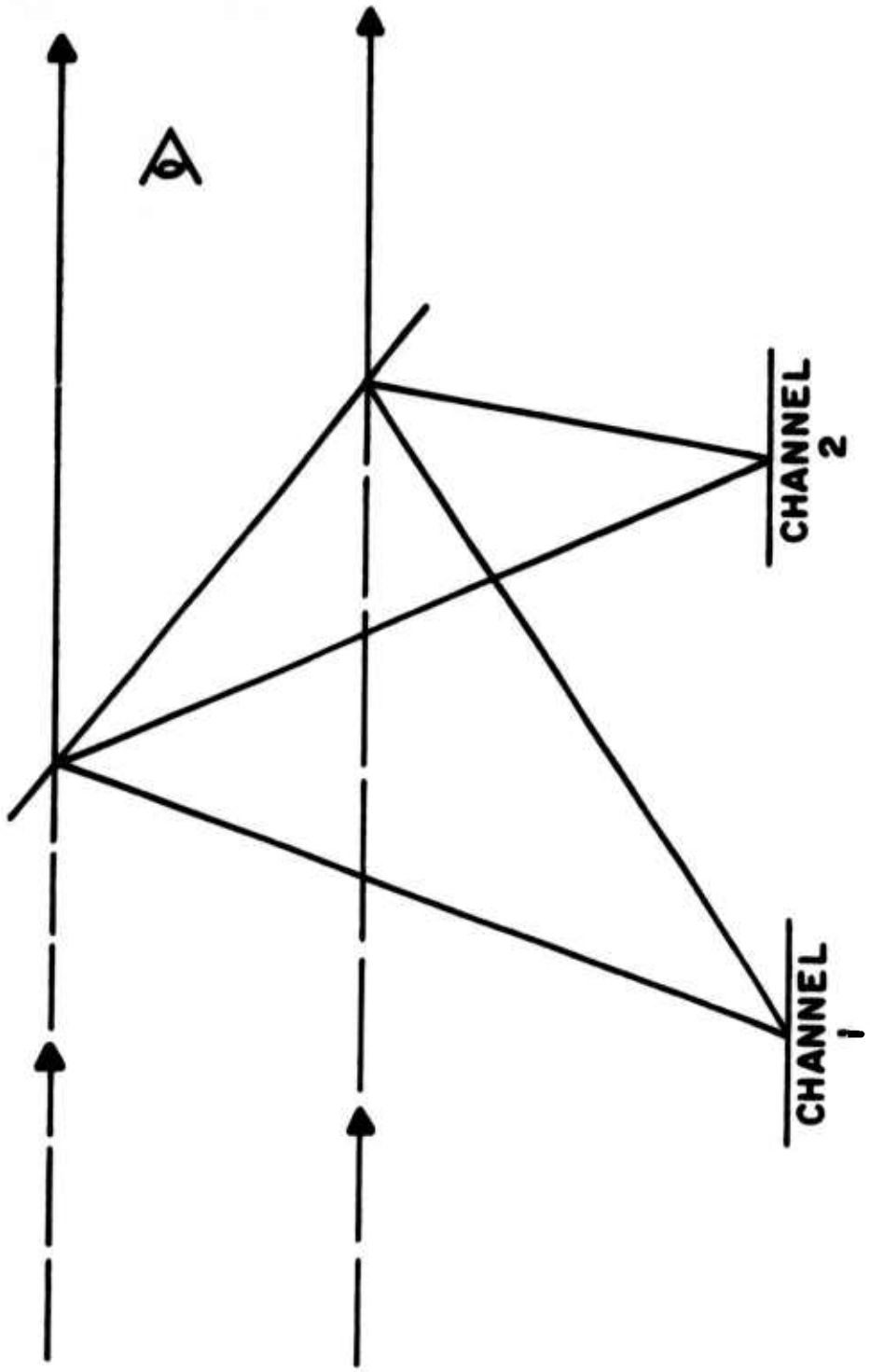

Figure 13. Original Concept of Two Channel System

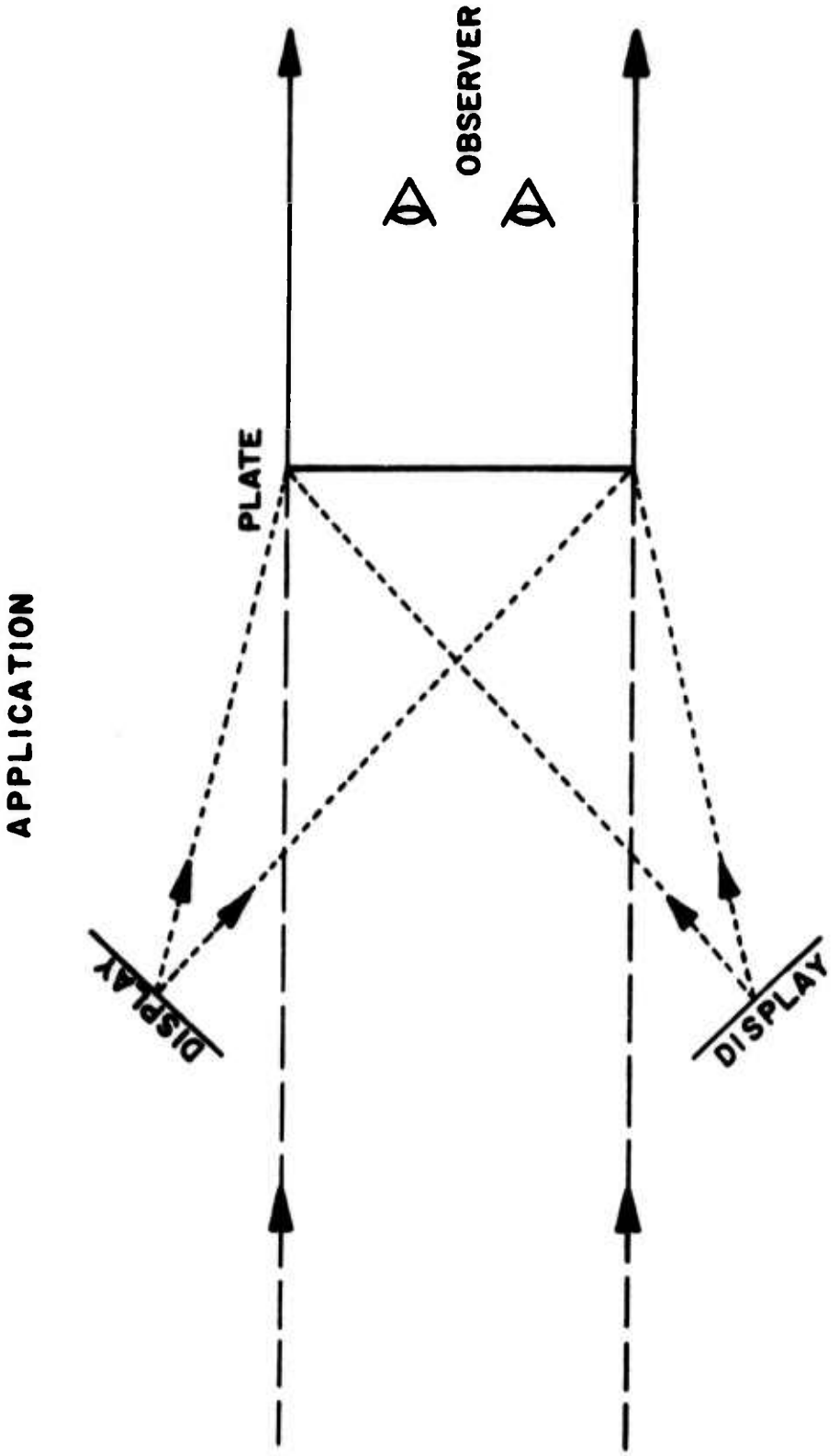

Figure 14. Symmetrical Two-Channel Lens System

each channel was 30°. This angle is small enough so that uniform high diffraction efficiencies could be maintained and have fairly good image quality and yet it is large enough so that direct view is not blocked. Equal angles for each channel greatly simplify exposure parameters since the sensitized plate could simply be rotated for the second exposure. The exposure positions are illustrated in figure 15. The specific exposure parameters can be found by first choosing the desired resultant display characteristics then calculating the required fringe inclination angles and spacings. These angles and spacings can be related to initial exposure parameters when account is taken of exposing wavelength and recording medium swelling during processing.

2. DISPLAY ILLUMINATION

As discussed previously, the recording light must be coherent and have a wavelength toward the blue end of the spectrum in order to efficiently expose the dichromated gelatin. The 488.0 nanometer line of an argon laser (except for some initial exposure testing) was used exclusively in the production of all gratings. This laser was tuned by means of an etalon to have a coherence length in excess of five meters. In exposure set ups, the path length difference was less than one-half meter, well within the coherence length. The illumination of the final display was chosen to be yellow sodium light (wavelength = 589.2 nonometers). This was chosen to demonstrate feasibility for two reasons: (1), the yellow light is closer to the peak eye response and (2), a sodium vapor lamp is less expensive initially and more efficient than a laser in terms of available illumination as a function of input electric power. To simplify measurements of diffraction efficiency and aberrations a krypton laser line with wavelength = 568.2 manometers was used in the evaluation measurements. Since this program was not directed toward a very specific application it was not necessary to optimize the system for final display.

3. DISPLAY GEOMETRY

As stated above the two input channels were chosen to be identical and each 30° off normal. The geometric parameters of rays diffracting from the grating having diameter 150 mm to a point Y located 30° off normal from point 0 at a distance of 460 mm are found to be as in figure 16.

$$\theta_{YB2E1} = 21° 16' \qquad \theta_{YB1E1} = 0°$$

$$\theta_{YB20} = 30° \qquad \theta_{YB10} = 0° \qquad (62)$$

$$\theta_{YB2E2} = 37° 26' \qquad \theta_{YB1E2} = 0°$$

Apply Snell's law and assuming recording has n = 1.5

$$\theta_{YB2E1} = 14° \qquad \theta'_{YB1E1} = 0°$$

$$\theta'_{YB20} = 19° 28' \qquad \theta'_{YB10} = 0° \qquad (63)$$

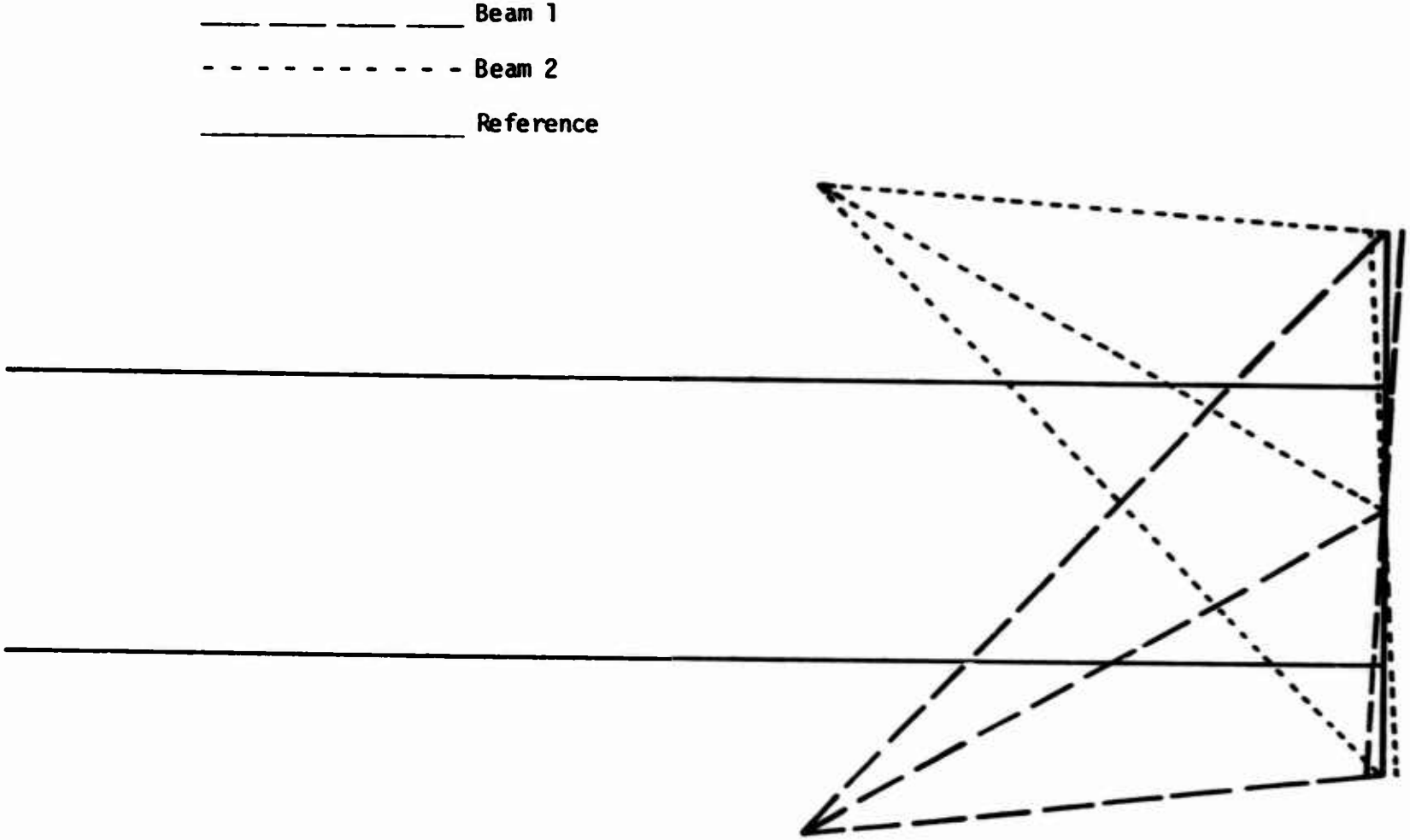

Figure 15. Plate Positions for Exposure

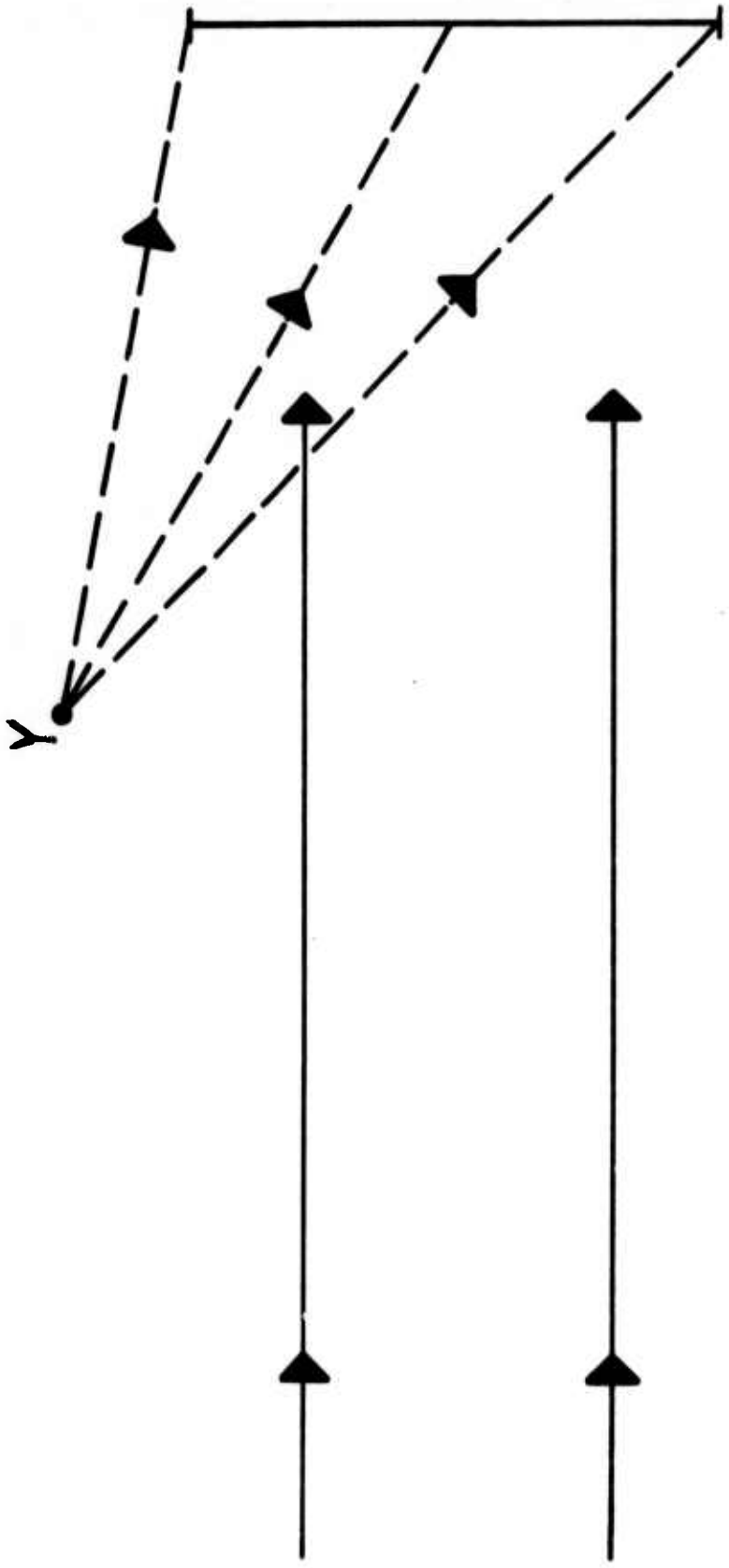

Figure 16. Desired Display Characteristic

$\theta'_{YB2E2} = 23° 54'$ $\theta'_{YB1E2} = 0°$

From these, the fringe inclinations and spacings at point O, E1, E2 are found to be:

$$\begin{aligned} \theta_{YE1} &= 7° & d_{YE1} &= 1554 \text{ nm} \\ \theta_{YFF} &= 9° 44' & d_{YFO} &= 1120 \text{ nm} \\ \theta_{YE2} &= 11° 57' & d_{YE2} &= 915 \text{ nm} \end{aligned} \quad (64)$$

Applying the "swell" equations the original fringe inclinations and spacings which resulted in the above are found to be:

$$\begin{aligned} \theta_{FE1} &= 8° 23' & d_{E10} &= 1549 \text{ nm} \\ \theta_{FO} &= 11° 38' & d_{00} &= 1113 \text{ nm} \\ \theta_{FE2} &= 14° 15' & d_{E20} &= 906 \text{ nm} \end{aligned} \quad (65)$$

The interference angles in blue light required to produce the above spacings are:

$$\phi_{E1} = 12° 4' \qquad \phi_0 = 16° 48' \qquad \phi_{E2} = 20° 42' \quad (66)$$

From these results the incident refracted ray directions at each point can be calculated.

$$\begin{aligned} \theta'_{B1E1} &= 2° 21' & \theta'_{B2E1} &= 14° 25' \\ \theta'_{B10} &= 3° 14' & \theta'_{B20} &= 20° 2' \\ \theta'_{B1E2} &= 3° 54' & \theta'_{B2E2} &= 24° 26' \end{aligned} \quad (67)$$

From Snell's law it is found that.

$$\begin{aligned} \theta_{B1E1} &= 3° 32' & \theta_{B2E1} &= 21° 56' \\ \theta_{B10} &= 4° 51' & \theta_{B20} &= 30° 55' \\ \theta_{B1E2} &= 5° 52' & \theta_{B2E2} &= 38° 38' \end{aligned} \quad (68)$$

These required incident blue rays are plotted in figure 17.

From figure 17 it is apparent that Beam 1 is almost collimated with an incident angle of approximately 4°30' and Beam 2 is off-normal from the center of the grating approximately 31° and is located approximately 450 mm away from the center of the grating. These were the parameters used to make the holographic lenses.

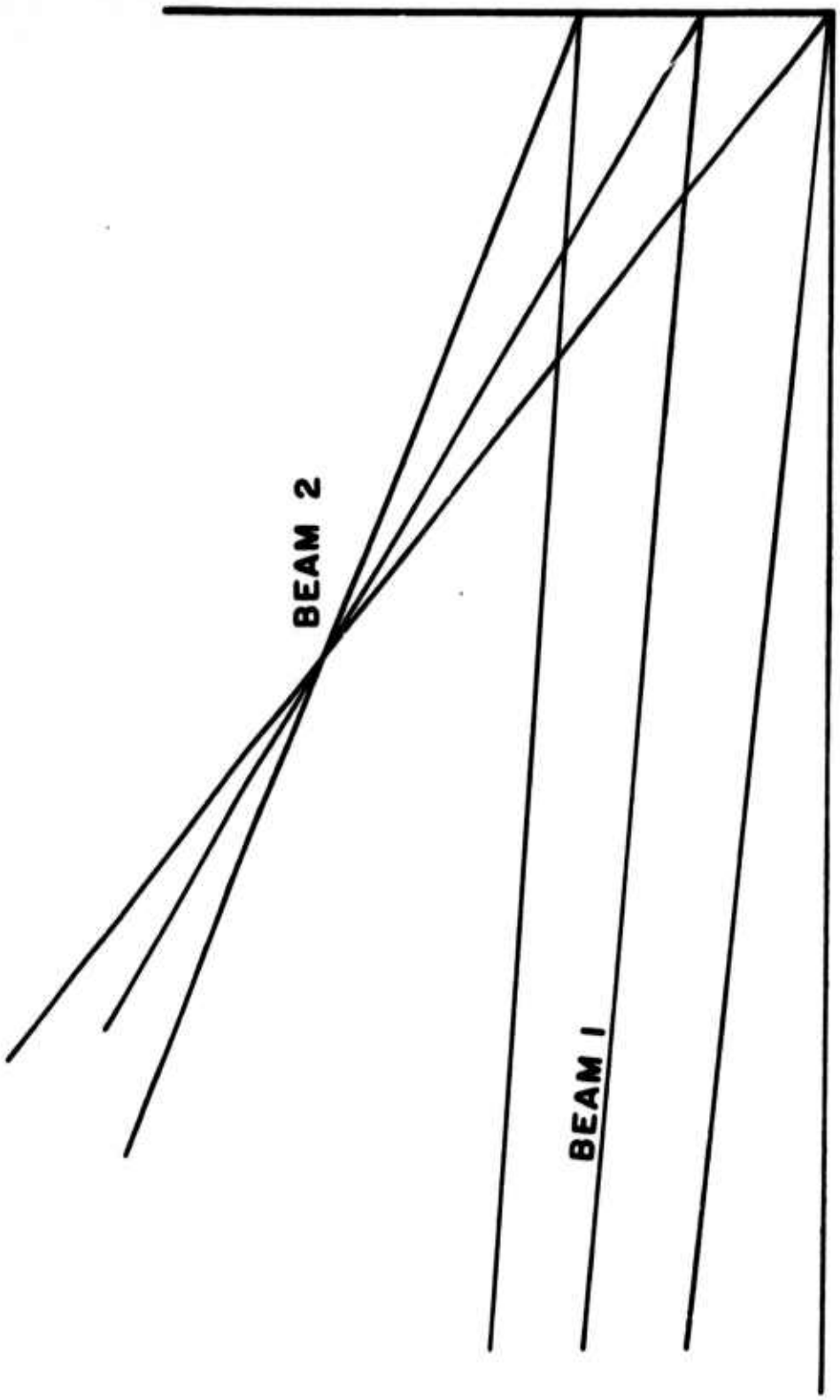

Figure 17. Required Exposure Angles

F. THEORY OF IMAGING AND ABERRATIONS[40,59]

In this section, the location of the Gaussian image, magnification, and third order aberrations of a quasi-rotationally-symmetric holographic lens are derived, following Meier.[40] In reality, the lenses made for the holographic heads up display (HHUD) were not rotationally symmetric; but a very good approximation was found by requiring that the object, reference, and readout beams be maintained at small angles relative to the axis. When the angles become large, aberrations of all orders, even and odd, enter into and complicate the imaging wavefront equations.[41] It was decided to use the rotationally-symmetric approximation in the design phase of the holographic lenses for the HHUD.

The basic arrangement for recording a holographic lens is shown in figure 17. A single coherent laser beam is divided into two beams by means of a partially transmitting and reflecting mirror. One of these beams, r, is collimated such that it appears to be a point source of light at infinity. The other beam o, is passed through a spatial frequency filter such that it appears to be a point source of light at a finite distance. (This finite distance will be nearly equal the focal length of the final holographic lens.) The two beams of light interfere and produce an irradiance distribution in the plane of the holographic plate represented by,

$$I = |O + r|^2 = |O|^2 + |r|^2 + O^*r + Or^* \qquad (69)$$

After proper exposure and suitable processing, a holographic lens is obtained from which the purely amplitude information of equation 69 has been removed and only the phase information remains.

When the holographic lens is illuminated with another coherent beam of light, c, two new wavefronts emerge:

$$H_R = c \cdot O^* \cdot r \qquad \text{and} \qquad H_V = c \cdot O \cdot r^* \tag{70}$$

One of these wavefronts is diverging and the other is converging. Since the lens is transparent, we are in reality concerned only with the composite phase of the three beams, and the irradiance of the reconstruction beam, c. From equation70 we see that the phases of the two emergent beams are given by:

$$\phi_R = \phi_c - \phi_o + \phi_r \tag{71}$$

$$\phi_R = \phi_c - \phi_o + \phi_r \tag{72}$$

To determine the actual phase of the beams, let us consider a point object $P(X_o, Y_o, Z_o)$ in a coordinate system whose origin lies in the center of the holographic plate with the X and Y axes in the plane of the emulsion, see figure 18. Let the wavelength of P be λ_o. The phase of the spherical wavefront from P at Q in the plane of the hologram relative to its phase at the origin is given by,

$$\phi_o(x,y) = \frac{2\pi d}{\lambda_o} = \frac{2\pi}{\lambda_o}\left(\overline{PQ} - \overline{PO}\right) \tag{73}$$

$$= \frac{2\pi}{\lambda_o}\left\{\left[(x-x_o)^2 + (y-y_o)^2 + z_o^2\right]^{\frac{1}{2}} - \left[x_o^2 + y_o^2 + z_o^2\right]^{\frac{1}{2}}\right\} \tag{74}$$

Assuming that $Z_o^2 > X_o^2 + Y_o^2$, we may expand equation74 as illustrated,

$$\phi_o(x,y) = \frac{2\pi}{\lambda_o}\left[\left(\frac{1}{2z_o}\right)\left(x^2 + y^2 - 2xx_o - 2yy_o\right) - \left(\frac{1}{2z_o}\right)^3 \left(x^4 + y^4 + 2x^2y^2\right.\right.$$

$$\left.\left. -4x^3x_o - 4y^3y_o - 4x^2yy_o - 4xy^2x_o + 6x^2x_o^2 + 6y^2y_o^2 + 2x^2y_o^2 + 2y^2x_o^2\right.\right.$$

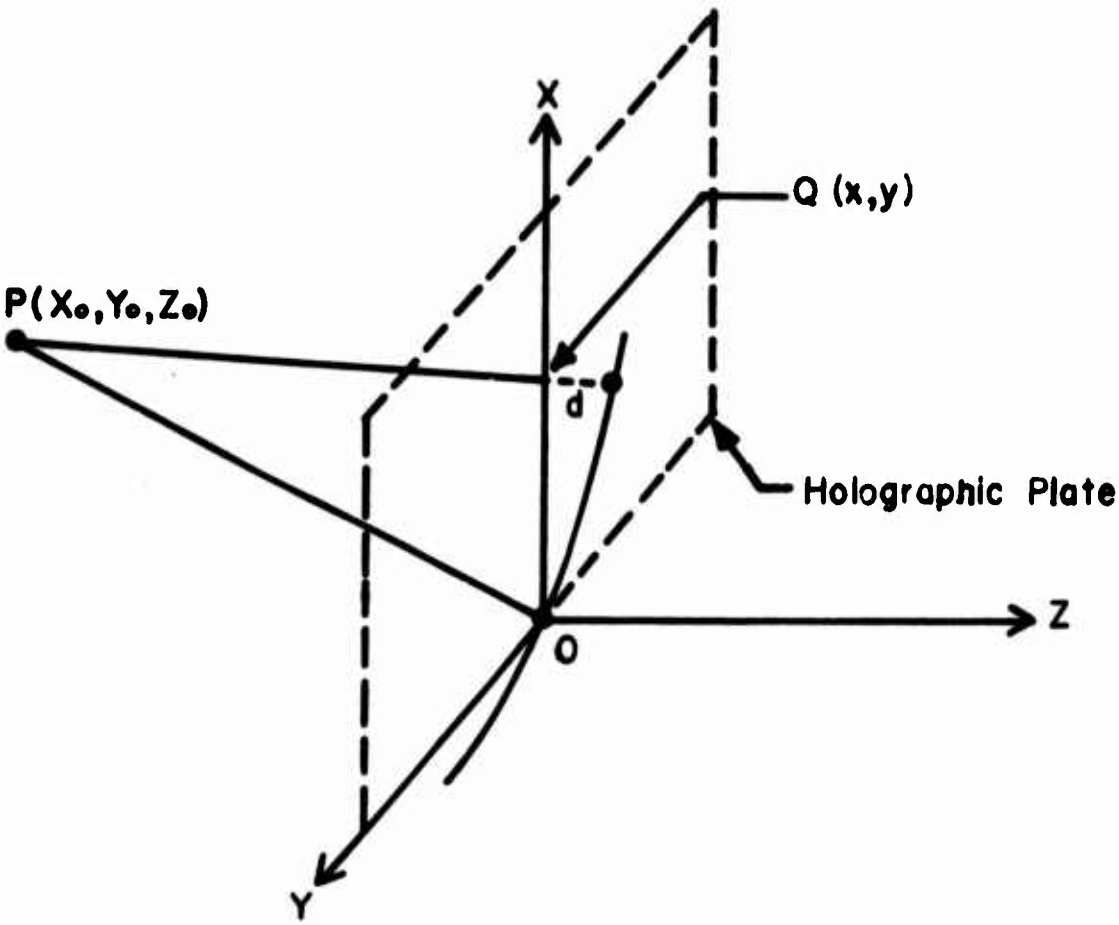

Figure 18. Coordinate System of Holographic System

$$+8xyx_o y_o - 4xx_o^3 - 4yy_o^3 - 4xx_o y_o^2 - 4yx_o^2 y_o)\Big] \qquad (75)$$

having neglected higher order terms. A similar expression holds for the phase of point source, r, at λ_o, and for the reconstruction point source, c at λ_c.

1. FIRST ORDER THEORY

To first order, the phase of the primary wave, V_1, is:

$$\phi_V^1 = \frac{2\pi}{\lambda_c}\,\frac{1}{2z_c}(x^2 + y^2 - 2xx_c - 2yy_c)$$

$$+ \frac{2\pi}{\lambda_o}\,\frac{1}{2z_o}(x'^2 + y'^2 - 2x'x_o - 2y'y_o)$$

$$- \frac{2\pi}{\lambda_o}\,\frac{1}{2z_r}(x'^2 + y'^2 - 2x'x_r - 2y'y_r) \qquad (76)$$

where primed coordinates refer to holographic parameters during the recording portion, and unprimed coordinates refer to holographic parameters during reconstruction. This allows for any scaling of the holographic grating by an amount, m, where,

$$x = m\,x'$$

$$y = m\,y' \qquad (77)$$

Define the wavelength ratio $\mu = \lambda_c / \lambda_o$, then substitute μ and m into 76 to yield,

$$\phi_V^1 = \frac{\pi}{\lambda_c}\left[(x^2+y^2)\left(\frac{1}{z_c}+\frac{\mu}{m^2 z_o}-\frac{\mu}{m^2 z_r}\right)-(2x)\left(\frac{x_c}{z_c}+\frac{\mu x_o}{m z_o}-\frac{\mu x_r}{m z_r}\right)\right.$$
$$\left.-(2y)\left(\frac{y_c}{z_c}+\frac{\mu y_o}{m z_o}-\frac{\mu y_r}{m z_r}\right)\right]. \qquad (78)$$

Let us now consider equation 78 as representing the first order term of a new sphere, the Gaussian reference sphere,

$$\phi_V^1 = \frac{\pi}{\lambda_c}\left(\frac{x^2+y^2-2xa_V-2b_V}{Z_V}\right). \qquad (79)$$

where, Z_V is its radius and a_V and b_V are the off-axis coordinates of its center. Solving from equation 78, we find that:

$$Z_V = \frac{m^2 z_c z_o z_r}{m^2 z_o z_r + \mu z_c z_r - \mu z_c z_o} \qquad (80)$$

$$a_V = \frac{m^2 x_c z_o z_r + \mu m x_o z_c z_r - \mu m x_r z_c z_o}{m^2 z_o z_r + \mu z_c z_r - \mu z_c z_o} \qquad (81)$$

$$b_V = \frac{m^2 y_c z_o z_r + \mu m y_o z_c z_r - \mu m y_r z_c z_o}{m^2 z_o z_r + \mu z_c z_r - \mu z_c z_o}. \qquad (82)$$

The expressions for the conjugate image, Z_R, may be obtained by changing the signs of Z_o and Z_r. Either of the two images may be real or virtual depending upon the sign of Z_R and Z_V, a negative sign meaning a virtual image.

To calculate the angular magnification, we choose Z_o as the distance from which the object is seen and Z_V or Z_R as the image viewing distance for mathematical convenience. The angular magnification for both images is given by:

$$M_{ang} = \frac{d(a/Z)}{d(x_o/z_o)} \tag{83}$$

$$M_{ang} = \mu/m \tag{84}$$

The lateral magnification for both images is given by:

$$M_{lat} = da/ax_o \tag{85}$$

where

$$M_{V\ lat} = \frac{m}{1 + (m^2 z_o/\ \mu z_c) - (z_o/z_r)} \tag{86}$$

$$M_{R\ lat} = \frac{m}{1 - (m^2 z_o/\ \mu z_c) - (z_o/z_r)} \tag{87}$$

The longitudinal magnification is calculated by:

$$M_{long} = dz_R\ /\ dz_o = -\frac{1}{\mu} M_{lat}^2 \tag{88}$$

The depth of focus of the holographic lens is given by:

$$\Delta Z = \pm(\Delta a/\tan \alpha_o)(\frac{1}{\mu}\ M_{lat}) \tag{89}$$

where Δa is the diameter of the tolerable circle of confusion, and α_o is the relative aperture on the object side.

2. THIRD ORDER THEORY

The third order components of the phase of the Gaussian reference sphere are given by,

$$\phi^3 = \frac{2\pi}{\lambda_C}\left[-\frac{1}{8Z^3}(x^4 + y^4 + 2x^2y^2 - 4x^3a - 4y^3b - 4xy^2a - 4x^2yb + 6x^2a^2 + 6y^2b^2 + 2x^2b^2 + 2y^2a^2 + 8xyab - 4xa^3 - 4yb^3 - 4xab^2 - 4ya^2b)\right] \quad (90)$$

Equation 90 was obtained by replacing the radius and off-axis coordinates in equation75 by those corresponding to the reference sphere. The third-order term in the true wavefront is the sum of ϕ_o, ϕ_r, and ϕ_c according to equation 71. After performing the summation required, we may sort the resulting terms into characteristic aberrations in the same manner as lens aberrations.

$$W = \frac{2\pi}{\lambda_C}\left[-\frac{1}{8}\rho^4 S \right. \quad \text{spherical}$$

$$\left. + \frac{1}{2}\rho^3(\cos\theta\, C_x + \sin\theta\, C_y) \right. \quad \text{coma}$$

$$-\frac{1}{2}\rho^2(\cos^2\theta\, A_x + \sin^2\theta\, A_y + 2\cos\theta\sin\theta\, A_xA_y) \quad \text{astigmatism}$$

$$-\frac{1}{4}\rho^2 F \quad \text{field curvature}$$

$$+\frac{1}{2}\rho\,(\cos\theta\, D_x + \sin\theta\, D_y) \quad \text{distortion} \qquad (91)$$

where we have defined

$$\rho^2 = x^2 + y^2$$
$$x = \rho\cos\theta \qquad (92)$$
$$y = \rho\sin\theta$$

For the conjugate image, we have

$$S_R = \frac{\mu}{m^4}\left[\left(\frac{\mu^2}{m^2}-1\right)\left(\frac{1}{z_o^3}-\frac{1}{z_r^3}\right)-\left(\frac{3\mu}{z_c}\right)\left(\frac{1}{z_o^2}+\frac{1}{z_r^2}\right)\right.$$
$$\left.+3\left(\frac{m^2}{z_c^2}-\frac{\mu}{m^2z_oz_r}\right)\left(\frac{1}{z_o}-\frac{1}{z_r}\right)+6\left(\frac{\mu}{z_oz_rz_c}\right)\right]. \qquad (93)$$

$$C_{Rx} = \frac{\mu}{mz_c^2}\left[\left(\frac{x_o}{z_o}-\frac{x_r}{z_r}\right)\right]-\frac{\mu}{m^3z_o^2}\left[\frac{x_o}{z_o}\left(1-\frac{\mu^2}{m^2}\right)+\frac{\mu\, x_c}{mz_c}\right.$$
$$\left.+\frac{\mu^2x_r}{m^2z_r}\right]+\frac{\mu}{m^3z_r^2}\left[\frac{x_r}{z_r}\left(1-\frac{\mu^2}{m^2}\right)-\frac{\mu\, x_c}{mz_c}+\frac{\mu^2x_o}{m^2z_o}\right]$$
$$+\frac{2\mu}{m^2}\left[\left(\frac{x_c}{z_c}-\frac{\mu x_o}{z_o}+\frac{\mu\, x_r}{m\, z_r}\right)\left(\frac{1}{z_oz_c}-\frac{1}{z_cz_r}+\frac{\mu}{m^2z_oz_r}\right)\right]. \qquad (94)$$

$$A_{Rx} = \frac{\mu x_c^2}{m^2 z_c^2}\left[\left(\frac{1}{z_o} - \frac{1}{z_r}\right)\right] - \frac{\mu x_o^2}{m^2 z_o^2}\left[\frac{1}{z_o}\left(1 - \frac{\mu^2}{m^2}\right) + \frac{\mu}{z_c} + \frac{\mu^2}{m^2 z_r}\right]$$

$$+ \frac{\mu x_r^2}{m^2 z_r^2}\left[\frac{1}{z_r}\left(1 - \frac{\mu^2}{m^2}\right) - \frac{\mu}{z_c} + \frac{\mu^2}{m^2 z_o}\right]$$

$$+ 2\frac{\mu}{m}\left[\left(\frac{1}{z_c} - \frac{\mu}{m^2 z_o} + \frac{\mu}{m^2 z_r}\right)\left(\frac{x_o x_c}{z_o z_c} - \frac{x_c x_r}{z_c z_r} + \frac{\mu x_o x_r}{m z_o z_r}\right)\right] \qquad (95)$$

$$F_R = A_x + A_y \qquad (96)$$

$$D_{Rx} = \frac{\mu}{m}\left[\left(\frac{\mu^2}{m^2} - 1\right)\left(\frac{x_o^3}{z_o^3} - \frac{x_r^3}{z_r^3} + \frac{x_o y_o^2}{z_o^3}\right) + \frac{3x_o}{z_o}\left(\frac{x_c}{z_c} + \frac{\mu x_r}{m z_r}\right)^2\right.$$

$$\left. - \left(\frac{\mu}{m}\right)\frac{\left(3x_o^2 + y_o^2\right)}{z_o^2}\left(\frac{x_c}{z_c} + \frac{\mu}{m}\frac{x_r}{z_r}\right) - 3\frac{x_c x_r}{z_c z_r}\left(\frac{x_c}{z_c} + \frac{\mu x_r}{m z_r}\right)\right] \qquad (97)$$

For the particular holographic lenses that are discussed in this report, the aberration equations are less cumbersome. Note that for $Z_R = Z_c = \infty$:

$$S_V = \frac{\mu}{m^4 z_o^3}\left(1 - \frac{\mu^2}{m^2}\right) \qquad (98)$$

$$C_{Vx} = \frac{\mu}{m^3 z_o^2}\left[\frac{x_o}{z_o}\left(1-\frac{\mu^2}{m^2}\right) - \frac{\mu}{m}\tan\alpha_c + \frac{\mu^2}{m^2}\tan\alpha_r\right] \tag{99}$$

$$C_{Vy} = 0 \tag{100}$$

$$A_{Vx} = -\frac{\mu}{m^2 z_o}\left[\frac{x_o^2}{z_o^2}\left(\frac{\mu^2}{m^2}-1\right) + \left(\tan\alpha_c - \frac{\mu}{m}\tan\alpha_r\right)^2 + 2\frac{\mu x_o}{m z_o}\left(\tan\alpha_c - \frac{\mu}{m}\tan\alpha_r\right)\right] \tag{101}$$

$$A_{Vy} = 0 \tag{102}$$

$$F_V = A_x \tag{103}$$

$$D_{Vx} = -\frac{\mu}{m}\left[\left(\frac{x_o^3}{z_o^3} - \tan^3\alpha_r\right)\left(1-\frac{\mu^2}{m^2}\right) + \left(\tan\alpha_c - \frac{\mu}{m}\tan\alpha_r\right)\cdot\left(-3\frac{x_o}{z_o}\tan\alpha_c + 3\frac{\mu x_o}{m z_o}\tan\alpha_r - \frac{\mu}{m}\frac{3x_o^2}{z_o^2} + 3\tan\alpha_c\tan\alpha_r\right)\right] \tag{104}$$

$$D_{Vy} = 0 \tag{105}$$

The corresponding expressions for the aberrations in the secondary image may be obtained by changing the sign of Z_o and Z_r (where $\tan\alpha_r = \frac{X_r}{Z_r}$, etc.).

SECTION III

EXPERIMENTAL ANALYSIS

A. COHERENCE LENGTH

Coherence requirements were satisfied by utilizing a spring-mounted, vibration isolated, enclosed table, and a long coherence length laser. The table used was a poured-in place, reinforced concrete, "U" cross section, platform. The dimensions are approximately four meters by two meters by one meter high. The top and wall thickness are approximately 0.2 meters and the weight is approximately 6,500 kilograms. The table is illustrated in figure 19. An enclosed wood frame structure is set on the table for air stability on the table's surface. The enclosure has sliding doors to provide access to the experimental area. The platform is supported by eight Barry spring isolation mounts which give the platform a natural frequency of approximately three Hertz. The laser used to expose the holograms was a Spectra-Physics Model 165 argon ion laser with a coherence extender consisting of an intra-cavity etalon. The laser head was mounted on the platform but outside the wood enclosure so that any thermal air currents generated by the laser head would not disturb the experimental area. The laser power supply was mounted off the platform to minimize vibration in the experimental area. All parts of the experimental set-up were locked to the platform and tested for stability.

The coherence length of the laser as described above was found to be in excess of ten meters. This was determined by setting up a Michelson-type interferometer and varying the path length of one of its arms. Fringe contrast was found to be visually undiminished when the path length difference was ten meters. As the path length difference in the experiment was not expected to exceed one meter, this was sufficient testing. A similar experiment was used to test the stability of the experimental set-up. This consisted of using the experimental set-up with a relatively small interference angle and projecting the produced fringes on a screen so that they may be visually observed. The fringes were found to drift, but at a rate slow enough such that exposure times in excess of five minutes would still have excellent contrast. Since exposure times of one or two minutes were expected, this was sufficient and no attempt was made to isolate or eliminate this long term instability.

B. EXPERIMENTAL SET-UP

The recording geometry was set-up as illustrated in figure 20. The laser beam was reflected from the laser off mirrors M_1 and M_2 to allow the beam to diverge to a size sufficient to fill the collimater objective L_3. Beam splitter "B.S." divided the beam into two parts. The transmitted beam reflected off mirror M_3 and was directed through the 50 mm focal length lens L_1. This lens focused the beam through a pinhole spatial filter S_1 which removed most of the high spatial frequency noise. The clean diverging beam coming from S_1 is then collimated by lens L_3 which is a 0.15 meter diameter and 1.5 meter focal length astronomical objective. The resultant collimated beam was of excellent uniformity. The reflected beam from "B.S." was directed by means of mirrors M_4 and M_5 through lens L_2 and spatial filter S_2 to emerge as a clean diverging beam. The recording plate was mounted

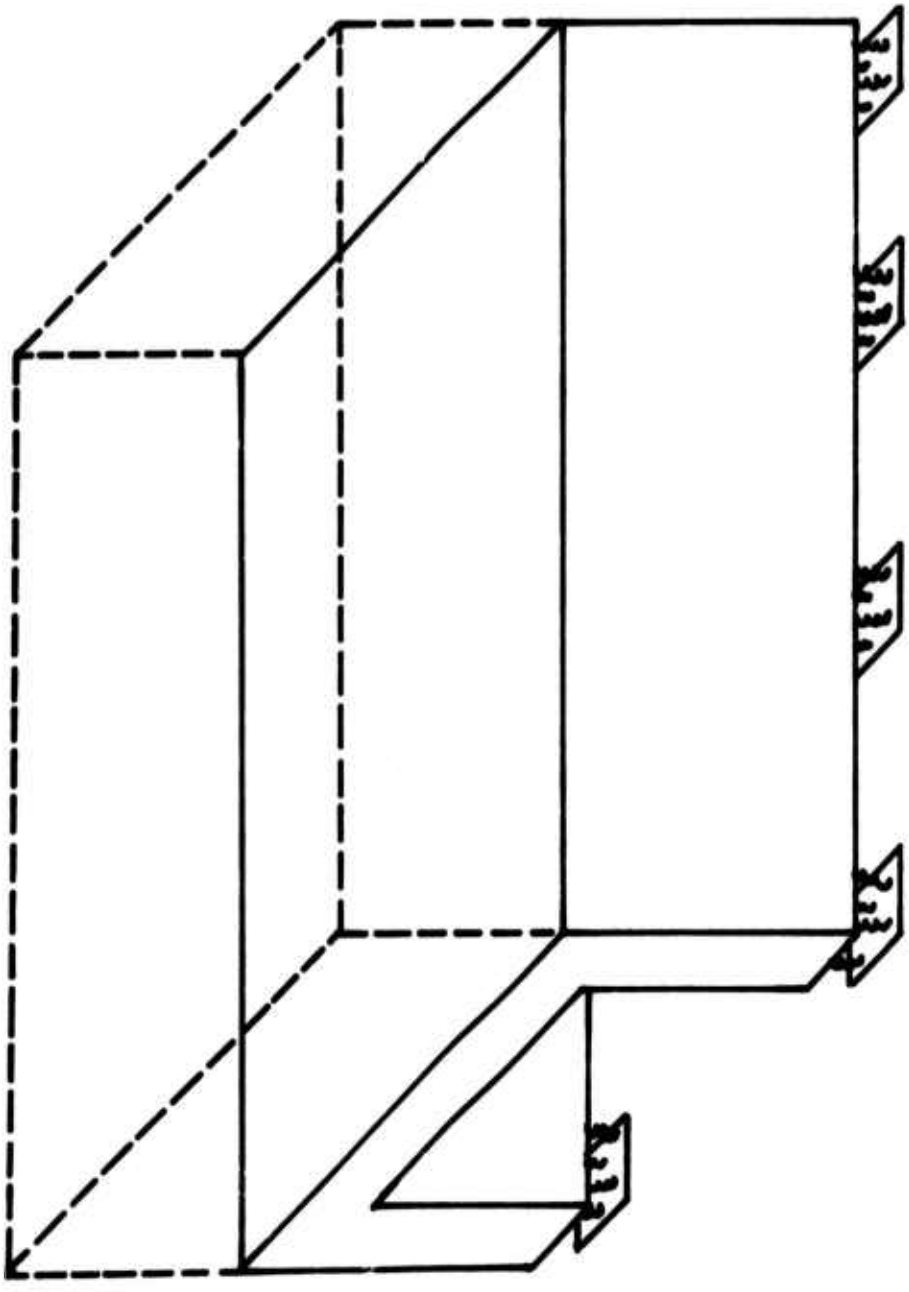

Figure 19. Table and Enclosure

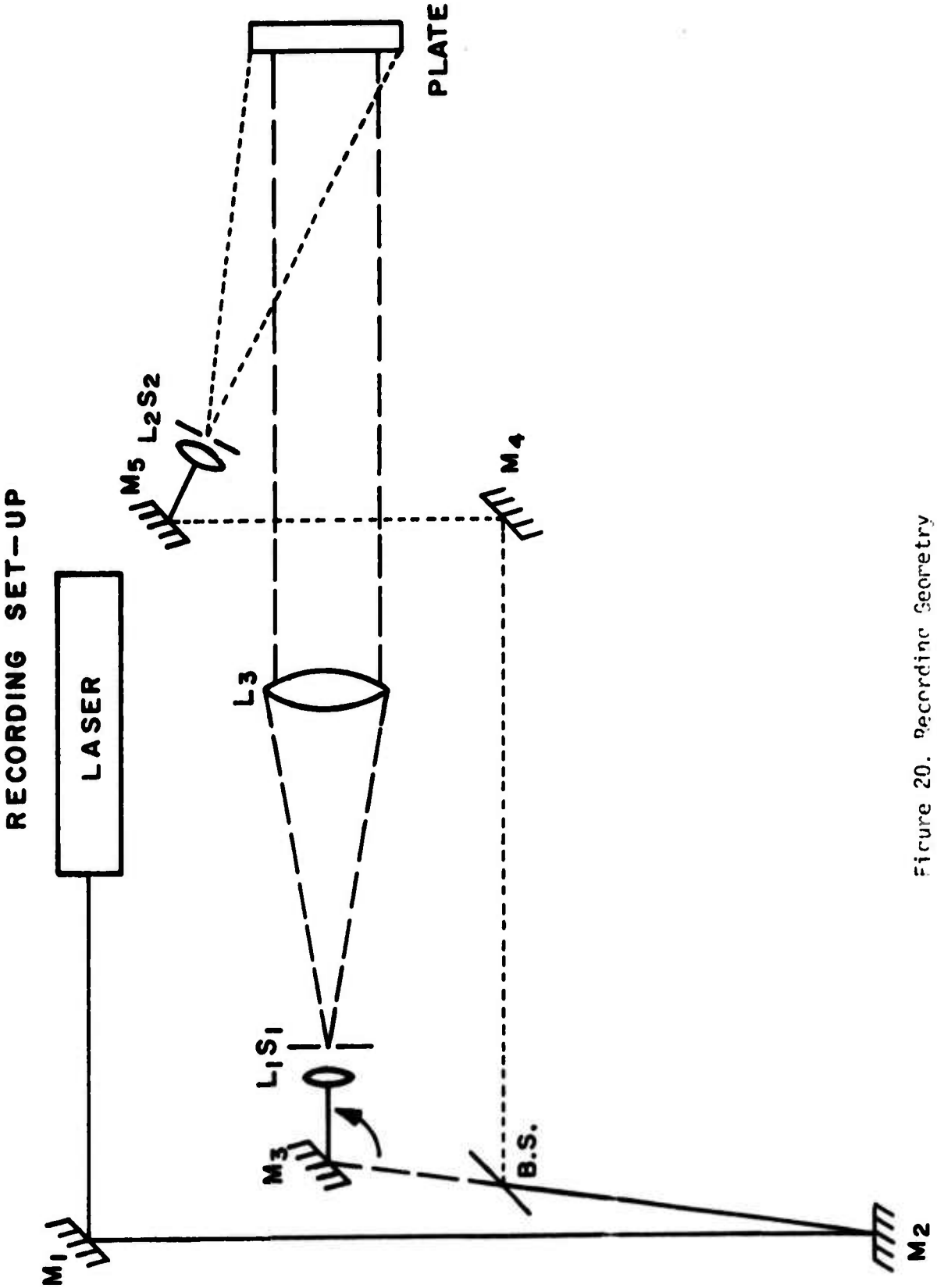

Figure 20. Recording Geometry

on a rotary table so that the angle of incidence of the collimated beam could be varied to any angle. The mirrors M_4 and M_5 as well as lens L_2 and spatial filter S_2 could be moved to any position such that the angle of incidence of the diverging beam could also be varied independently.

In figure 21 are some of the experimental beam configurations used. Figure 21(a) illustrates an interference angle at the plate center of 60° with the emulsion normal parallel to the collimated beam. Figure 21(b) has an interference angle of 30° with the plate normal parallel to the collimated beam. Figure 21(c) has a 30° interference angle with the plate normal bisecting the two beams. Figure 21(d) has a 90° interference angle with the plate normal bisecting the two beams. Experiments were run with all of these configurations with results indicating that highest diffraction efficiencies are obtained with 30° interference angles while the most uniform plates were those in which the plate normal bisected the angle of interference. The latter effect was expected since the fringes are parallel to the emulsion normal and are unaffected by swelling or shrinking. The smaller interference angles lead to larger fringe spacings and correspondingly less stringent requirements on resolution capability of the recording medium.

With this recording set-up and the laser described above, the power density of the recording plate could be varied from 10^{-3} to 3×10^{-1} milliwatts/cm^2. This was accomplished by manipulating the power of the laser, the position of variable beam splitter B.S. or by changing the focal length and hence the divergence of lens L_2.

Before any exposures were made the recording set-up was checked by visual observation and/or test exposure of a conventional silver halide plate to determine whether there were any stray reflections or other undesired light sources which could expose the experimental plate. These light sources could usually be eliminated by appropriate aperturing of the laser beams or by shielding the experimental plate. Ten minutes before exposures, the air handling unit was deactivated in the laboratory so that air motion would be minimized during exposures.

C. MATERIALS EVALUATION

The choice of the materials to be used in the final display was limited by the system requirement of simultaneous two eye viewing. To allow for some head motion the diameter of the display grating should be at least 0.15 meters. This requirement eliminated photo-chromics and other exotic materials since they were not commercially available in the quantity and format required for experimentation.

1. BLEACHED SILVER HALIDE

Although several techniques were tried no satisfactory bleached holograms could be produced. Diffraction efficiencies in excess of 50% were obtained using the bleach procedures described in appendix A. Unfortunately the resultant processed plates were extremely non-uniform in efficiency and were milky in appearance. Diffraction efficiency tended to degrade with time. This was remedied by sealing the processed plate under a cover glass, partially verifying the effects noted in reference 15. The processing procedure noted in reference 17 appears to combine the sensitivity of silver-halides

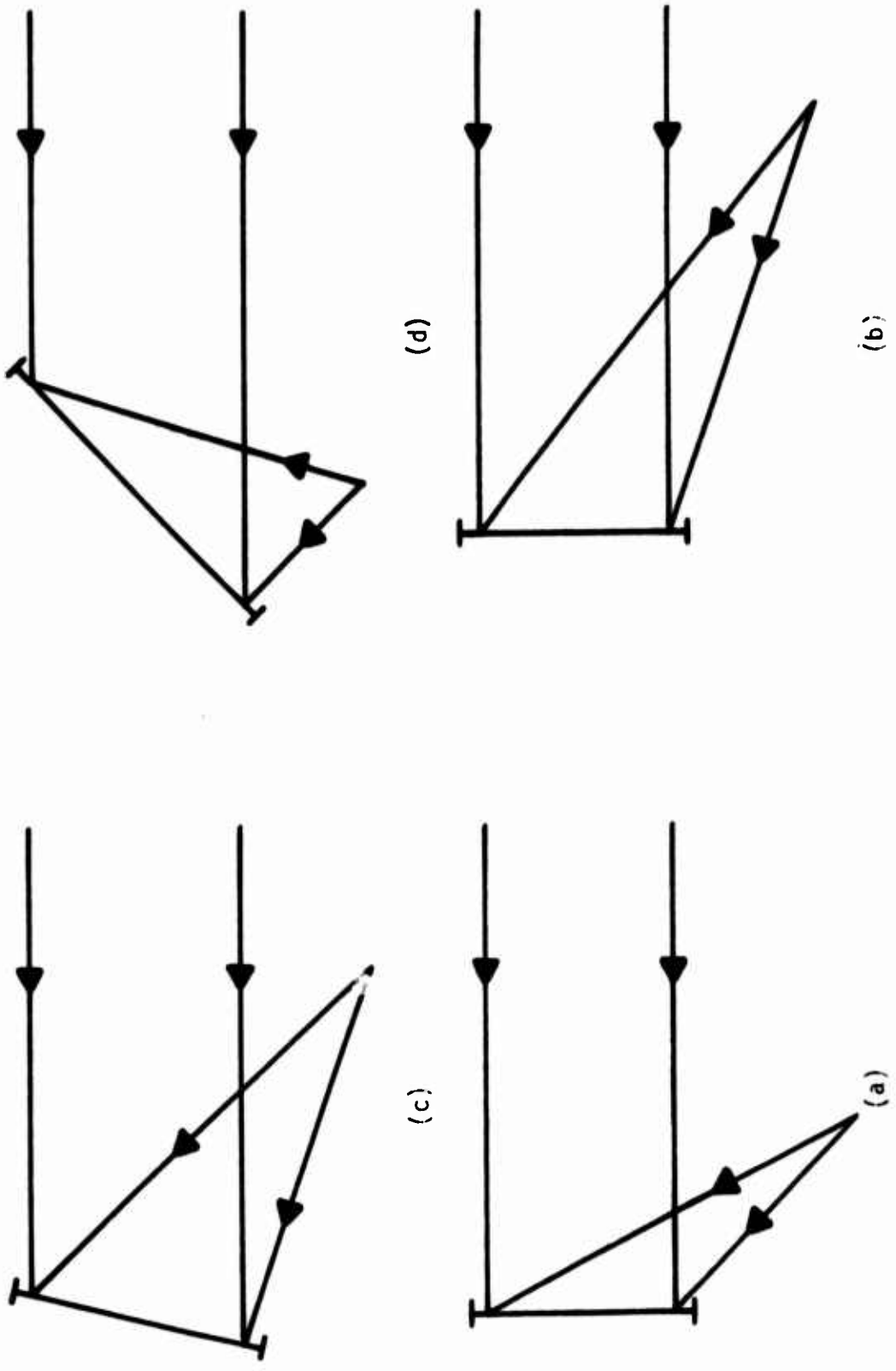

Figure 21. Experimental Beam-Plate Configurations

with the quality of the dichromate process but it required a successful bleaching procedure as a first step. This procedure is listed in appendix A also for future consideration. Other bleaching techniques offer less hope for success than those attempted, some because of complexity, resultant non-clear plate, or scattering noise, and others due to inherent faults for this application. Fortunately, the investigations into the properties of bleached silver halide emulsions were good preparation for the work to follow on dichromated gelatins.

2. PHOTOPOLYMERS

A requirement imposed by the power of the laser used was that the material be capable of being exposed by power densities of 0.3 milliwatts/cm^2. Although more than 500 mw were available at 488.0 nm from the laser the efficiency of the recording system was such that a power density of 0.3 mw/cm^2 was the maximum obtainable.

The only photopolymer obtained was a sample of an experimental photopolymer material prepared by B. L. Booth of E.I. duPont deNemours and Company. This photopolymer had a threshold power density of >0.5 mw/cm^2. Although this material could not be used in the holographic recording system, as arranged for the final display, it was tested using a different recording system which was capable of 15 mw/cm^2. The instructions indicated a relatively short shelf life and heeding this the samples were exposed within a few days of receipt. The resultant gratings were of 40-50% diffraction efficiency when the exposure instructions were followed.

The problems associated with the testing of this material were low sensitivity and small field angle. The latter was due to the formed grating being fairly thick which limited the available acceptance angle range to less than 1°. As these materials become more commercially available they might be applied to other holographic optical element applications. They are extremely easy to expose and processing is negligible.

3. DICHROMATES

After much trial and error experimentation based on the dichromate sensitization and processing procedures described in appendix A the following procedures were developed for Eastman Kodak 649-F plates on glass 200 x 250 x 6mm thick.

a.	Fix	Kodak Rapid Fixer w/hardener 68°F	10 minutes
b.	Wash	Filtered Running Water 68°F	20 minutes
c.	Wash	Methanol Room Temp	10 minutes
d.	Wash	Fresh Methanol Room Temp	5 minutes

e.	Sensitize	4.5% solution Ammonium Dichromate in water	10 minutes
f.	Dry	Blot edge and dry with plate tilted ~ 10° from horizontal emulsion up, room temp & 45-80% R.H.	Overnight
g.	Clean	Wipe excess dried crystals from glass side of plate	
h.	Expose	Glass side toward exposing light 488 nm, 200-300 microwatts/cm^2	120 seconds
i.	Wait		2-3 hours
j.	Wash	Running filtered water 68°F until yellow tint is gone	5-10 minutes
k.	Soak	50/50 Isopropanol and water 40°F	2 minutes
l.	Soak	90/10 Isopropanol and water 40°F	2 minutes
m.	Soak	Isopropanol 40°F	15 minutes
n.	Dry	Closed cycle air circulation with desiccant in line	30-60 minutes
o.	Seal	Cover glass with epoxy around edges.	

The reasoning and experimental conclusions leading to this processing procedure are as follows:

Step (a). Several attempts to coat gelatin on clean glass plates were made. The results were poor non-uniform coatings. Since there was no reason not to use commercially available flat plates this procedure was followed. This step removed the silver halide from the 649-F emulsion and partially hardened the gelatin.

Step (b). This wash removed the fixer.

Steps (c,d). These steps removed the sensitizing dye from the emulsion and left a clear gelatin.

Step (e). After sensitizing plates with various concentrations of ammonium dichromate it was found that 4.5% concentration was the best trade-off between sensitivity of the sensitized plate and

opacity or cloudiness in the processed plate. Concentrations of 1% to 10% were prepared and exposed to reach this conclusion.

Step (f). Due to the relatively high humidity present in our laboratory the plates required overnight to dry.

Step (g). Excess crystals were cleaned off the glass side of the plate by wiping them with a soapy towel then a water-soaked towel and finally dry towels.

Step (h). It was found that the total exposure could be varied from 10 to 60 millijoules/cm^2 without significant change in diffraction efficiency. An exposure of 30 millijoules/cm^2 was used for the final display plate. The glass side toward the exposing light minimized multiple reflection effects.

Step (i). It was found that a waiting time of two to twelve hours between exposure and processing gave the best and most consistent diffraction efficiencies.

Step (j). After washing the plates five minutes the lights were turned on and the wash continued until the yellow tint disappeared.

Steps (k,l,m). The successively high concentrations of chilled isopropanol soaks take the water out of the gelatin. It was found that room temperature or warmer isopropanol baths led to cloudy and non-uniform diffraction efficiency of plates.

Step (n). A closed cycle air circulation system was used with an indicating desiccant in the line to rapidly dry the processed plates. This system is shown schematically in figure 22. Other drying methods such as the method described in reference 2 as well as using dry air and dry nitrogen in an open cycle configuration did not give consistent results.

Step (o). A variety of sealing materials were used to seal a cover glass over the gelatin. Cyano-methyl acrylates such as Eastman 910 adhesive seemed to be the most promising but plates sealed in this manner deteriorated to low diffraction efficiency in four to six months. Cellulose acetate adhesive sealed plates did not completely cure and diffraction efficiency gradually deteriorated. The best and longest lasting sealing material was a two-part clear epoxy such as "EPOXI-PATCH" manufactured by Hysol Division of the Dexter Corporation. This material was mixed and applied around the perimeter of the cover glass. The dried plate was then quickly placed on the cover glass and left to set overnight.

After the processing procedure was optimized to that described above, two double exposure techniques were tried to find the best method of producing the two-channel display lens. The methods tried were:(1) sensitized plate was exposed then rotated 180° about emulsion normal and re-exposed and (2)

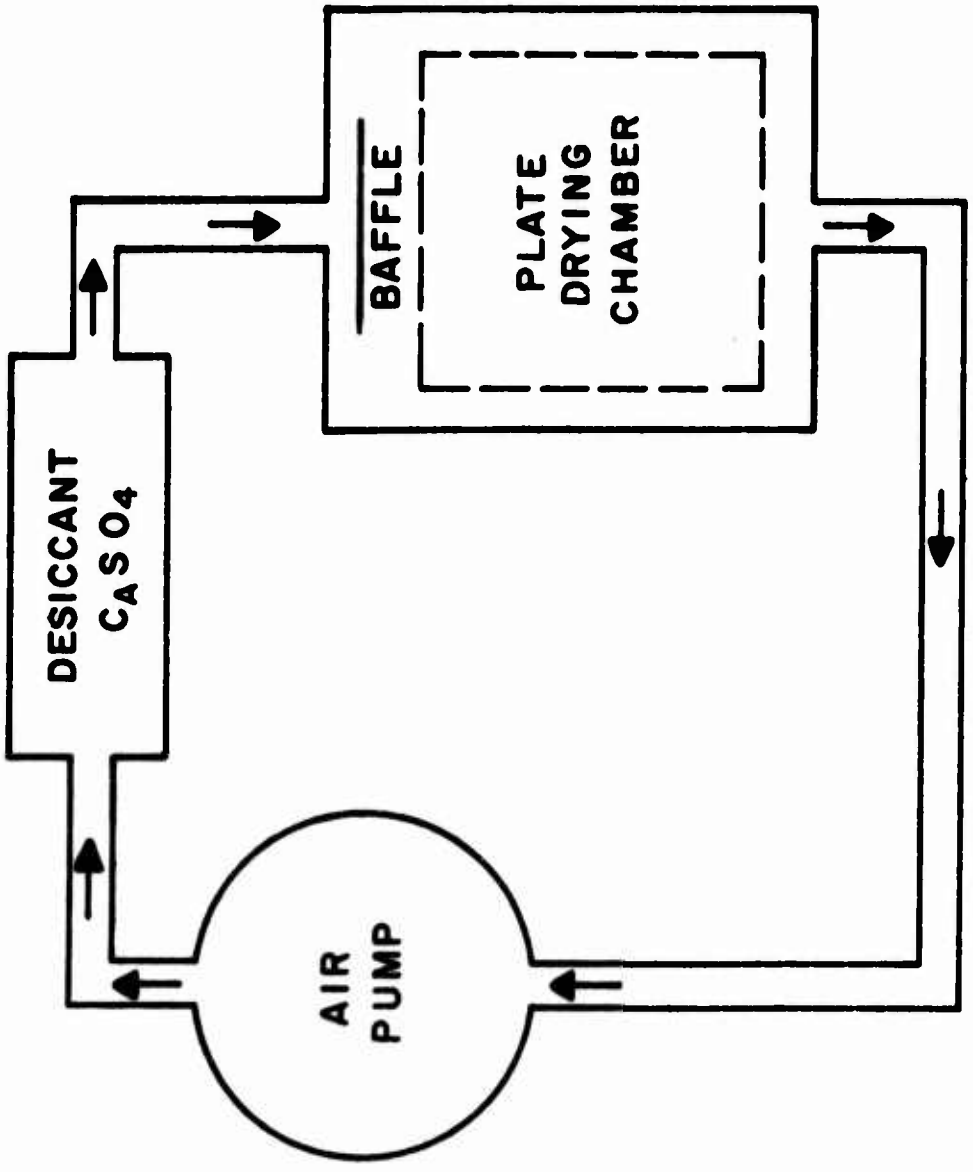

Figure 22. Plate Drying System

sensitized plate was exposed and processed through step (j) of the processing procedure. The plate was then resensitized by repeating steps (e), (f), and (g) and re-exposed with the plate rotated 180° and reprocessed by continuing through steps (i) to (o). It was found that there was significant differences in the results of these two methods. Method 1, usually yielded a plate in which the diffraction efficiency of the first exposure was much greater than that of the second exposure; e.g., 70% in first and 10% in second. The second method led to almost equal diffraction efficiencies e.g., 35% in first and 45% in second. The second method was used for the production of the display lens.

D. MULTIELEMENT LENS

Although the final display lens was chosen to operate as a two-channel system, each channel acting as a single hologram lens some investigations were directed toward the use of multielements to allow resolvable images in white light.[53] This technique essentially allows the first hologram lens to redirect, chromatically disperse and collimate the light from the white light illuminated object. The second hologram lens is located a finite distance away in the path of the light from the first lens. The second lens redirects the light into its original direction, and undisperses the chromatically dispersed light while retaining image collimation. The net result is that the observer sees a single color image whose color and apparent size varies as the observer's head moves vertically. This system can also be made multichannel by having individual first hologram lenses and a dual channel second hologram lens. The details of this type of system are described in reference 53.

E. THE COMPUTER PROGRAM AND ITS USES

A computer program was developed for the Wang Laboratories Model 720 programmable electronic desk calculator as an analytical tool in the design and evaluation of the holographic lenses discussed in this report. The program was based on equations derived in Section I and was used to calculate (1) the lateral position in a known plane of light rays after diffraction by the lens, (2) the first order portion of the diffracted wavefronts, (3) the third order portion of diffracted wavefronts (including the various aberrations), (4) ray slopes, and (5) wavefront error in the diffracted wavefronts. The program is listed in Appendix B. It proved to be a very useful tool in designing and analyzing the final holographic lens element.

1. FOCAL LENGTH [40,46]

The theoretical focal length of the holographic lens was calculated, using equation 80, for several different wavelengths. Then the actual focal length of the lens was measured experimentally in order to verify the theory. Figure23 illustrates the resulting comparison for one holographic lens. The theoretical focal length was within two percent of the experimental focal length at all wavelengths tested. Figure 24 illustrates the resulting comparison for another holographic lens. The theoretical focal length was within two percent of the experimental focal length in the red region of the spectrum but varied approximately twelve percent in the blue region. This greater variation in the blue region was attributed to emulsion swelling and the fact that the shorter focal length of this particular lens placed a greater strain on our rotationally symmetric approximation.

The amount of longitudinal chromatic aberration in both lenses can be estimated directly from figures 23 and 24. The theoretically predicted amount for the first lens (from 476.2 nm to 632.8 nm) was 120 mm and for the second lens was 91 mm. The experimentally measured amount for the first lens was 121 mm and for the second lens was 121 mm.

From the experimental verifications, we determined that the theoretical predictions for focal length could be used as an aid in designing the desired holographic lens element.

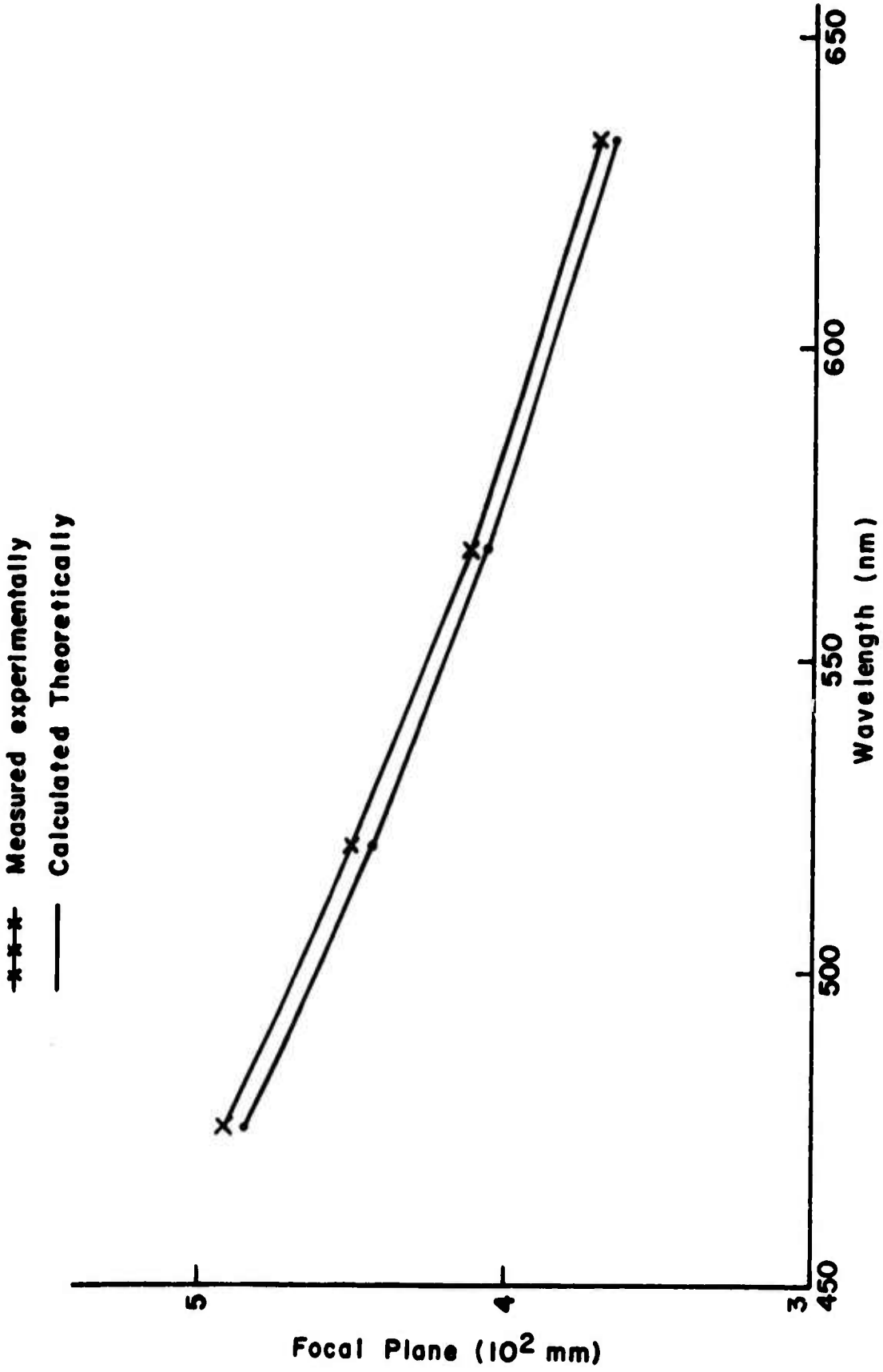

Figure 23. Comparison of Experimental to Theoretical Focal Lengths for Lens A

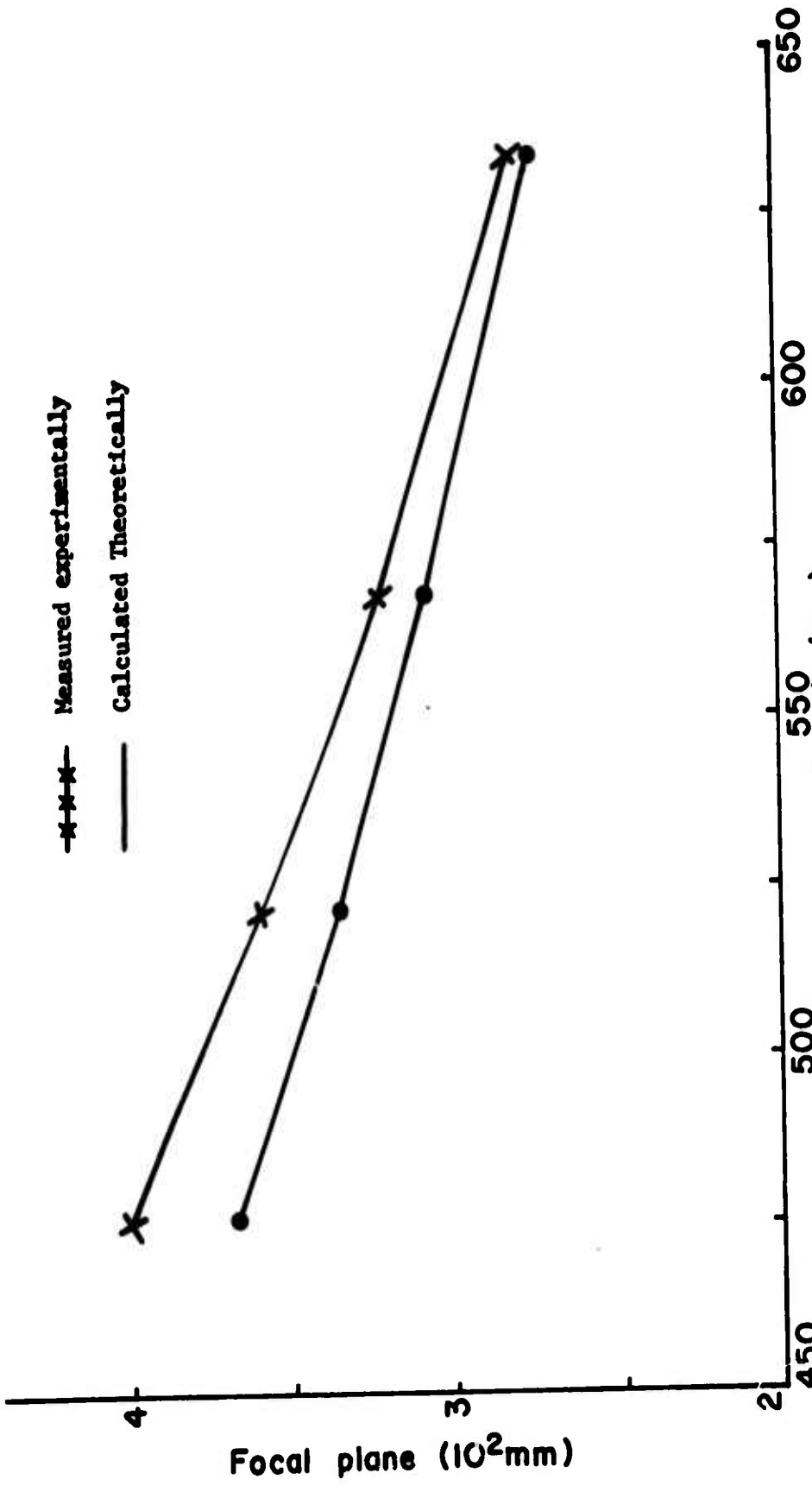

Figure 24. Comparison of Experimental to Theoretical Focal Lengths for Lens B

2. HARTMANN GRAPHS[60]

The direction of light rays after diffraction by the holographic lens was determined using equations 91,98 and 105 Theoretical meridional and skew ray fans were passed from an infinitely distant point object through the holographic element to the region of their intersection. Identical ray fans were experimentally passed through actual holographic lenses in order to verify the theory. Plots of the diffracted ray fans are given in figures 25 through 40 which illustrate the resulting comparisons for one exemplary holographic lens. The off-axis angle of the focal area in the experimental case varied considerably from the theoretical case. This difference is attributed to emulsion swelling in the experimental case and a breakdown of the rotationally symmetric approximation in the theoretical case. In lieu of this angular difference, much useful information can be obtained from the ray graphs concerning the holographic lenses; and it was determined that the computer program was of design value concerning these ray graphs.

a. Tangential Focal Length[50]

By comparing figure 25 with figure 33, the amount of difference between theoretically calculated and experimentally measured tangential focal length for lens c at λ = 476.2 nm may be obtained, e.g., Δf = 447 mm - 442 mm = 5 mm. And, similarly for figures 27,29,31,35,37,39 the focal lengths at other wavelengths may be calculated.

b. Sagittal Focal Length

By comparing figure 26 with figure 34, the amount of difference between theoretically calculated and experimentally measured sagittal focal length for lens C at λ = 476.2 nm may be obtained, e.g., Δf = 460 mm - 437 mm = 23 mm. And, similarly for figures 28,30,32,36,38,40, the focal lengths at other wavelengths may be calculated.

c. Spherical Aberration.

The amount of longitudinal spherical aberration in the sagittal plane can be estimated by measuring the distance from where the "marginal" ray crosses the reference ray axis to where a "paraxial" ray crosses the reference ray axis. From figure 26, the theoretical longitudinal spherical

aberration is 11 mm. From figure 34, the experimental longitudinal spherical aberration is 10 mm.

d. Coma.

The amount of coma can be judged by measuring the distance across the focal area in a direction perpendicular to the central reference ray. For example, from figure29 the theoretical coma in the meridional plane of lens C at λ = 568.2 nm is 2.5 mm. For comparison, the experimentally measured spot size for this wavelength and plane was 5 mm.

e. Astigmatism.

The amount of astigmatism in lens C at λ = 476.2 nm may be obtained by comparing the focal lengths in each pair of figures. From figures25 and 26 the amount of theoretically calculated astigmatism is 447 mm - 460 mm = -13 mm and from figures 33 and 34 the amount of experimentally measured astigmatism is 442 mm - 437 mm = +5 mm.

f. Chromatic Aberration.

An estimate of the amount of longitudinal chromatic aberration can be obtained by reading the focal lengths from selected figures and plotting them against wavelength. For example, figures 25,27,29,31 yield a theoretical chromatic aberration measure of 19 mm for the tangential focal plane.

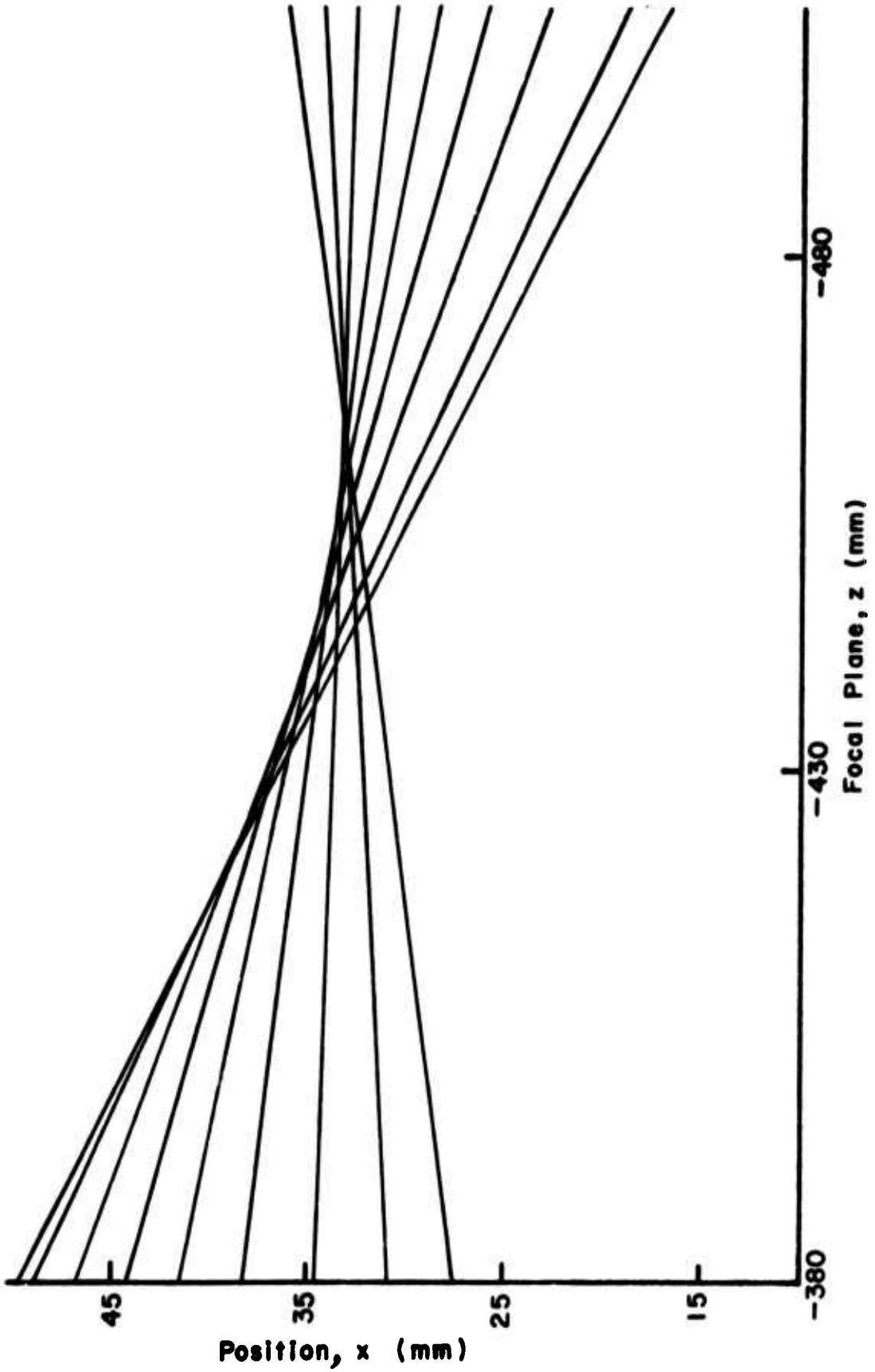

Figure 25. Theoretical Meridional Ray Fan Graph for Lens C at λ = 476.2 nm

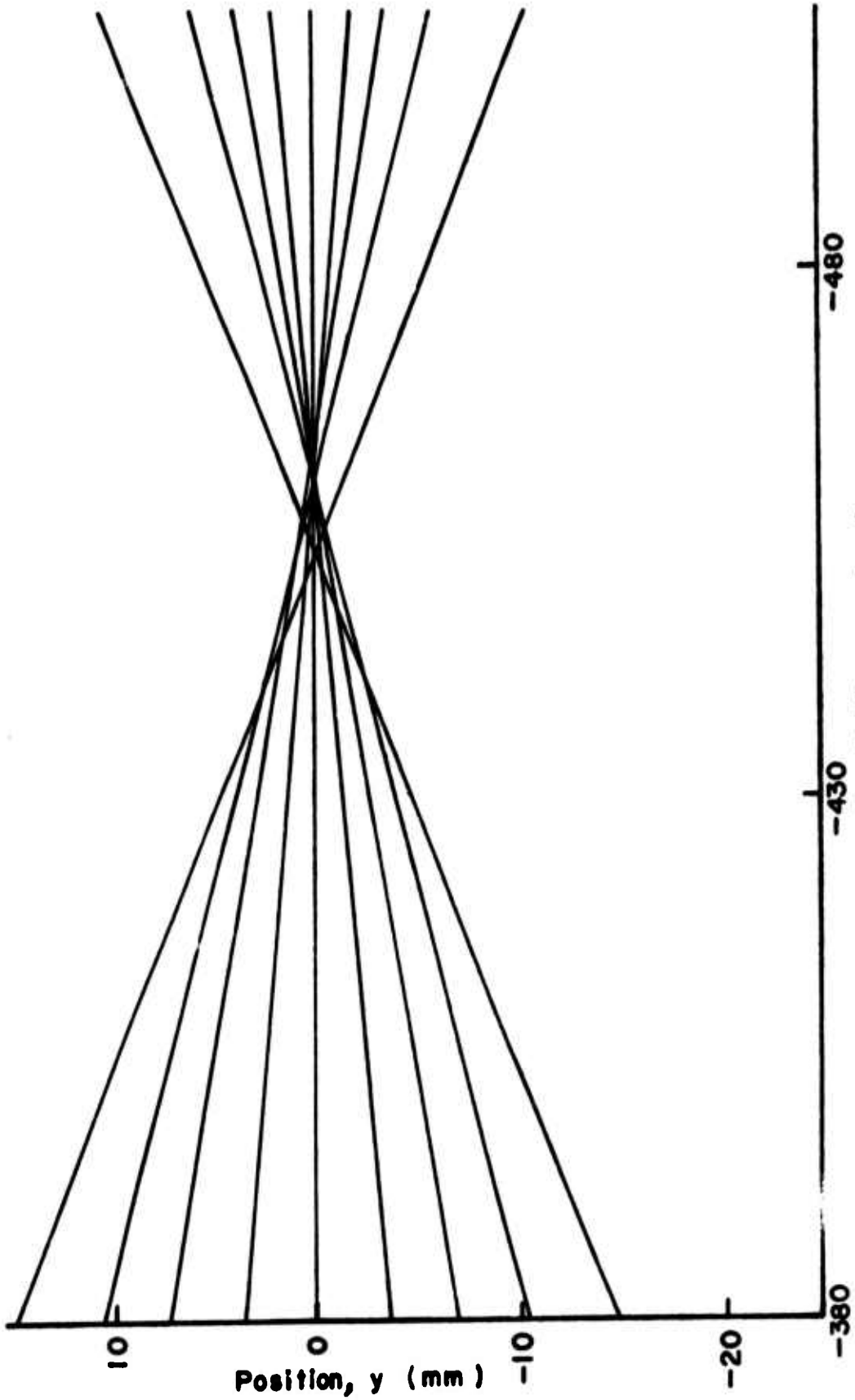

Figure 26. Theoretical Skew Ray Fan Graph for Lens C at λ = 476.2nm

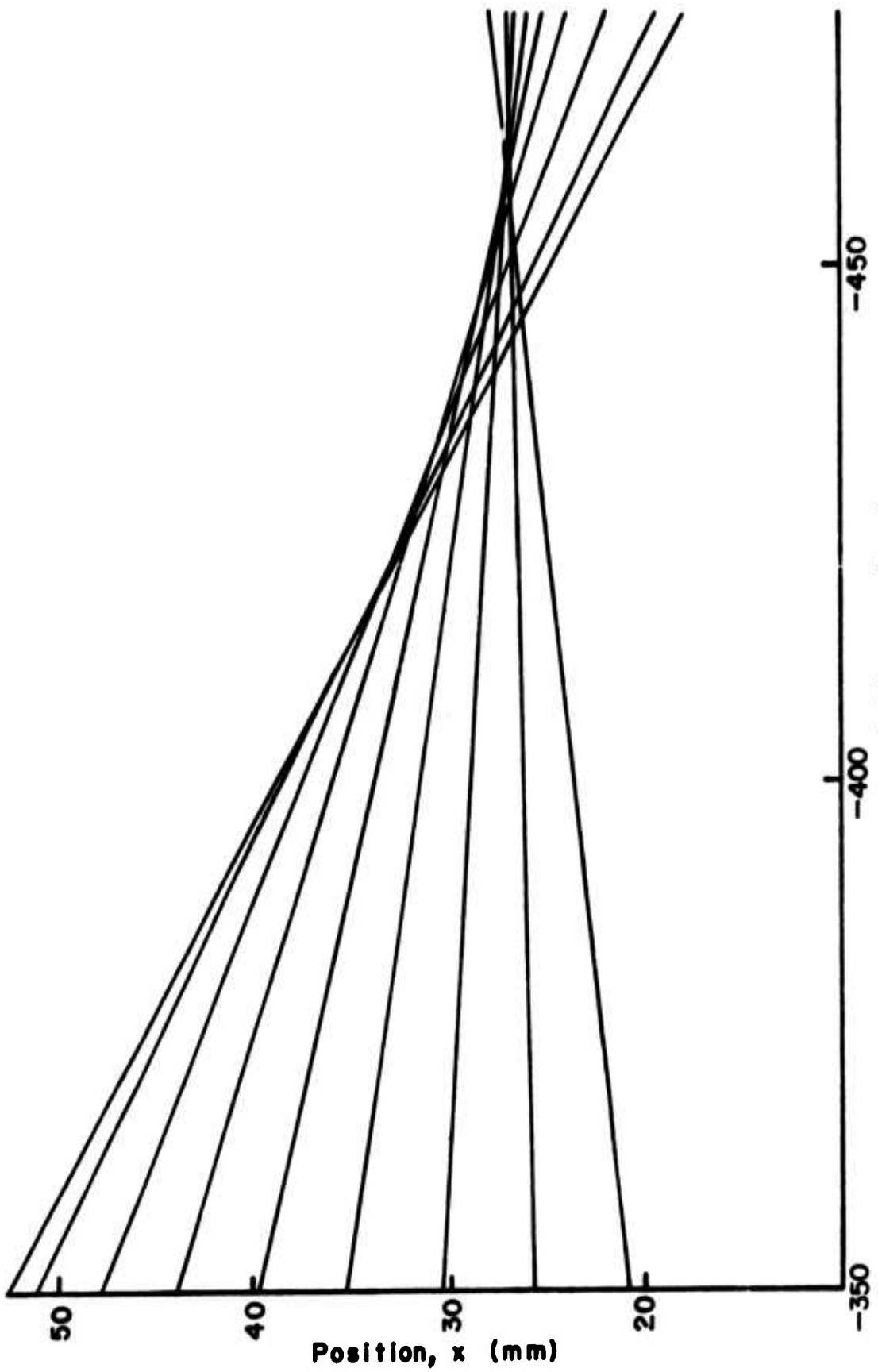

Figure 27. Theoretical Meridional Ray Fan Graph for Lens C at λ = 520.8 nm

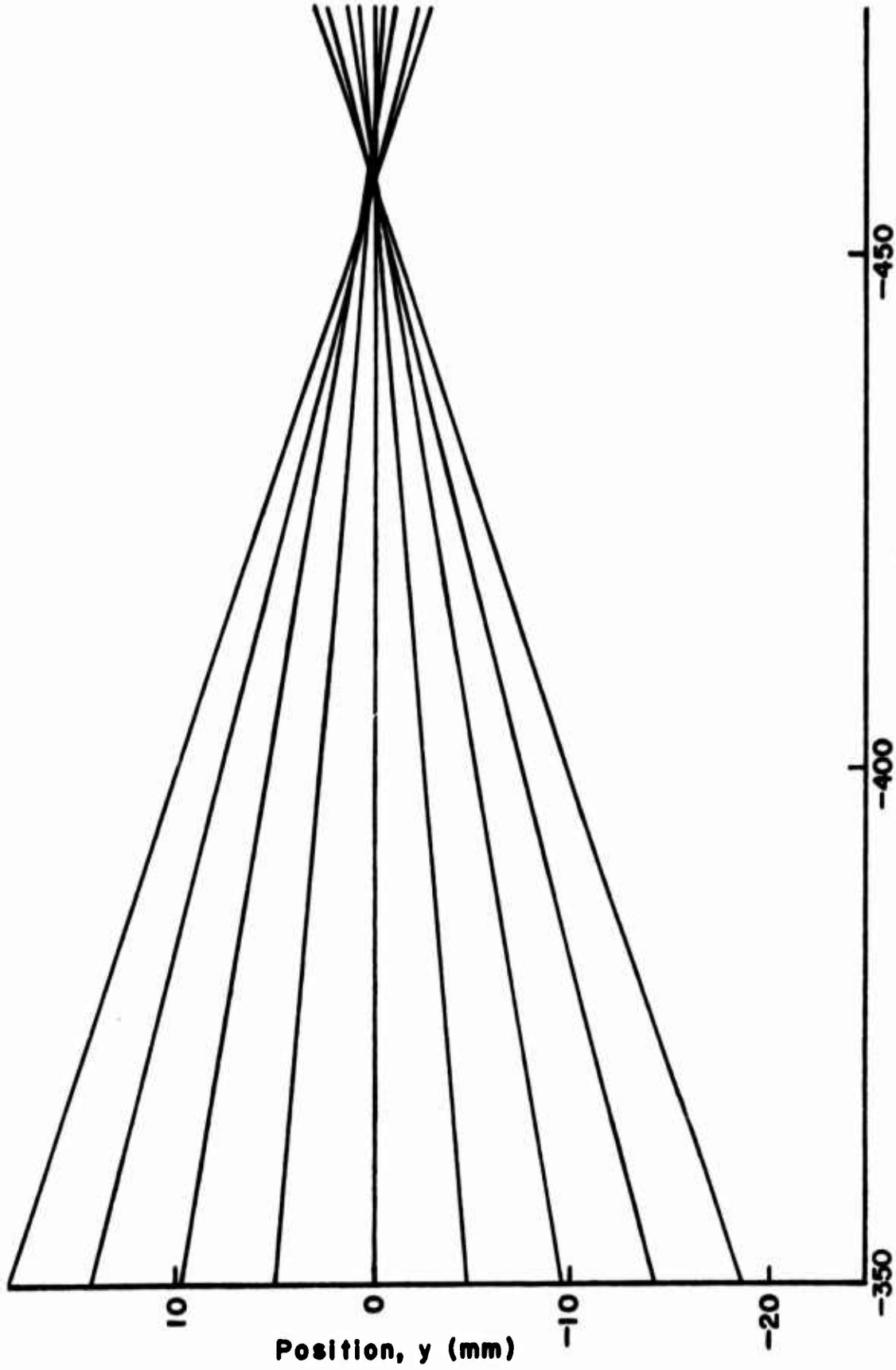

Figure 28. Theoretical Skew Ray Fan Graph for Lens C at λ = 520.8 nm

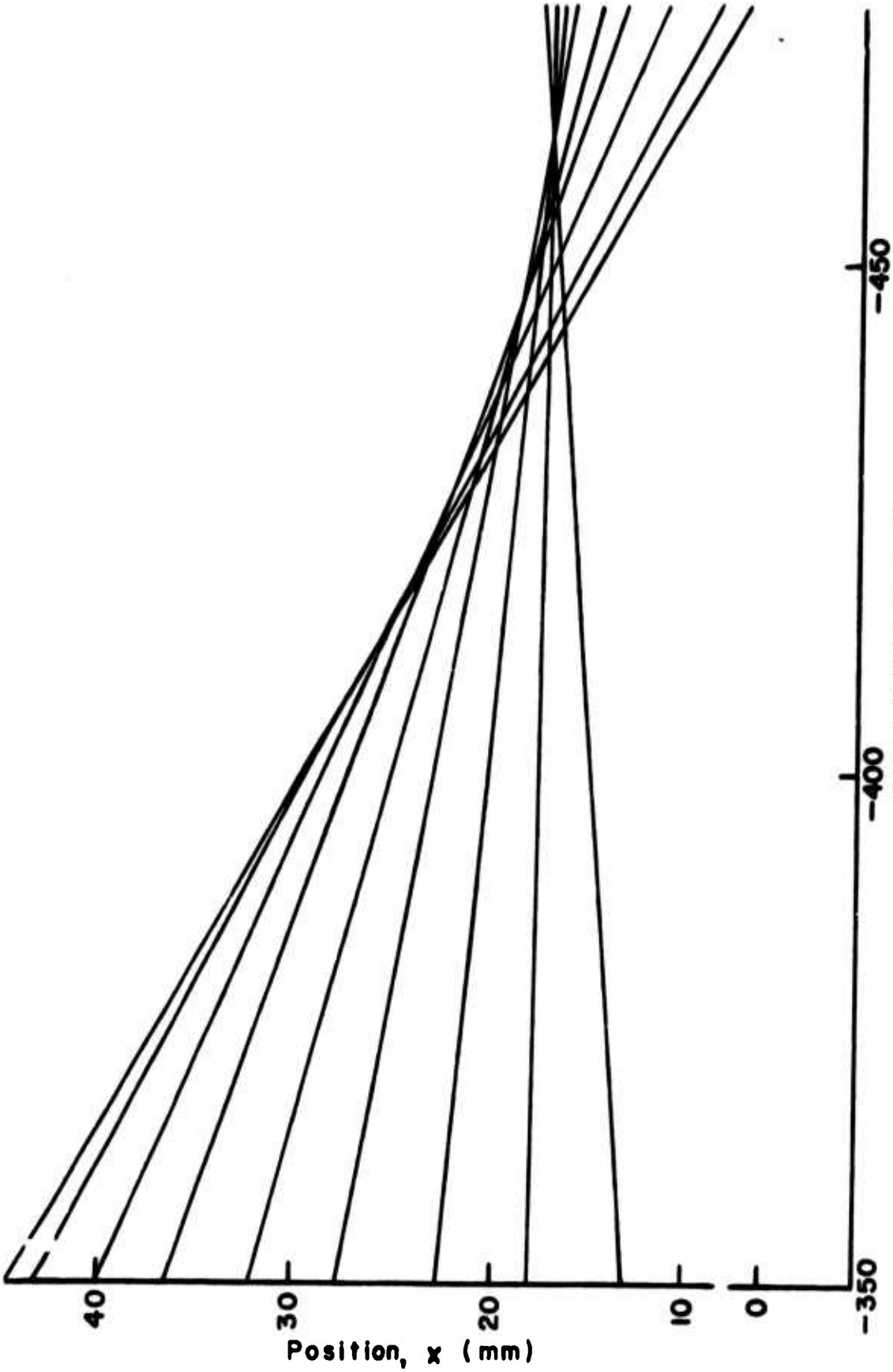

Figure 29. Theoretical Meridional Ray Fan Graph for Lens C at λ = 568.2 nm

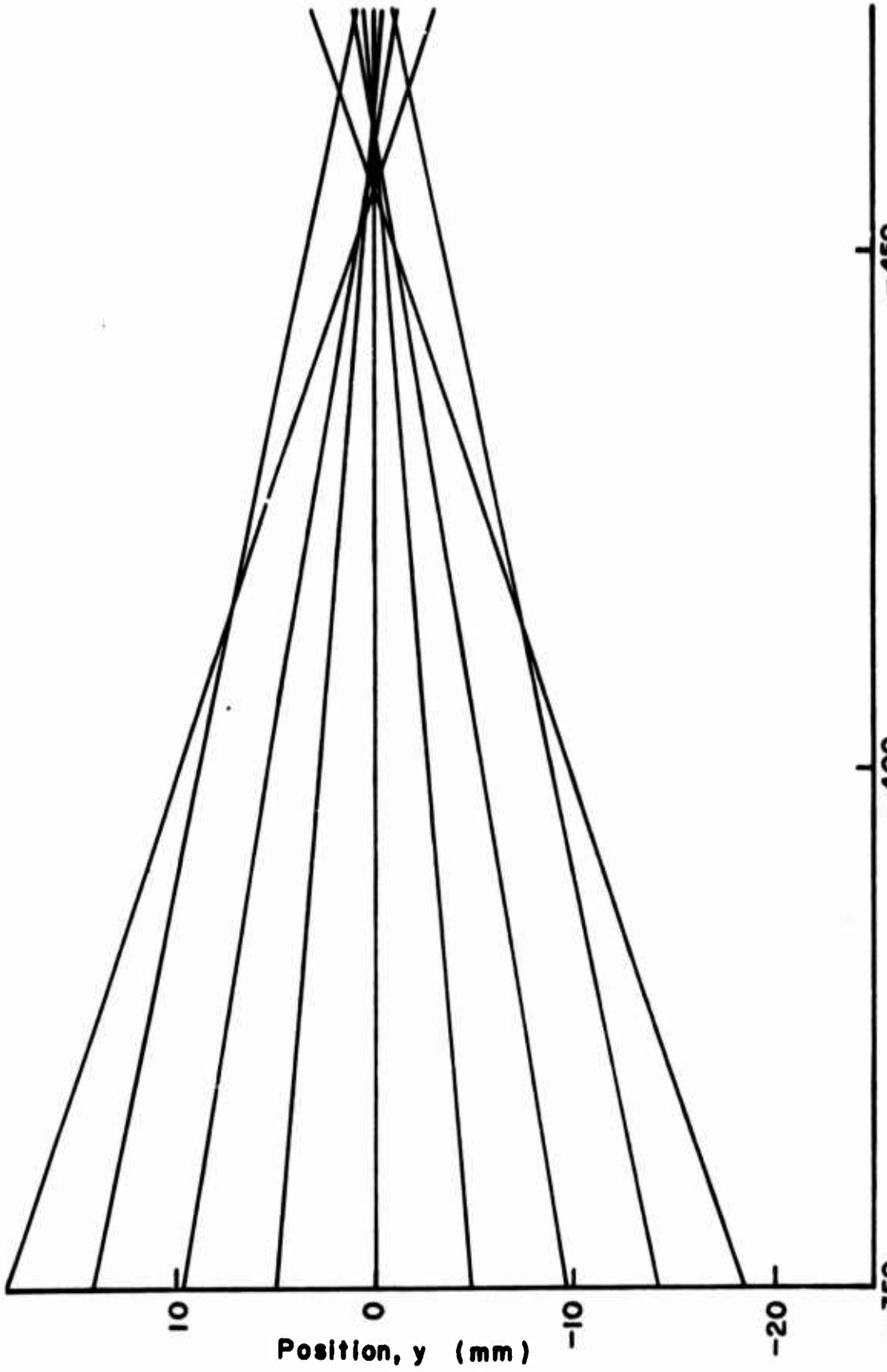

Figure 30. Theoretical Skew Ray Fan Graph forLens C at λ = 568.2 nm

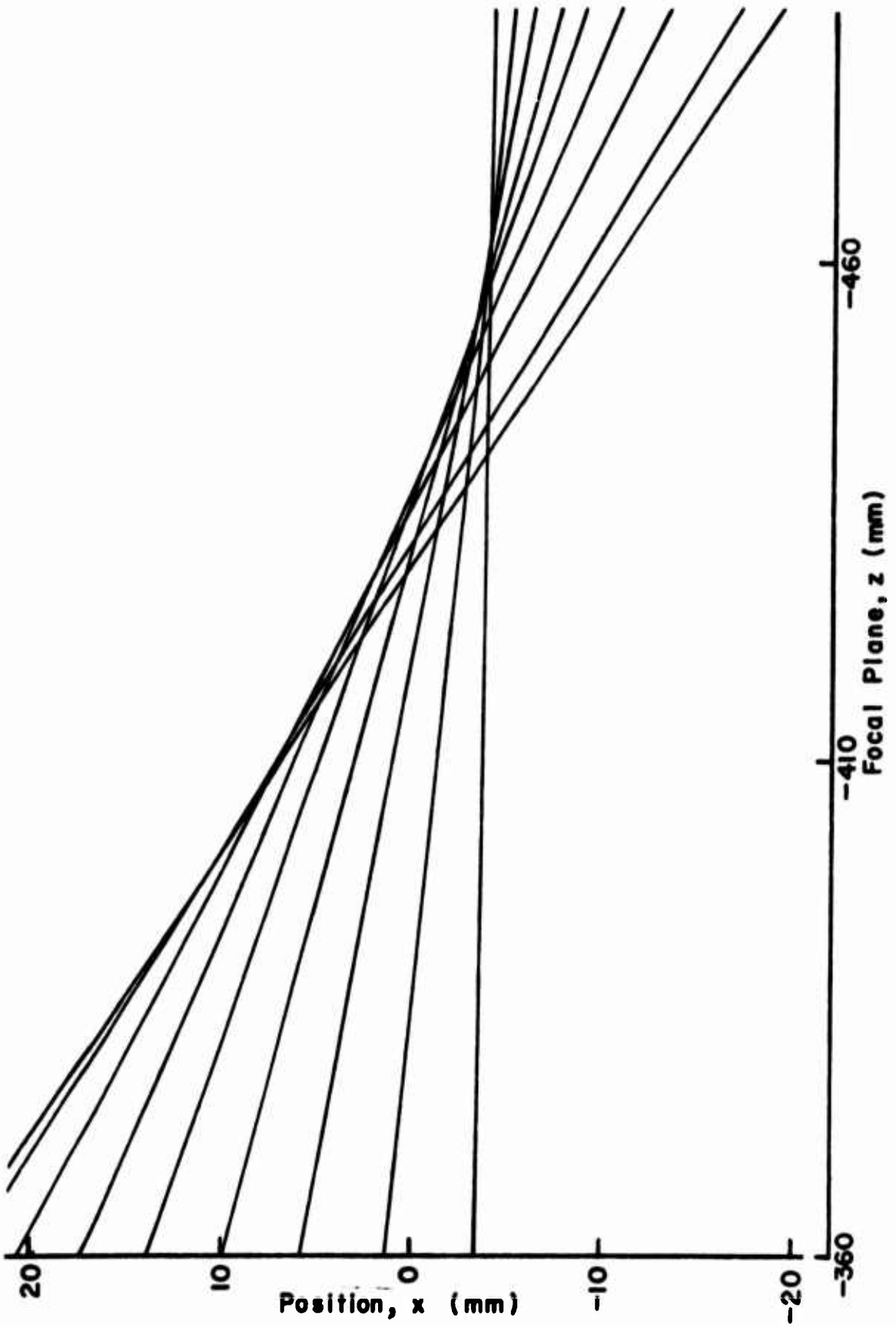

Figure 31. Theoretical Meridional Ray Fan for Lens C at λ = 632.8 nm

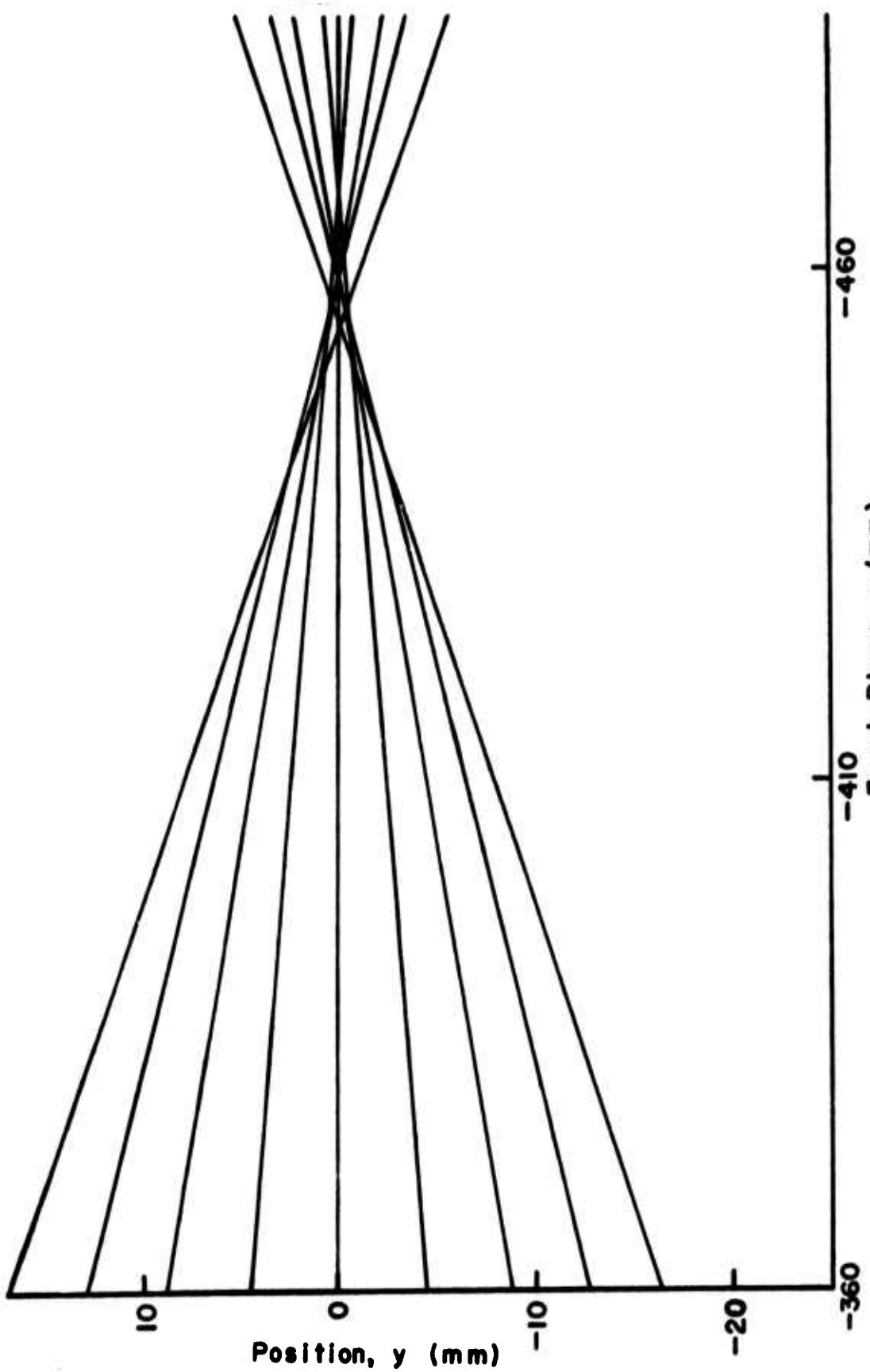

Figure 32. Theoretical Skew Ray Fan Graph for Lens C at λ = 632.8 nm

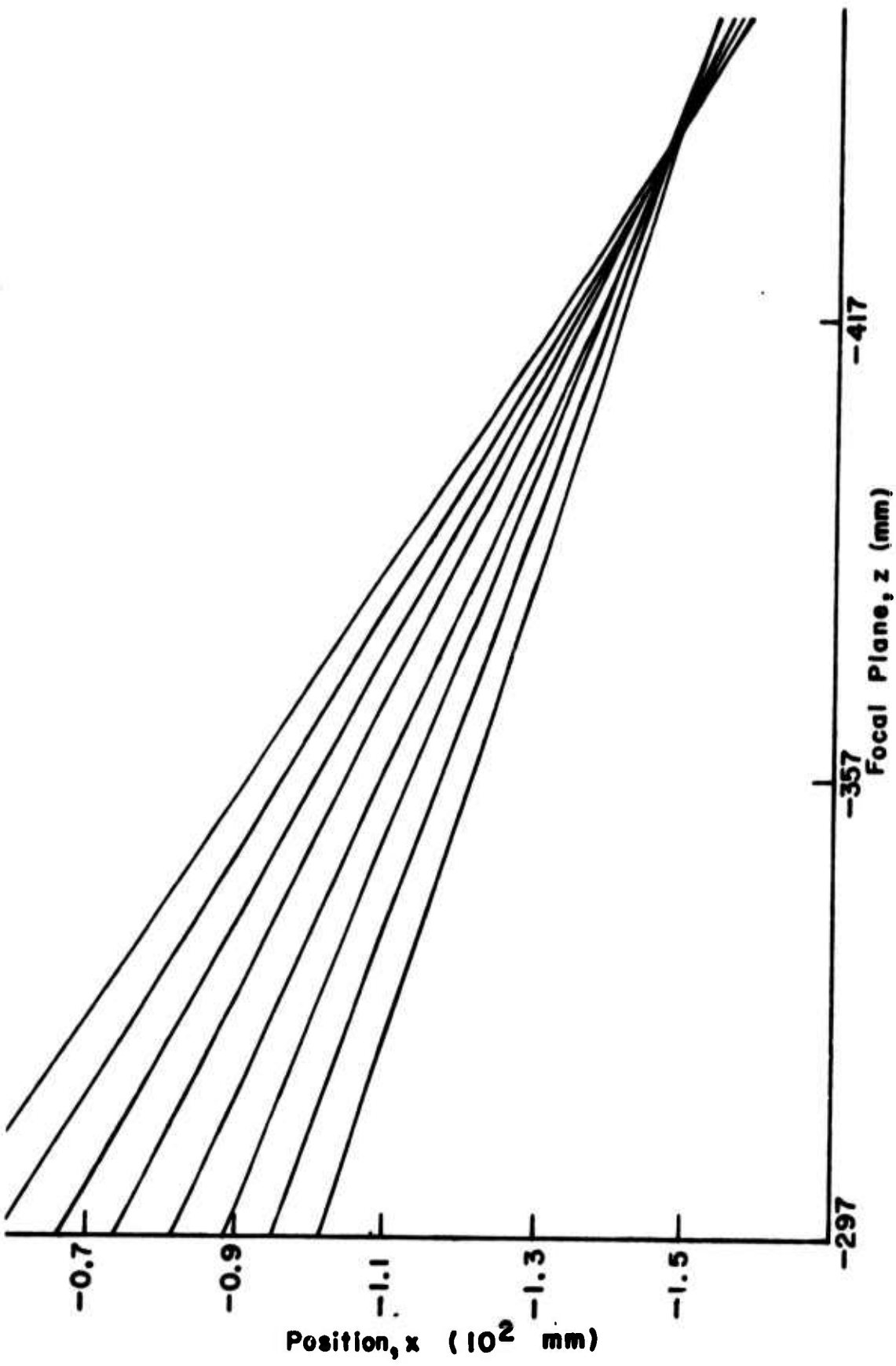

Figure 33. Experimental Meridional Ray Fan Graph for Lens C at λ = 476.2 nm

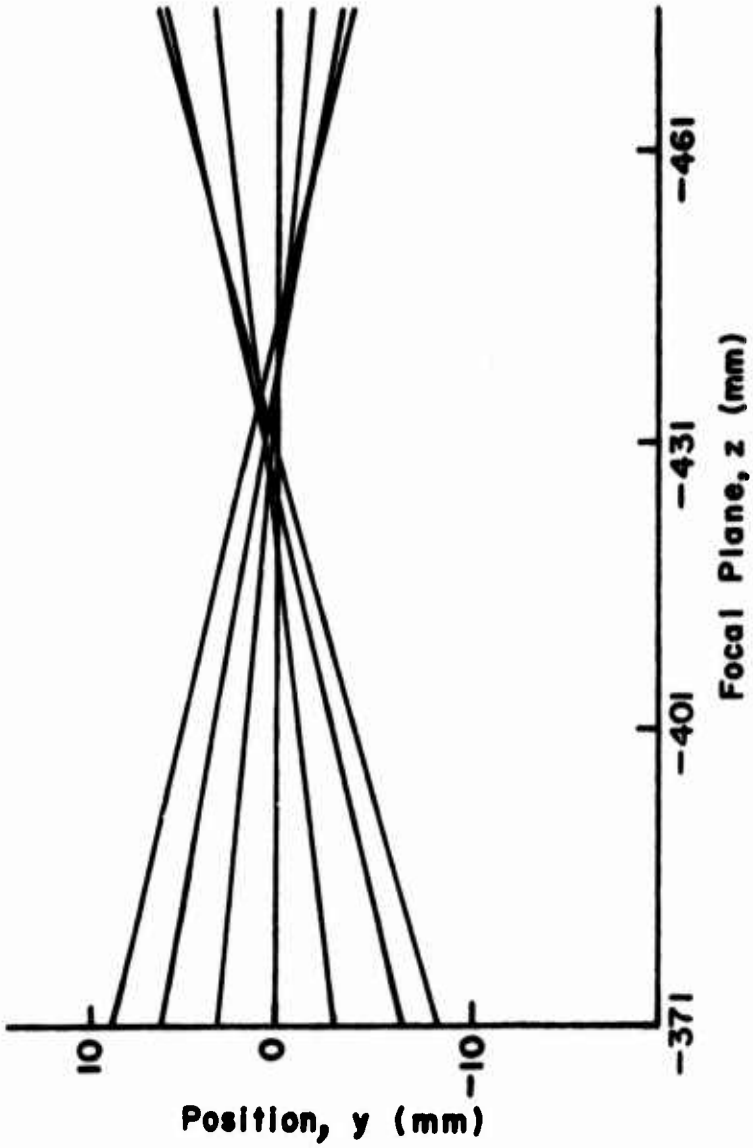

Figure 34. Experimental Skew Ray Fan Graph for Lens C at λ = 476.2 nm

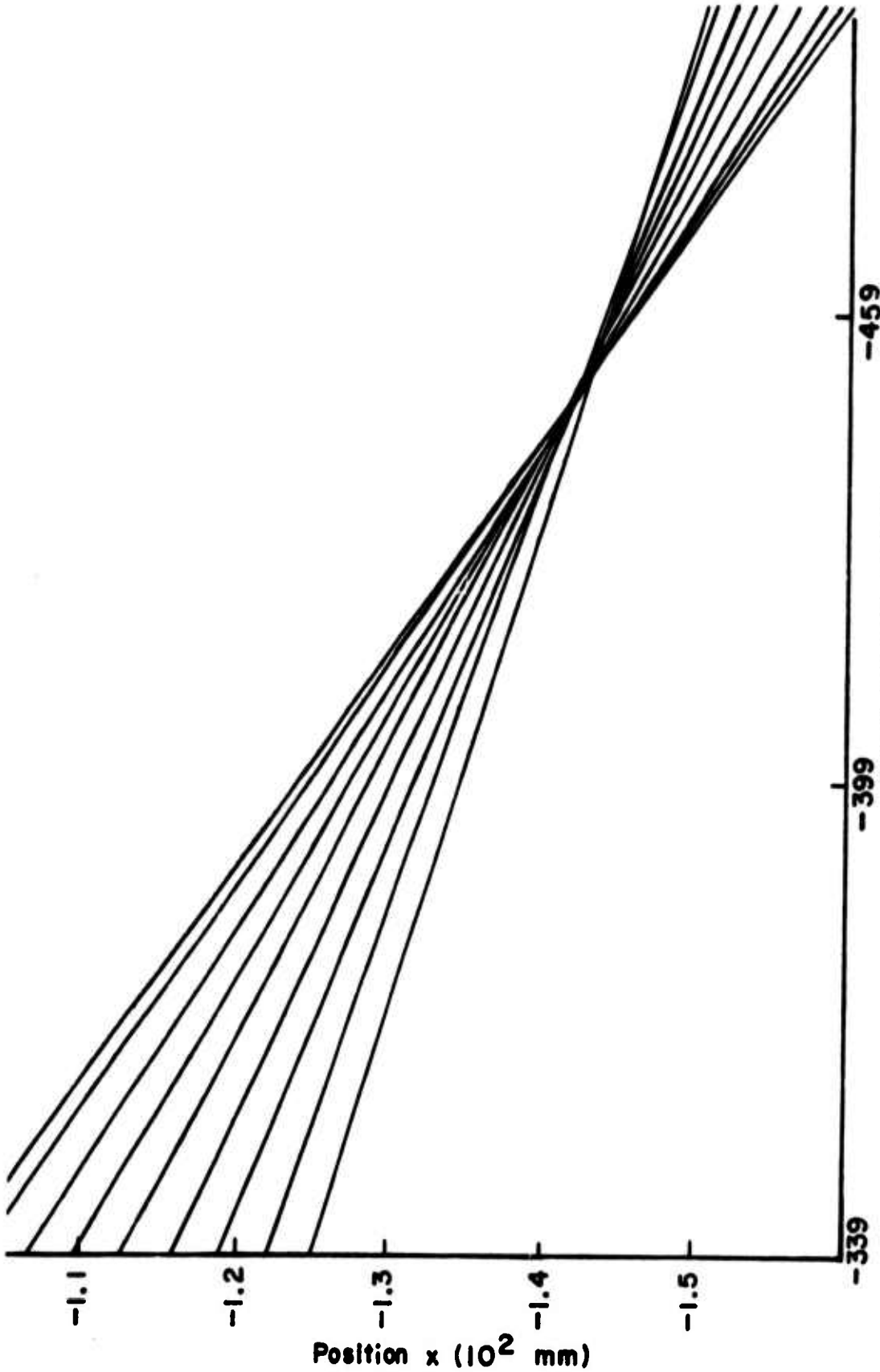

Figure 35. Experimental Meridional Ray Fan Graph for Lens C at λ = 520.8 nm

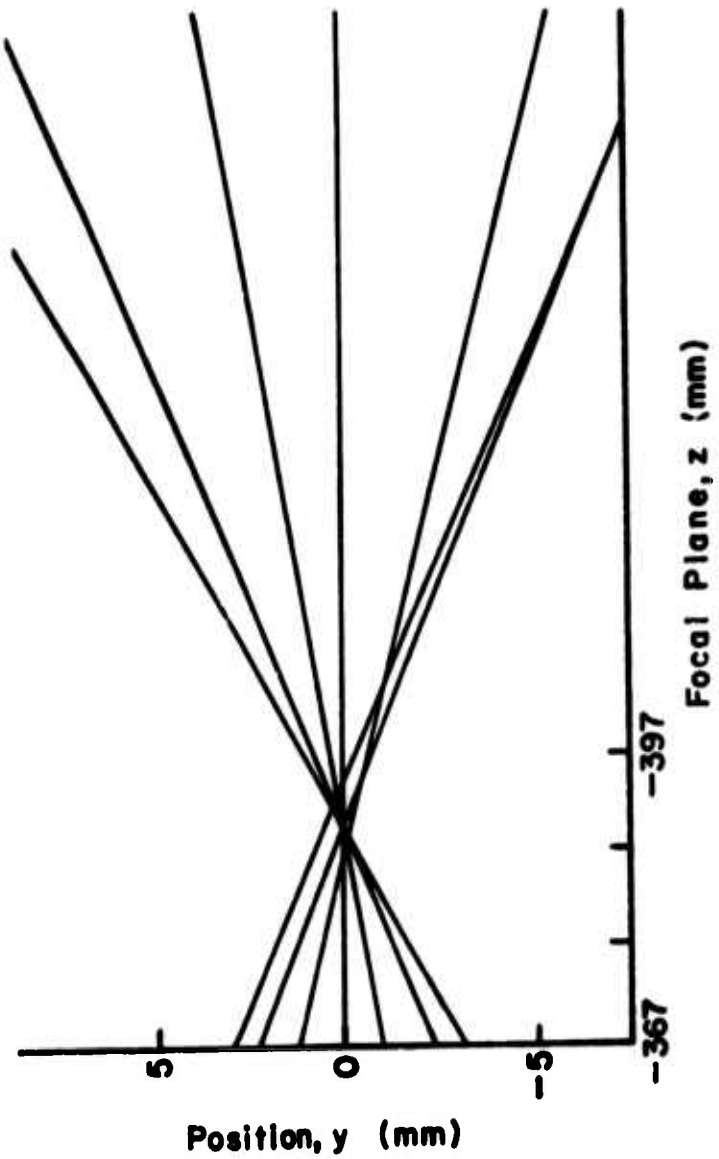

Figure 36. Experimental Skew Ray Far Graph for Lens C at λ = 520.8 nm

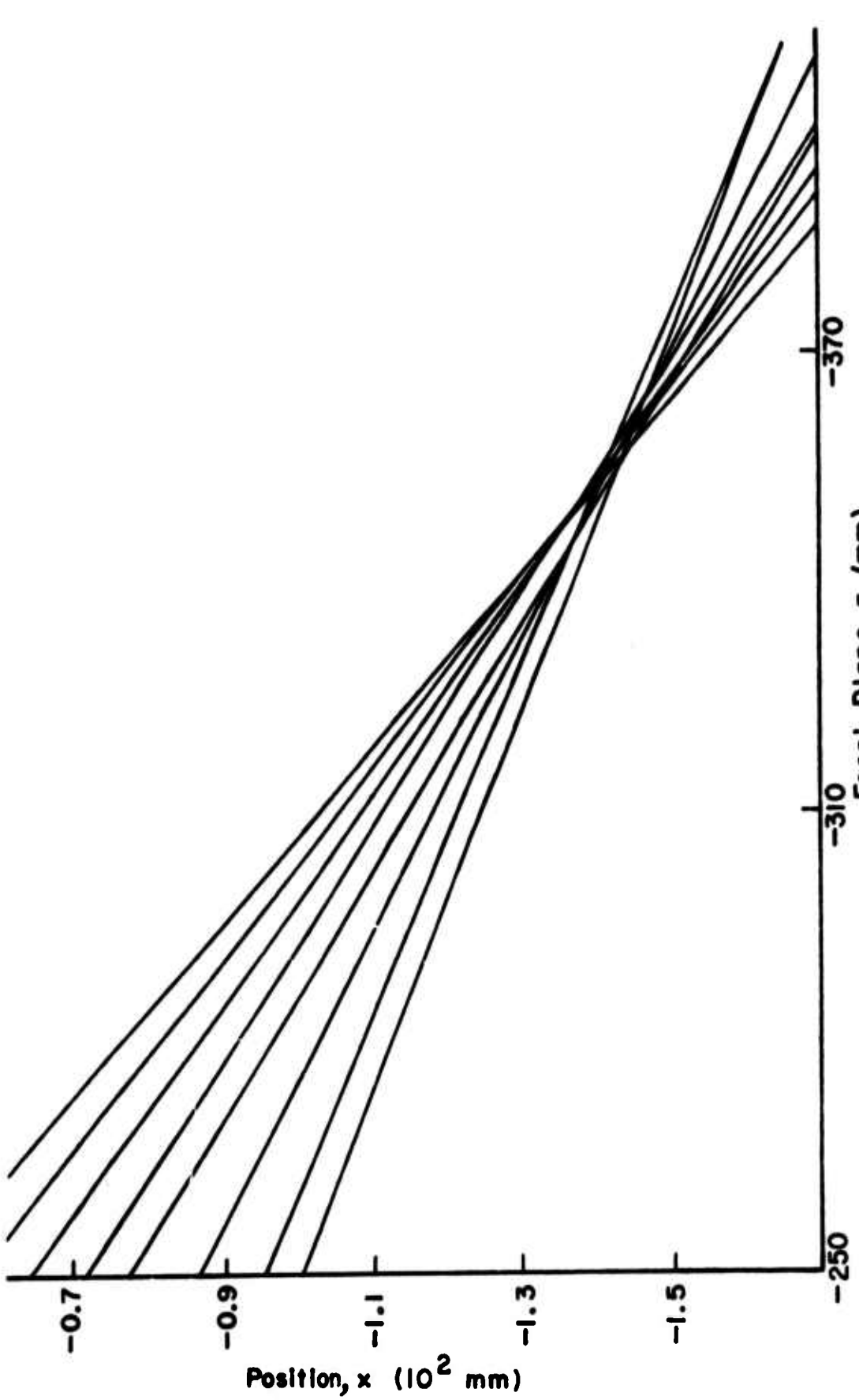

Figure 37. Experimental Meridional Ray Fan Graph for Lens C at λ = 568.2 nm

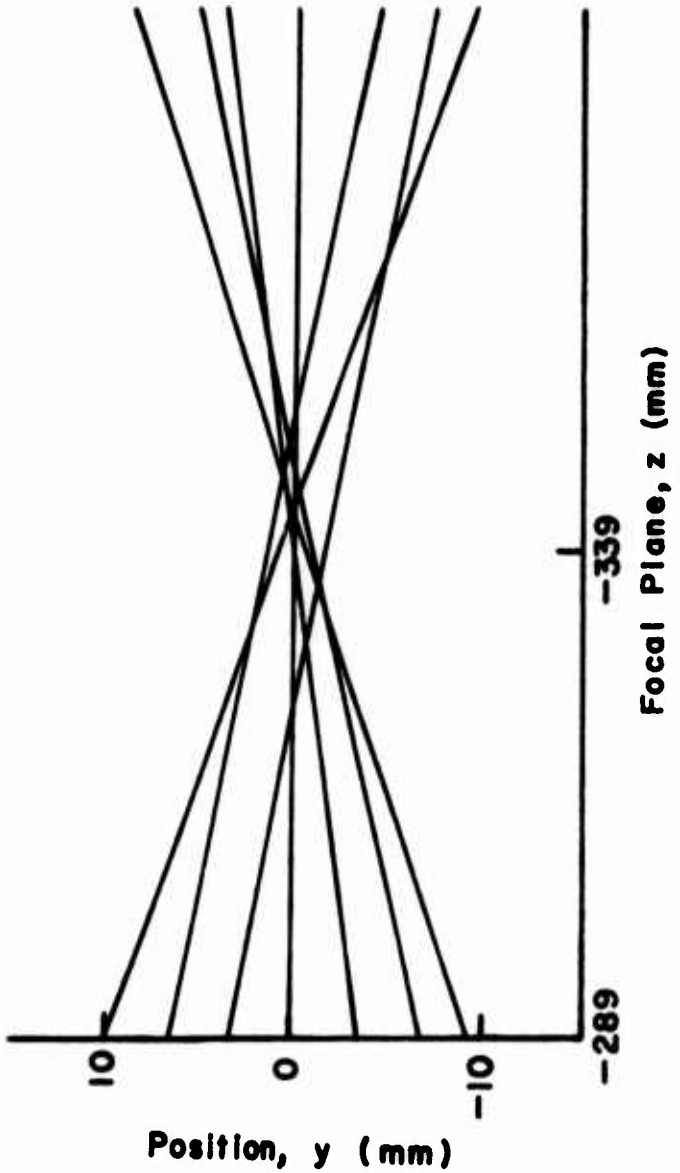

Figure 38. Experimental Skew Ray Fan Graph for Lens C at λ=568.2 nm

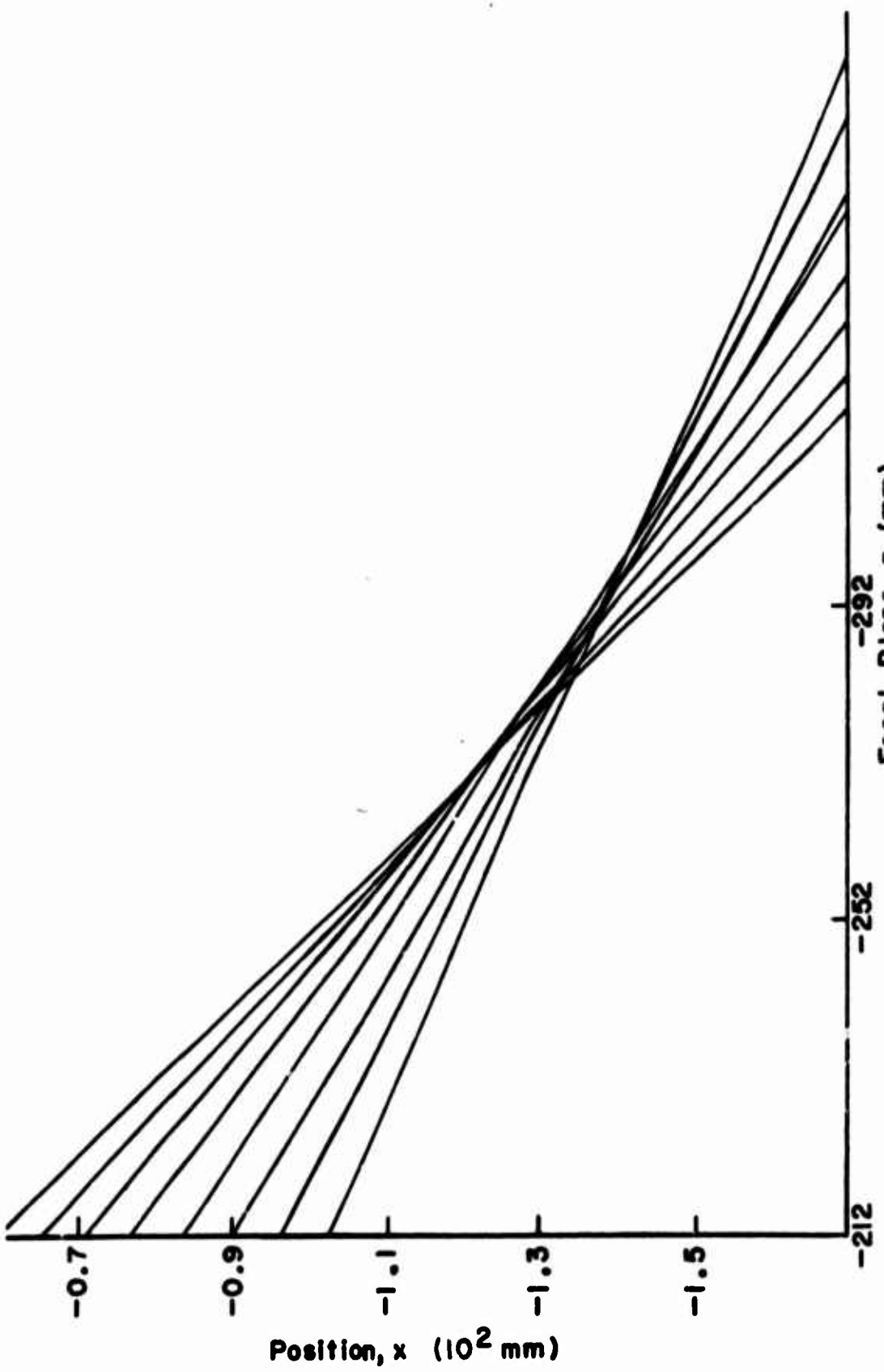

Figure 39. Experimental Meridional Ray Fan Graph for Lens C at λ = 632.8 nm

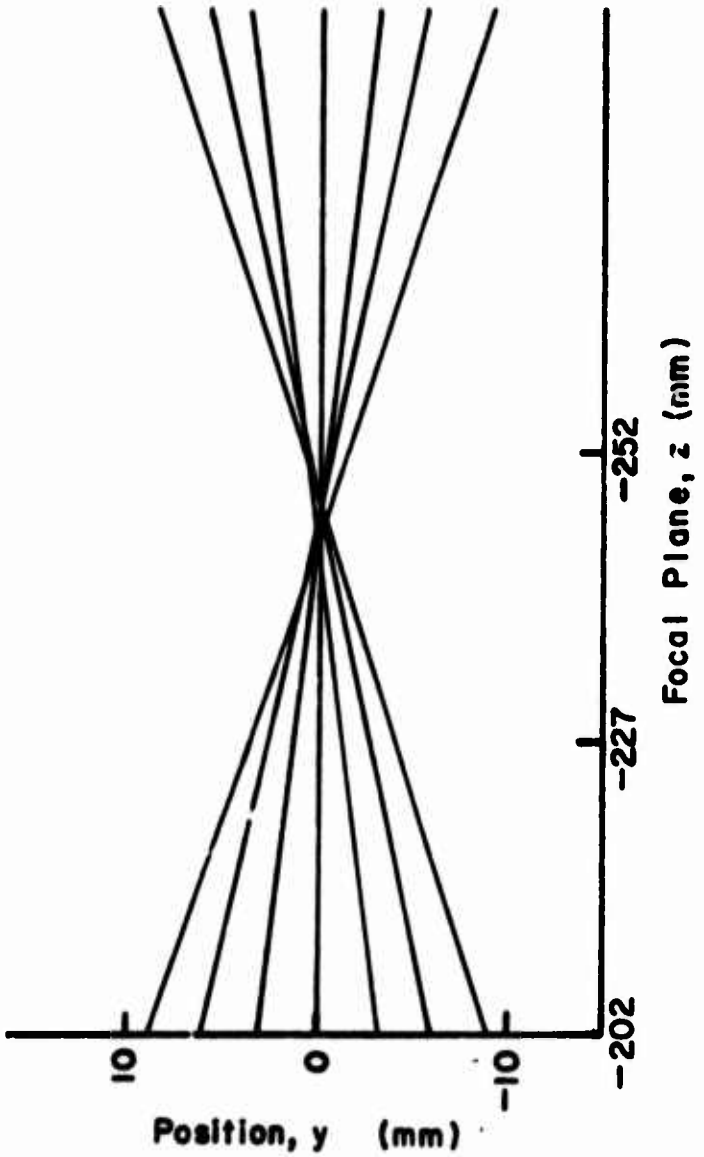

Figure 40. Experimental skew Ray Fan Graph for Lens C at λ = 632.8 nm

3. WAVEFRONT ERROR

The amount of wavefront error in the diffracted wavefront from the holographic lens was calculated from equations 91 and 98-105. The theoretical wavefront error for holographic lens D was calculated at four wavelengths for several relative aperture heights. The results are plotted in figure 41. From the figure one can see that the nearer the readout wavelength is to the constructing wavelength the less the wavefront error will be.

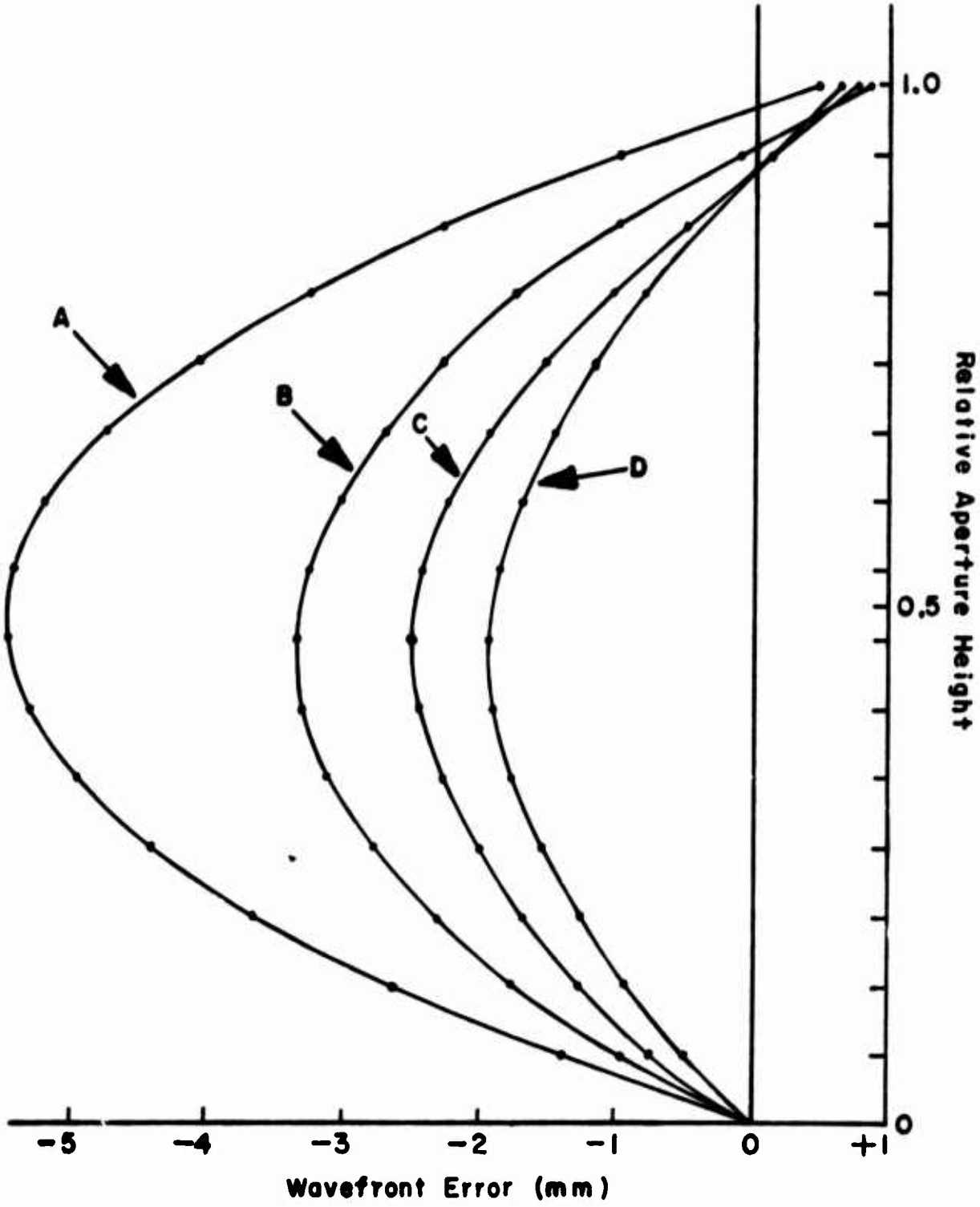

Figure 41. Theoretical Wavefront Error at Various Wavelengths vs. Aperture Height; A,632.8 nm; B,568.2 nm; C,520.8 nm; D,476.2 nm

F. EVALUATION OF DISPLAY HOLOGRAPHIC LENS[60,69]

Optical evaluation of the final holographic lens was separated into several areas: diffraction efficiency, resolving power, Hartmann graphs, spherical aberration, coma, astigmatism, field curvature, distortion, chromatic aberration, and angle of diffracted light. The evaluation did not always conform to conventional methods of evaluating glass refractive elements because holographic lenses are not "conventional". For example, the aberrations that are found in rotationally symmetric glass lens elements may be separated into third, fifth, and higher odd orders. However, the aberrations in nonsymmetric holographic lenses may be of any order, even or odd.[41] Also, at the surfaces of glass refractive lenses, blue wavelengths are deviated more than red wavelengths. But, in holographic diffractive lenses, red wavelengths are deviated more than blue. By this time, the reader should be aware that we have used such terms as spherical aberration, astigmatism, and coma in an accommodative sense. The holographic aberrations had a similar appearance to those of glass elements; hence, the accommodative naming.

The final holographic lens used in the holographic heads up display (HHUD) proved to have satisfactory optical quality for the virtual image display in all areas tested except chromatic aberration. For this reason the final display was forced to be monochromatic, using a sodium lamp for illumination. Further, research into achromatizing holographic lenses is required in order to obtain a full color display of good quality. It seems clear that such achromatization can be accomplished by developing holographic doublets and triplets similar to glass lenses.

1. DIFFRACTION EFFICIENCY

The diffraction efficiency at one point in an holographic element is defined as the amount of light diffracted into the first order image divided by the amount of light impinging on the hologram times one hundred percent. For the final holographic lens element, the diffraction efficiency was measured for both channels by means of a 4- by 4-inch square array of apertures illuminated with light of wavelength 568.2 nm. Figure 42 illustrates the results for channel 1, and figure 43 illustrates the results for channel 2. Channel 1 had a reasonably consistent twenty-five percent diffraction efficiency. Channel 2 was consistently at forty-five percent diffraction efficiency. These amounts are quite good and at the state-of-the-art for area diffraction efficiencies in double exposure holographic elements. The diffraction efficiency proved to be at a satisfactory level for the field angles used in the HHUD.

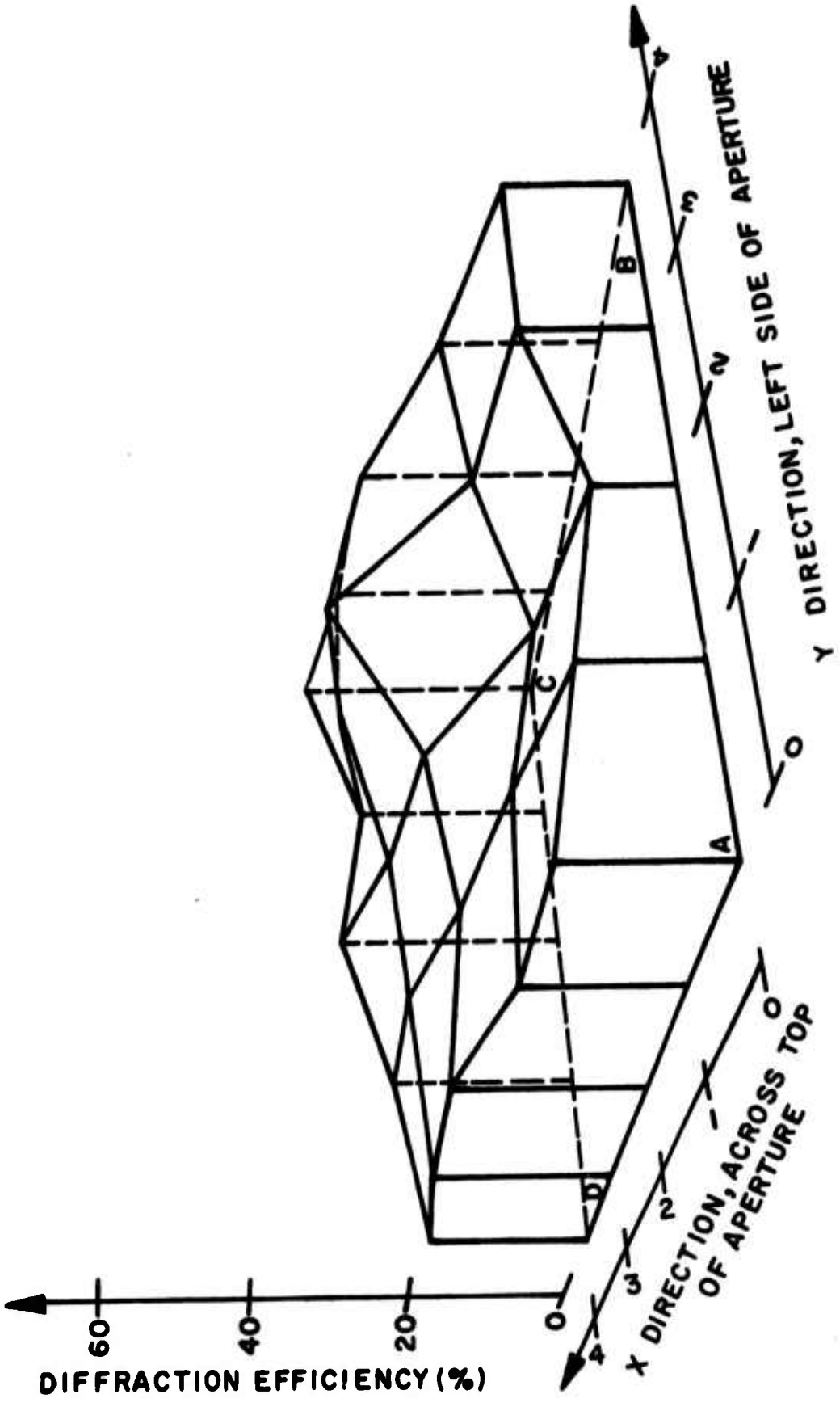

Figure 42. Experimental Diffraction Efficiency vs. Aperture Position for Channel 1 of Final Holographic Element at λ = 568.2 nm

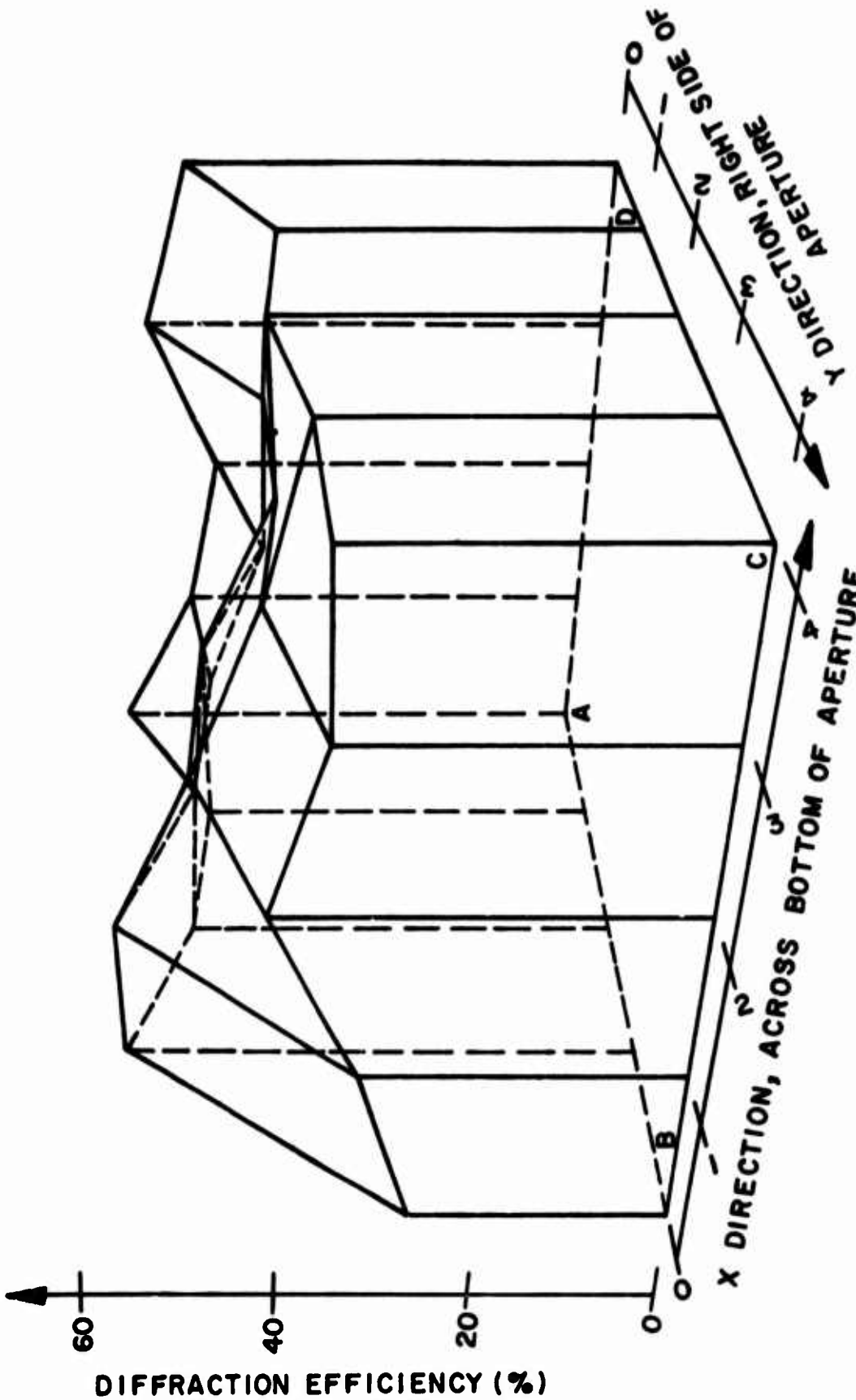

Figure 43. Experimental Diffraction Efficiency vs. Aperture Position for Channel 2 of Final Holographic Element at λ = 568.2 nm

2. RESOLVING POWER

A standard Air Force resolution target was placed at the focal point of each channel and projected with 568.2 nm light to yield a virtual image at infinity. The target was read with the naked eye and yielded one minute of arc resolution for both channels. The target was read with a 60 X telescope and yielded one-half minute of arc resolution for both channels. The resolution target in each channel was photographed at f/90 and the results are shown in figure 44at a magnification of 0.74. The resolution was satisfactory for the virtual image display in the HHUD.

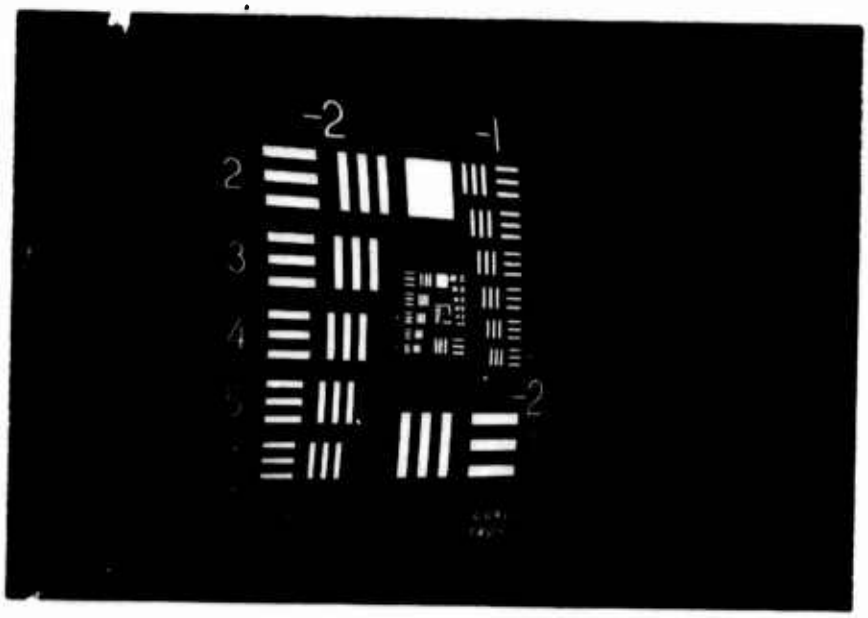

(a)

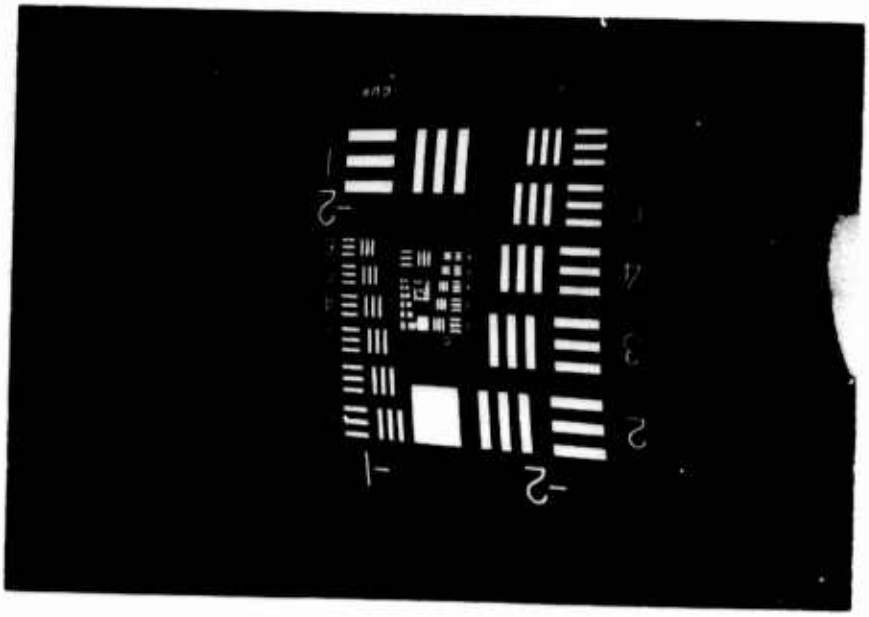

(b)

Figure 44. Photograph of Resolution Target Projected by Final Holographic Element at λ = 568.2 nm: (a) Channel 1; (b) Channel 2

3. HARTMANN GRAPHS

Meridional and skew ray fans were passed from a point source at infinity through both channels of the final holographic lens and through the regions of the two foci. The light used was 568.2 nm in wavelength from a krypton laser.

The rays were intercepted at two known focal planes and the resulting slopes are plotted in figures 45 through 48.

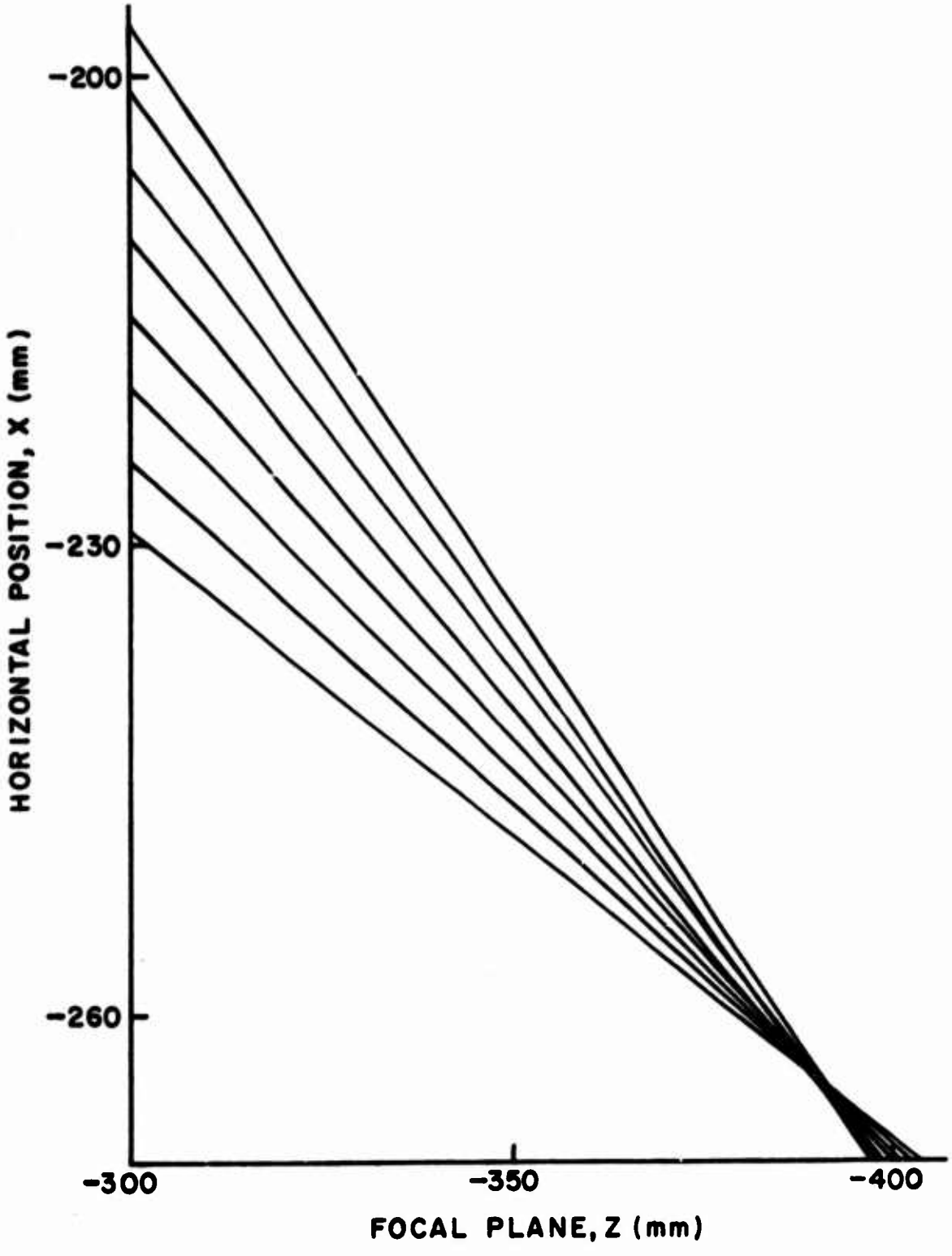

Figure 45. Experimental Meridional Ray Fan Graph for Channel 1 of Final Lens at λ = 568.2 nm

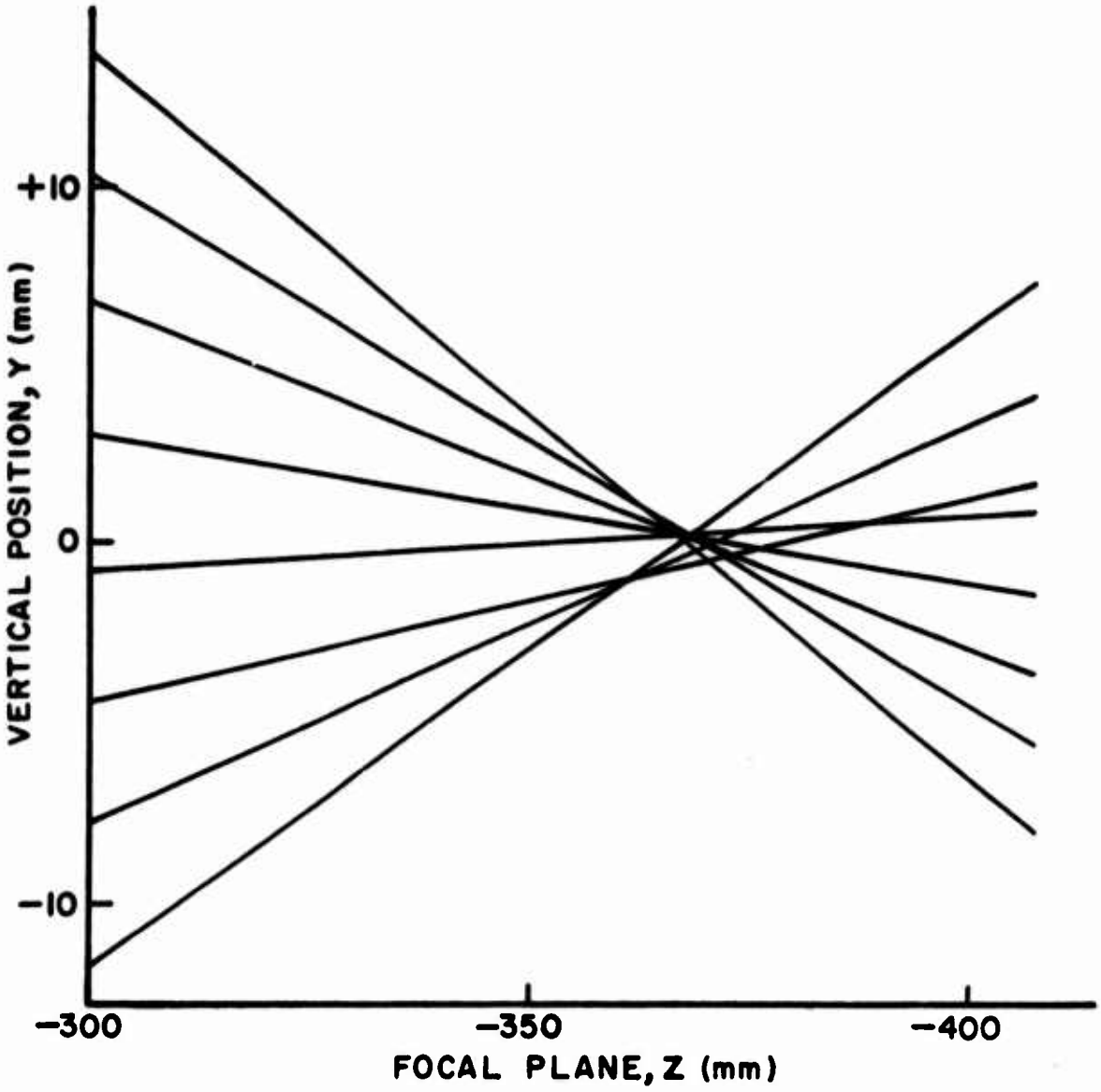

Figure 46. Experimental Skew Ray Fan Graph for Channel 1 of Final Lens at λ = 568.2 nm

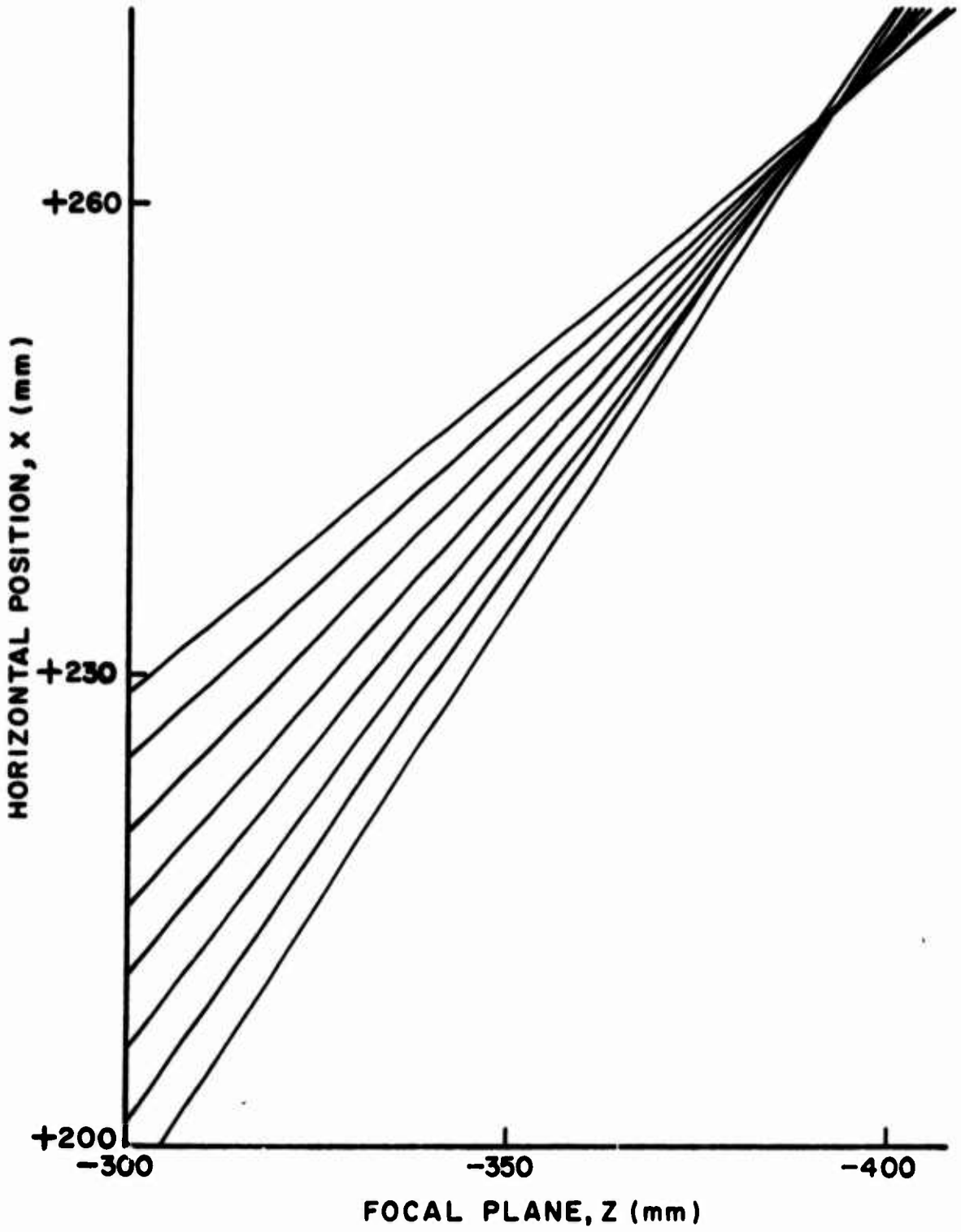

Figure 47. Experimental Meridional Ray Fan Graph for Channel 2 of Final Lens at λ = 568.2 nm

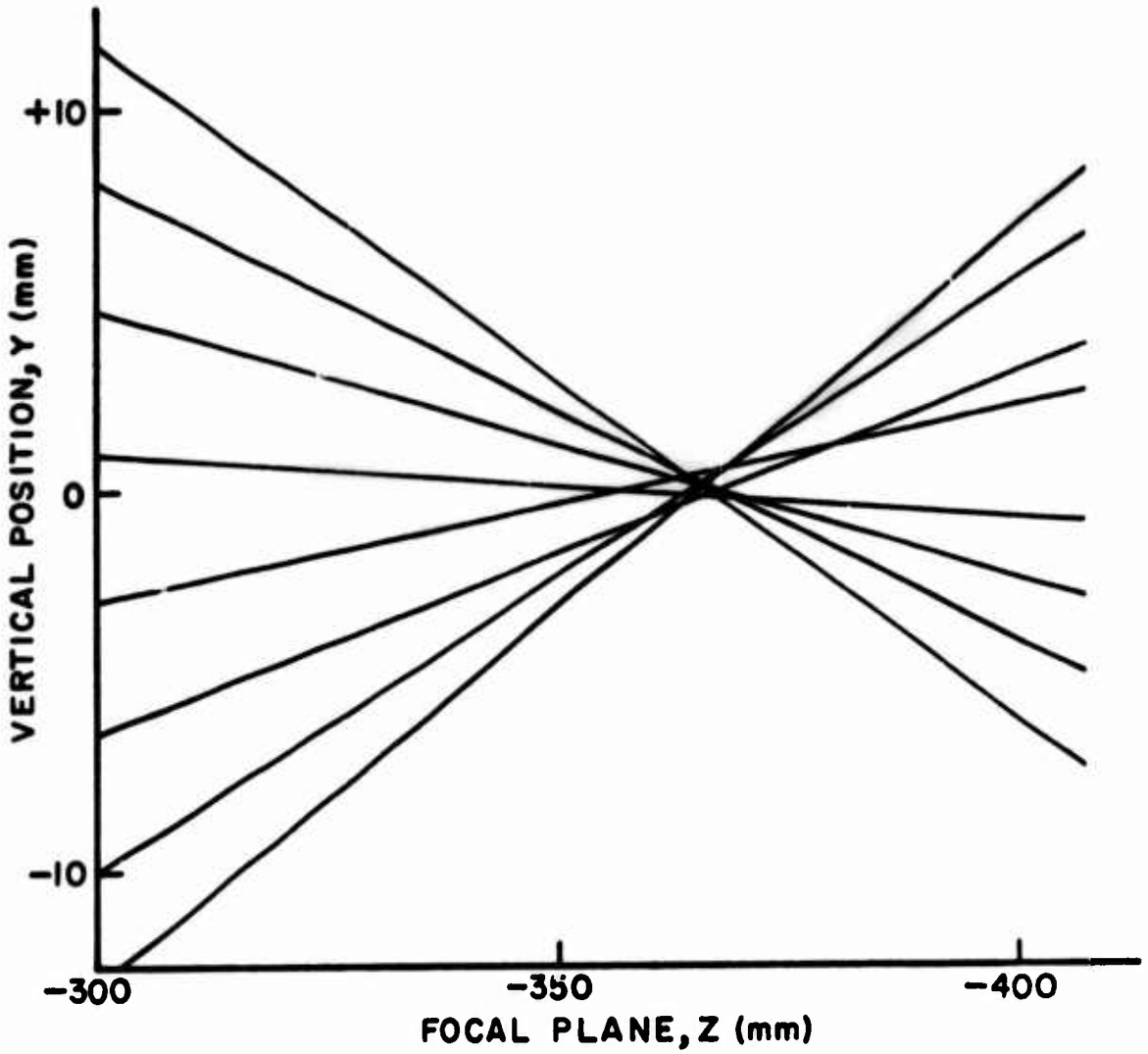

Figure 48. Experimental Skew Ray Fan Graph for Channel 2 of Final Lens at λ = 568.2 nm

4. SPHERICAL ABERRATION

The minimum spot size at the angle of maximum diffraction efficiency for λ = 568.2 nm was used as a measure of the lateral spherical aberration. The minimum spot size was 5 mm in diameter for both channels of the final lens. The minimum spot for each channel was photographed at a magnification of 0.6 and the photographs are shown in figure 49.

Also, a measure of longitudinal spherical aberration was obtained from the ray fan graphs in figures 45 to48 as described in Section III.E.2. For channel 1, the skew ray fan yielded 11.5 mm of longitudinal spherical aberration. For channel 2, the skew ray fan yielded 7 mm of longitudinal spherical aberration.

These amounts of spherical aberration proved to be acceptable for the HHUD.

(a)

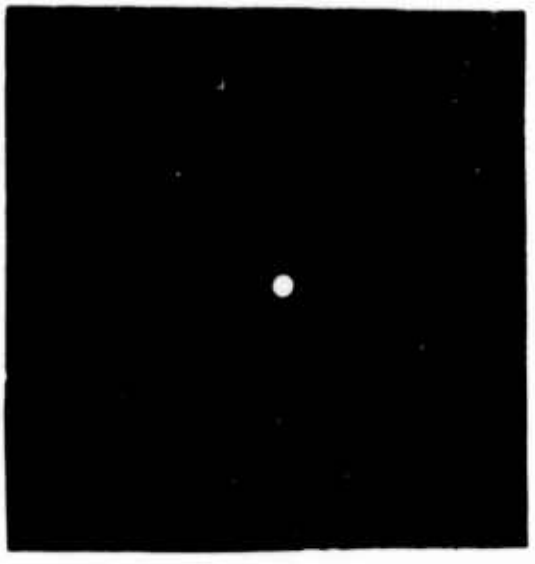

(b)

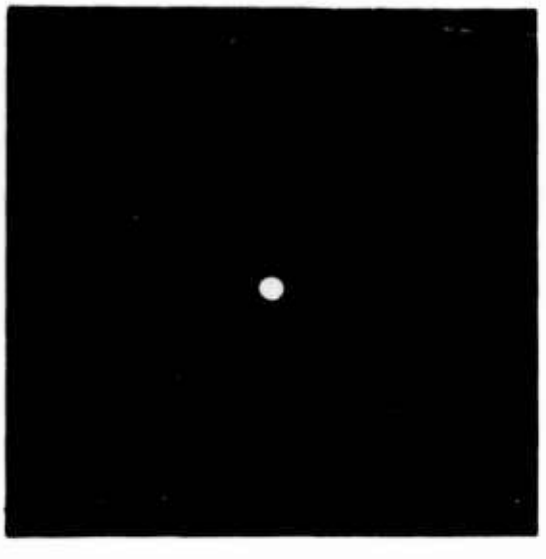

Figure 49. Minimum Spot at Angle of Maximum Diffraction Efficiency for Final Lens at λ = 568.2 nm: (a) Channel 1; (b) Channel 2

5. COMA

A measure of the amount of coma in the final holographic lens was obtained from the ray fan graphs of figures 45 to48 according to the method described in Section III.E.2. For channel one, there was a measure of 0.9 mm; and for channel two, there was a measure of 0.7 mm.

Photographs were made of the focal spot of each channel to illustrate the comatic aberration. Collimated light of wavelength 568.2 nm was passed through the lens on-axis to its best focal point, e.g., minimum spot size. A photograph was made of this image and is shown in 0° for both channels in figures 50 and 51. Then the collimated light was passed through the lens at various meridional angles and the focal images were photographed in the same plane as the 0° image. The resulting photographs are shown in figures 50 and 51 at a 0.6 magnification.

The best focal plane was determined for various meridional angles for both channels and the diameter of the minimum spot was measured. The results are plotted in figures 42 and 43. For comparison, the minimum spot size was measured versus object field angle for a masked off-axis glass lens element. The glass lens had a 152 mm aperture (same as holographic lens) and a 285 mm focal length (holographic lens was 380 mm). Three-fourths of the lens was masked in order to give it similar physical characteristics to channel 1 of the off-axis holographic lens. The results are plotted in figure 44. Comparing figure 44 with figure 42, one sees that the holographic lens had a slightly larger minimum spot size for field angles from -30° to -12°; but the holographic lens always had a smaller minimum spot for field angles from -12° to +30°.

The amount of coma in the final holographic lens was tolerable for the virtual image display in the HHUD.

(a) [illegible]

(b) +11°

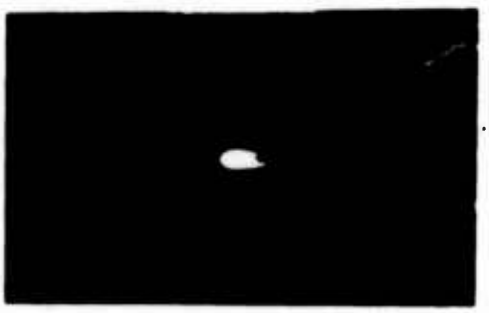

(c) +3°

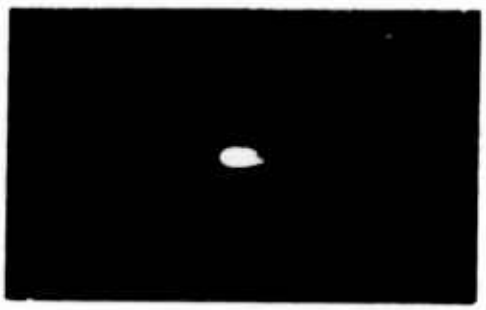

(f) +2°

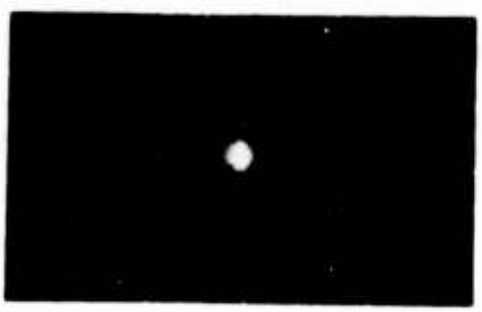

(i) -1°

(j) -2°

(m) -8°

(n) -11°

Figure 50. Focal Image In Plane Of Smallest Spot At Various Meridional Angles For Channel 1 Of Final Holographic Lens (Part 1 of 2)

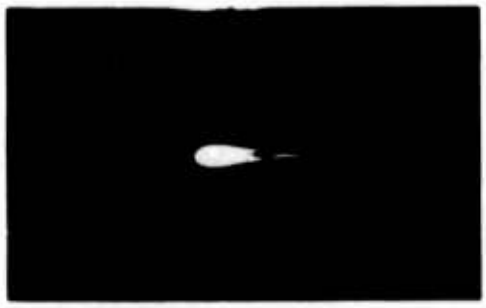

(c) +3°

(d) +5°

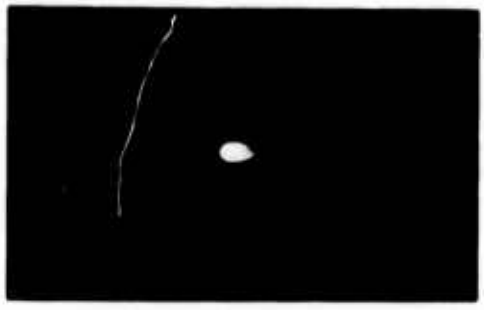

(e) +1°

(h) 0°

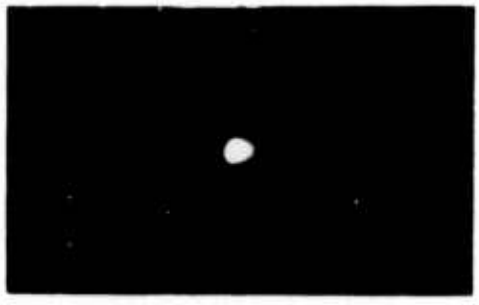

(k) -3°

(l) -5°

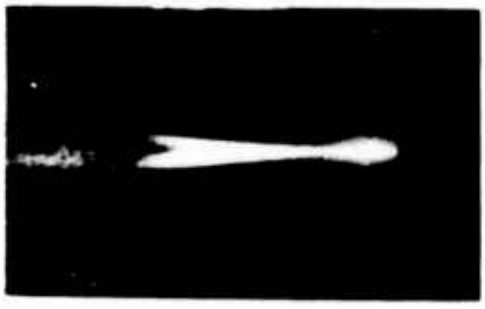

(o) -18°

Figure 50. Focal Image In Plane Of Smallest Spot At Various Meridional Angles For Channel 1 Of Final Holographic Lens (Part 2 of 2)

(a) -18^{o}

(b) -11^{o}

(e) -3^{o}

(f) -2^{o}

(i) $+1^{o}$

(j) $+2^{o}$

(m) $+8^{o}$

(n) $+11^{o}$

Figure 51. Focal Image In Plane Of Smallest Spot At Various Meridional Angles For Channel 2 Of Final Holographic Lens (Part 1 of 2)

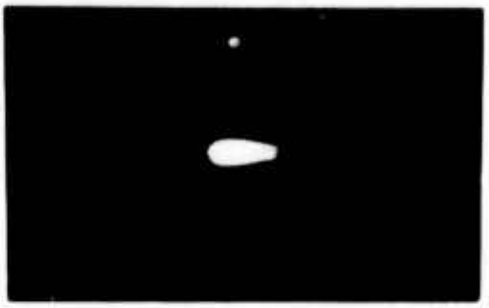

(c) -8^{o}

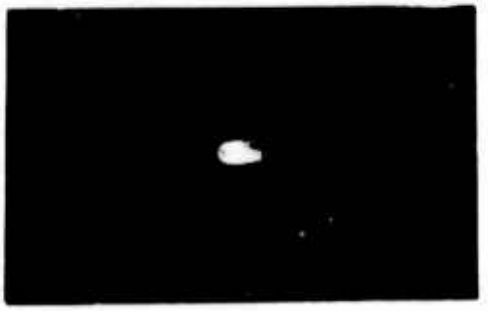

(d) -4^{o}

(g) -1^{o}

(n) 0^{o}

(k) $+3^{o}$

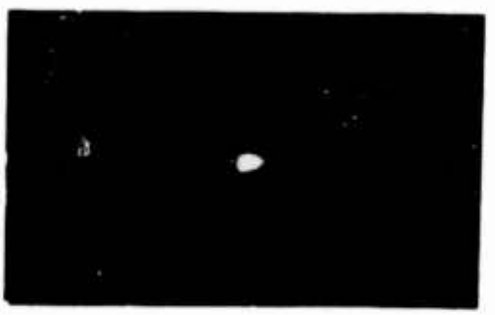

(l) $+4^{o}$

(o) $+18^{o}$

Figure 51. Focal Image In Plane Of Smallest Spot At Various Meridional Angles For Channel 2 Of Final Holographic Lens (Part 2 of 2)

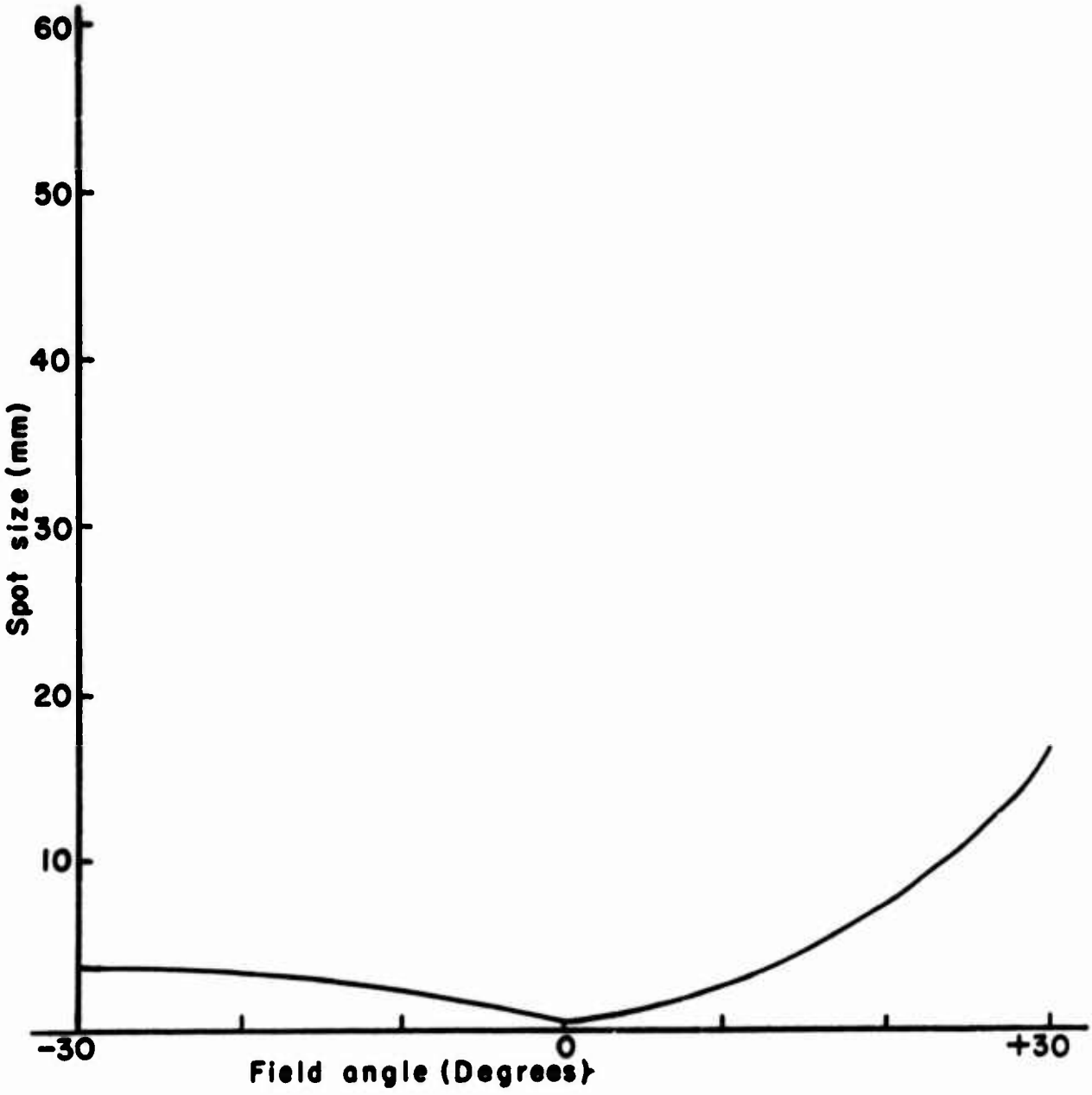

Figure 52. Minium Spot Size vs. Object Field Angle for Channel 1 of Final Lens at λ = 568.2 nm

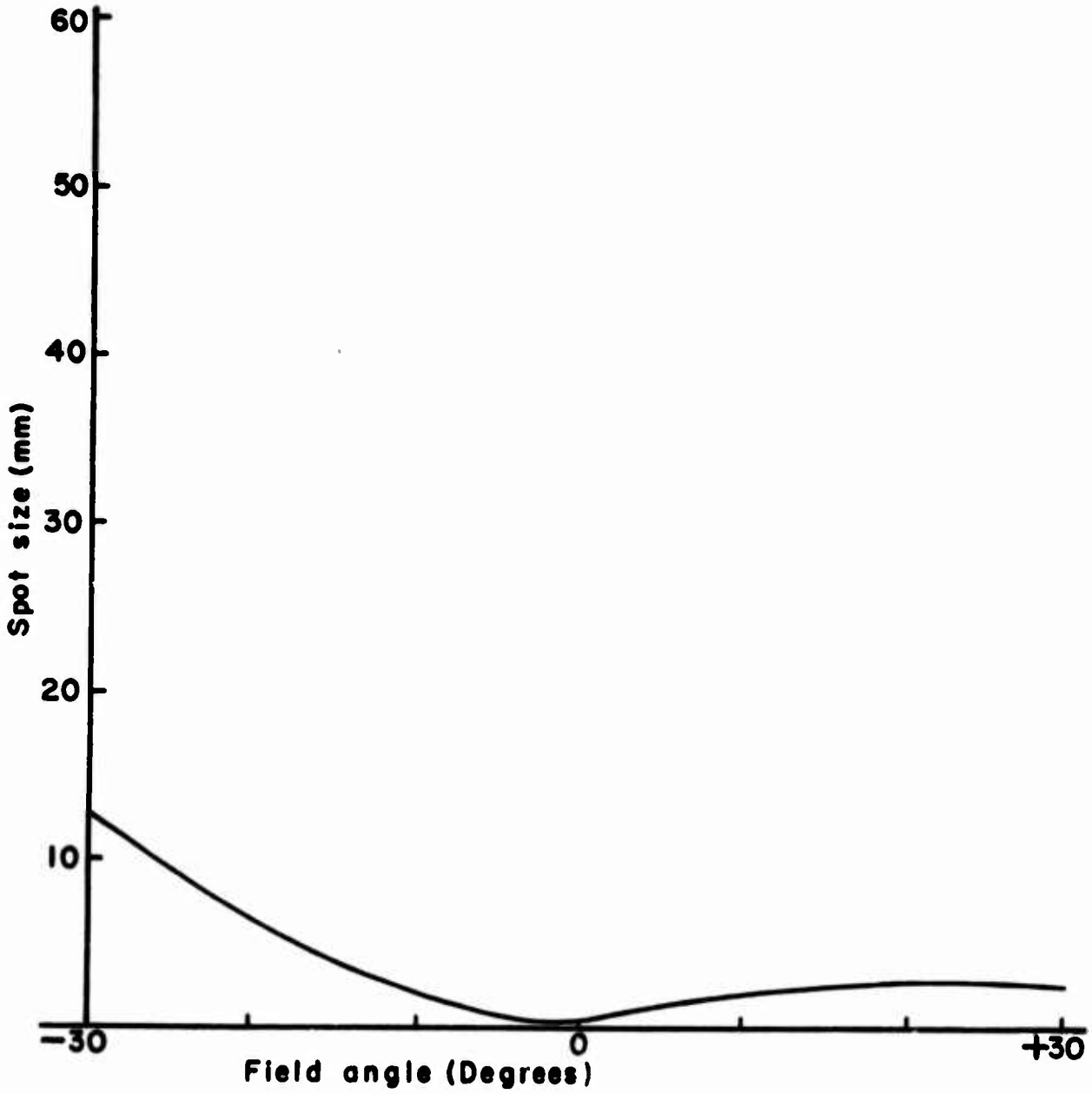

Figure 53. Minimum Spot Size vs. Object Field Angle for Channel 2 of Final Lens at λ = 568.2 nm

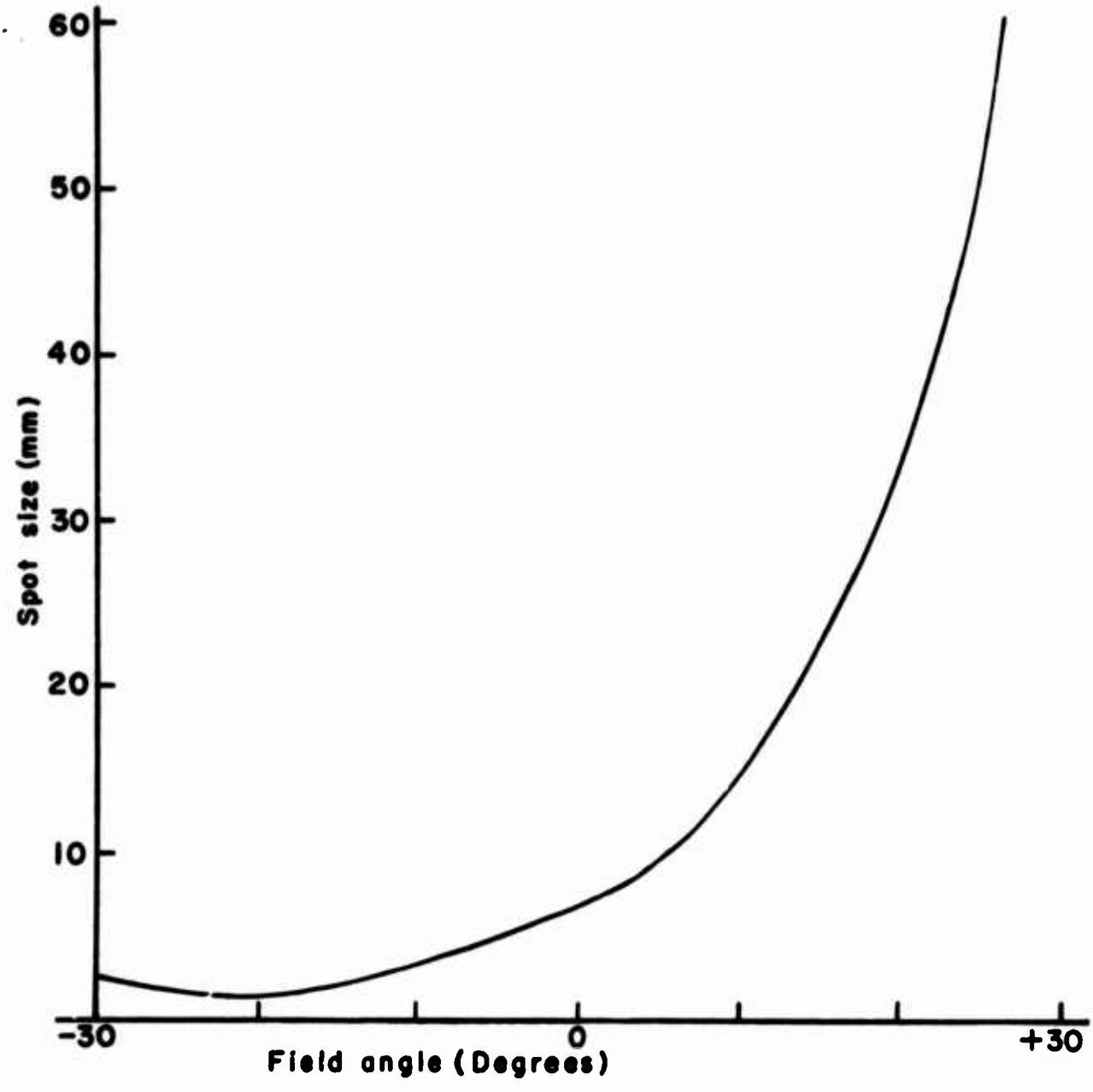

Figure 54. Minimum Spot Size vs. Object Field Angle for a Masked, Off-Axis Glass Lens at λ = 568.2 nm

6. ASTIGMATISM

The astigmatism for each channel for the final holographic lens was obtained from the ray fan graphs according to the method of Section III.E.2. Comparing figures 45 and 46 one finds 22 mm of astigmatism for channel 1. Comparing figures 47 and 48 one finds 25 mm of astigmatism for channel 2.

The amount of astigmatism at various off-axis object field angles was determined by passing collimated, 568.2 nm light through the holographic lens and measuring the distance from the center of the holographic lens to the tangential and sagittal focal planes, respectively. The measurements for channel 1 are illustrated in figures 55 and 56. The measurements for channel 2 are illustrated in figures 57 and 58. The astigmatism increases continually until an object field angle of $\pm$ 25° is attained; then the astigmatism begins to decrease.

Photographs were made of the on-axis astigmatic foci and the results are shown in figure 59 at a 0.6 magnification.

This amount of astigmatism was found tolerable in the virtual image HHUD.

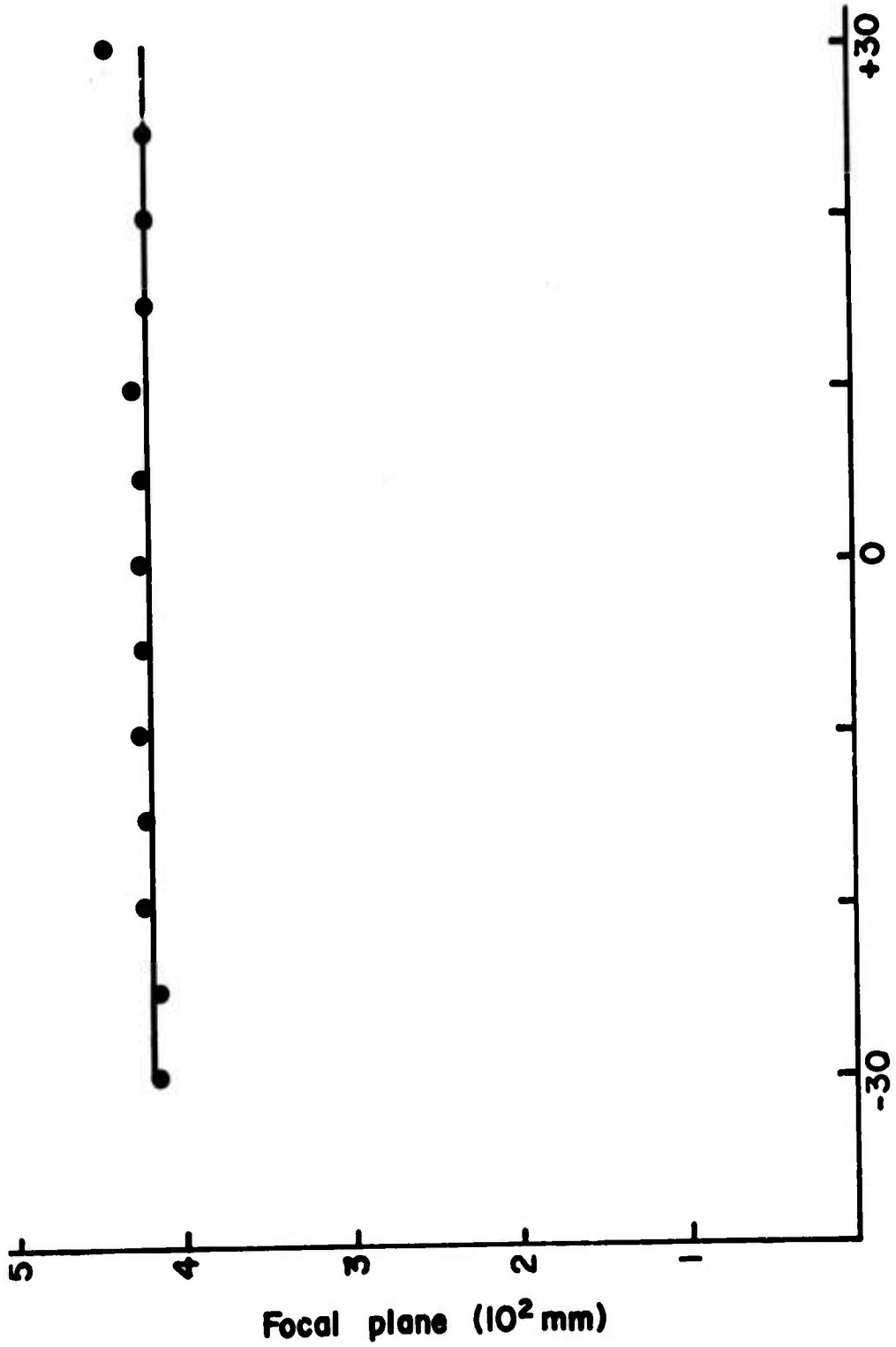

Figure 55. Plane of Sagittal Focus vs. Object Field Angle for Channel 1 of Final Lens at λ = 568.2 nm

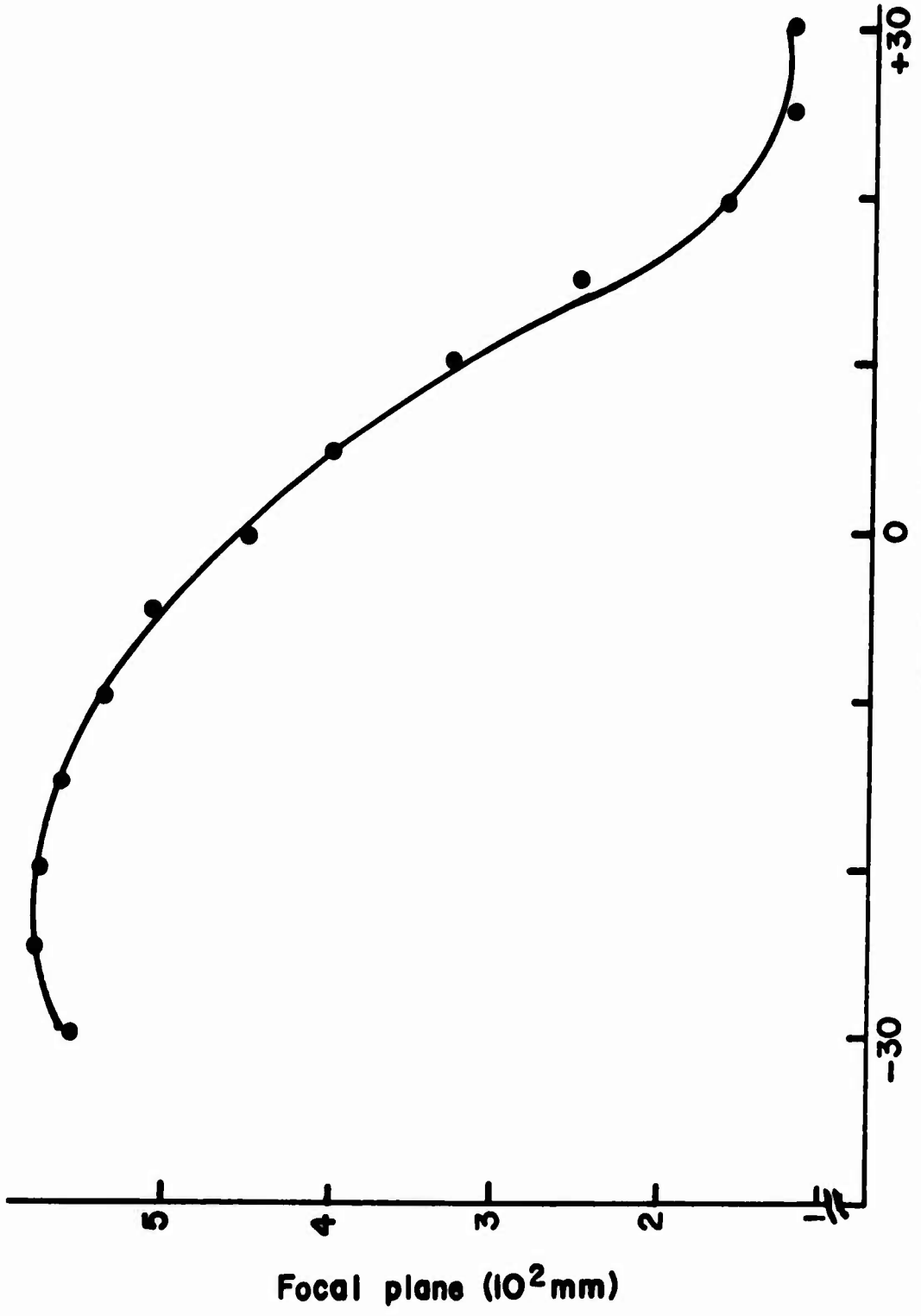

Figure 56. Plane of Tangential Focus vs. Object Field Angle for Channel 1 of Final Lens at λ = 568.2 nm

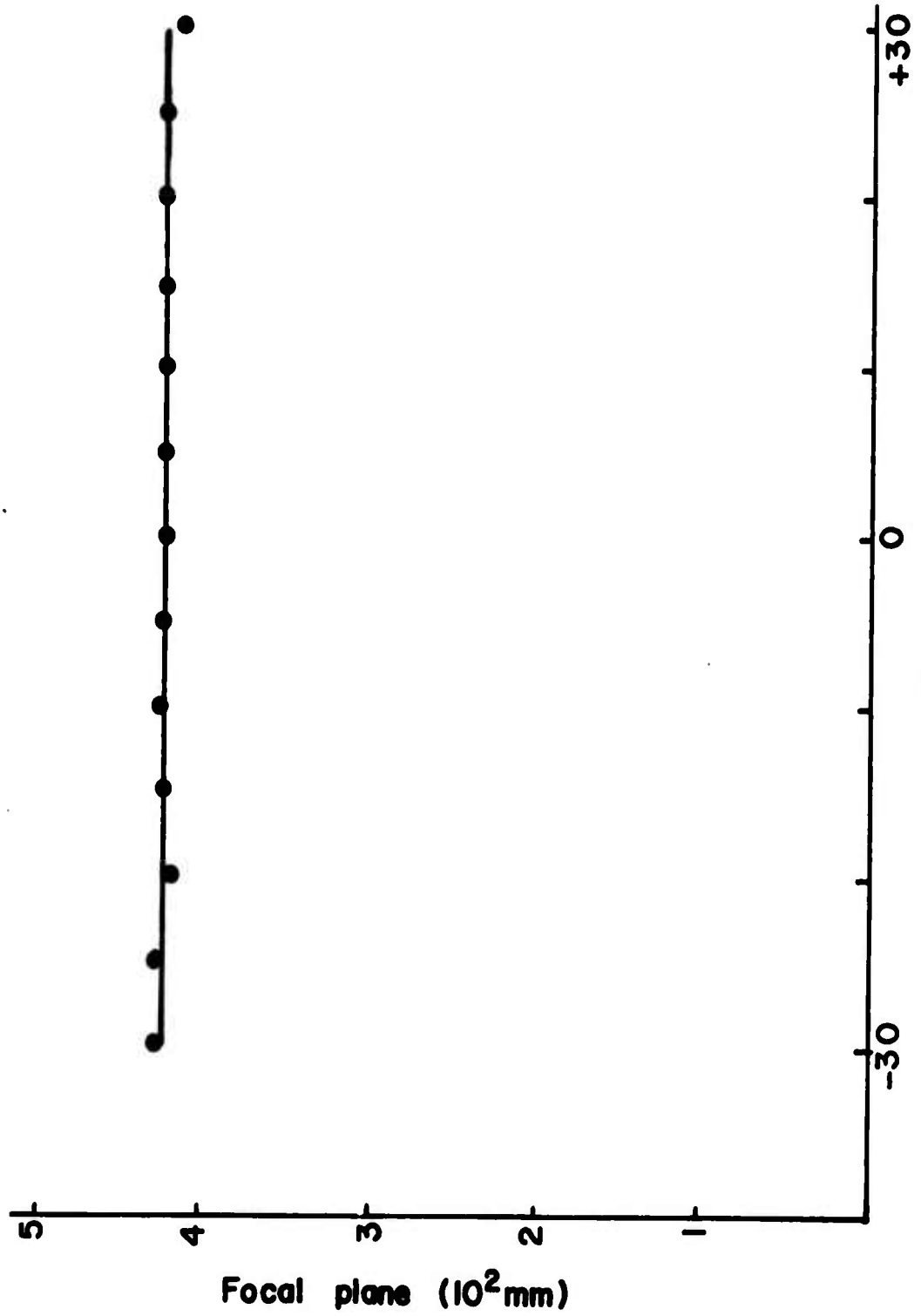

Figure 57. Plane of Sagittal Focus vs. Object Field Angle for Channel 2 of Final Lens at λ = 568.2 nm

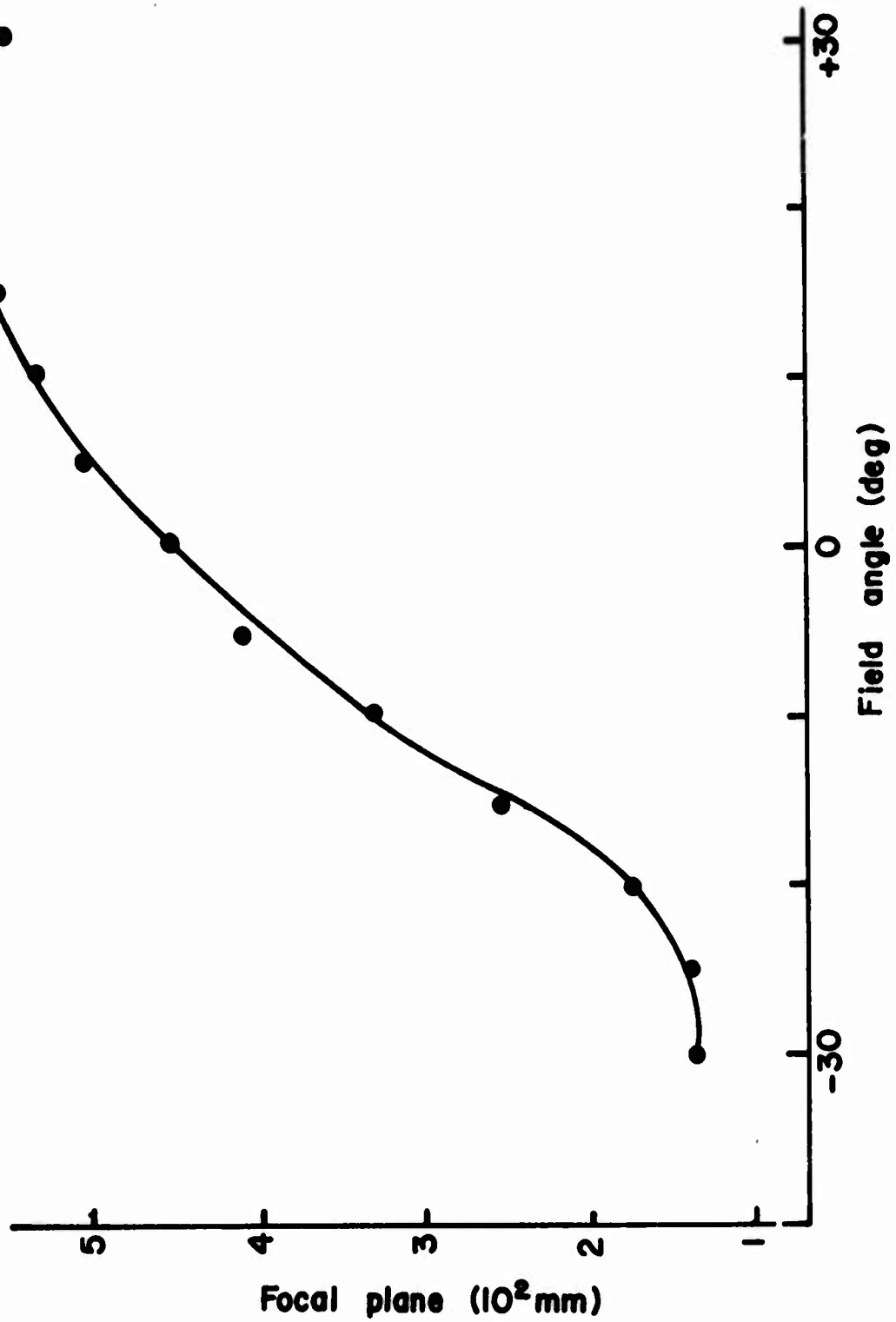

Figure 58. Plane of tangential Focus vs. Object Field Angle for Channel 2 of Final Lens at λ = 568.2 nm

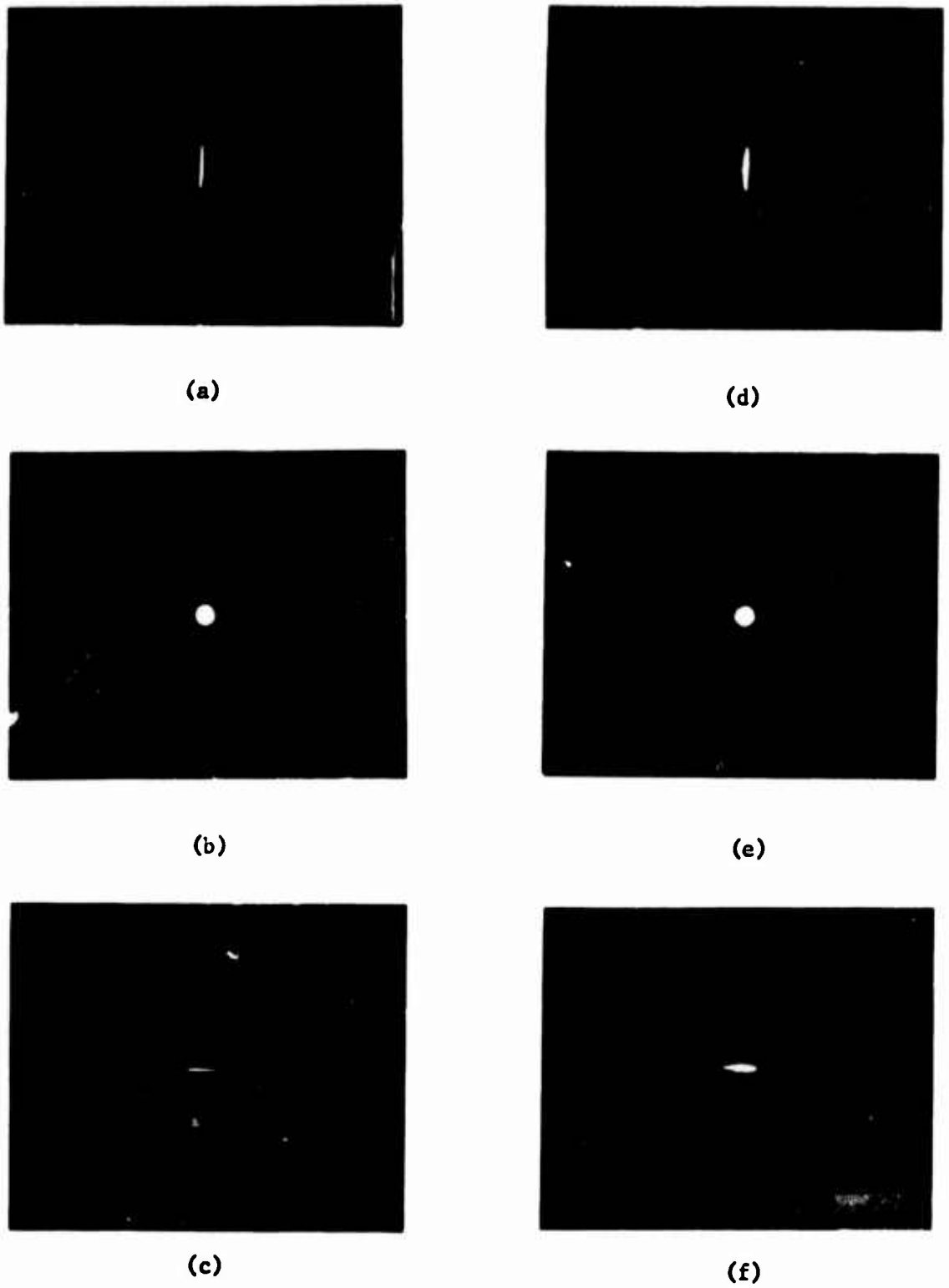

Figure 59. Astigmatic Foci for Final Lens at
λ = 568.2 nm: (a,b,c) Channel 1; (d,e,f) Channel 2

7. FIELD CURVATURE

The field curvature in each channel of the final holographic lens was determined by passing collimated, 568.2 nm light through the holographic lens at various object field angles and measuring the distance from the center of the holographic lens to the plane of best focus. The results are plotted in figures 60 and 61.

For comparison the field curvature in a masked off-axis glass lens element (same lens as in 5) was measured in the same manner. The results are plotted in figure 62. One can see that the field curvature was greater for the holographic lens than for the glass lens. Also, both channels of the holographic lens yielded an inflection point in the graph, whereas the glass lens did not.

The field curvature in the final holographic lens was tolerable since only about $\pm$ 8° of the field was actually used in the HHUD.

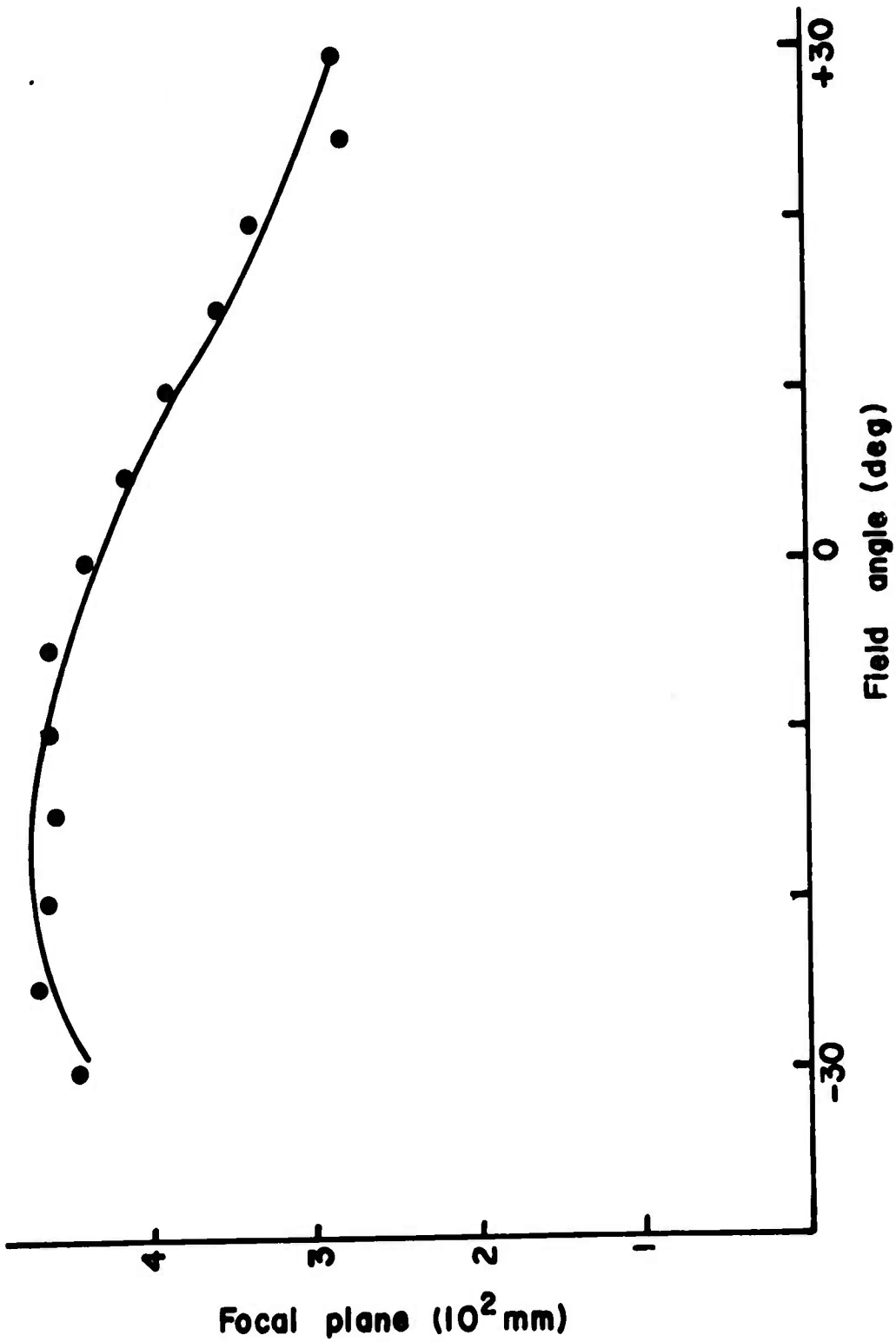

Figure 60. Plane of Best Focus vs. Object Field Angle for Channel 1 of Final Lens at λ = 568.2 nm

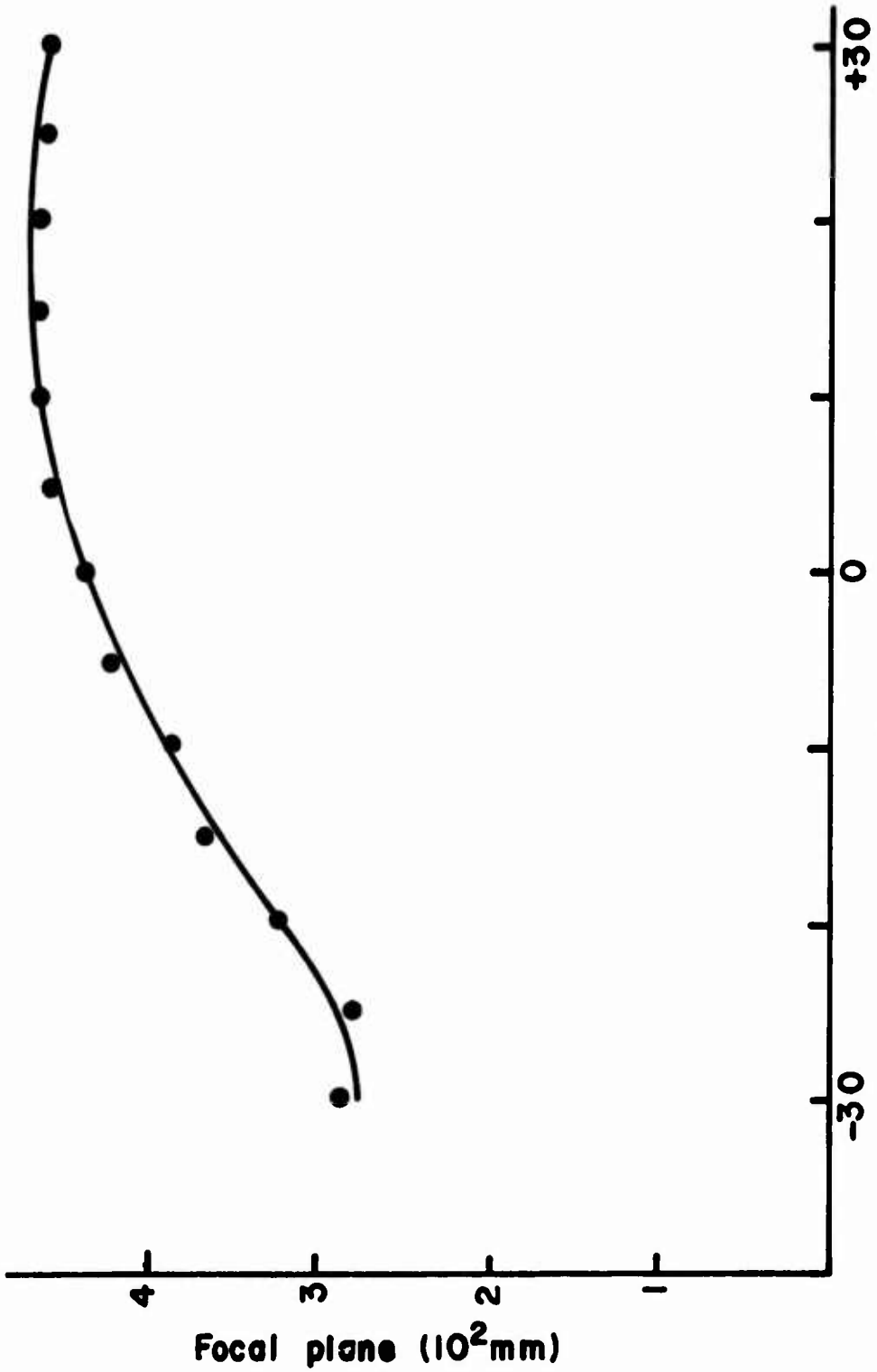

Figure 61. Plane of Best Focus vs. Object Field Angle for Channel 2 of Final Lens at λ = 568.2 nm

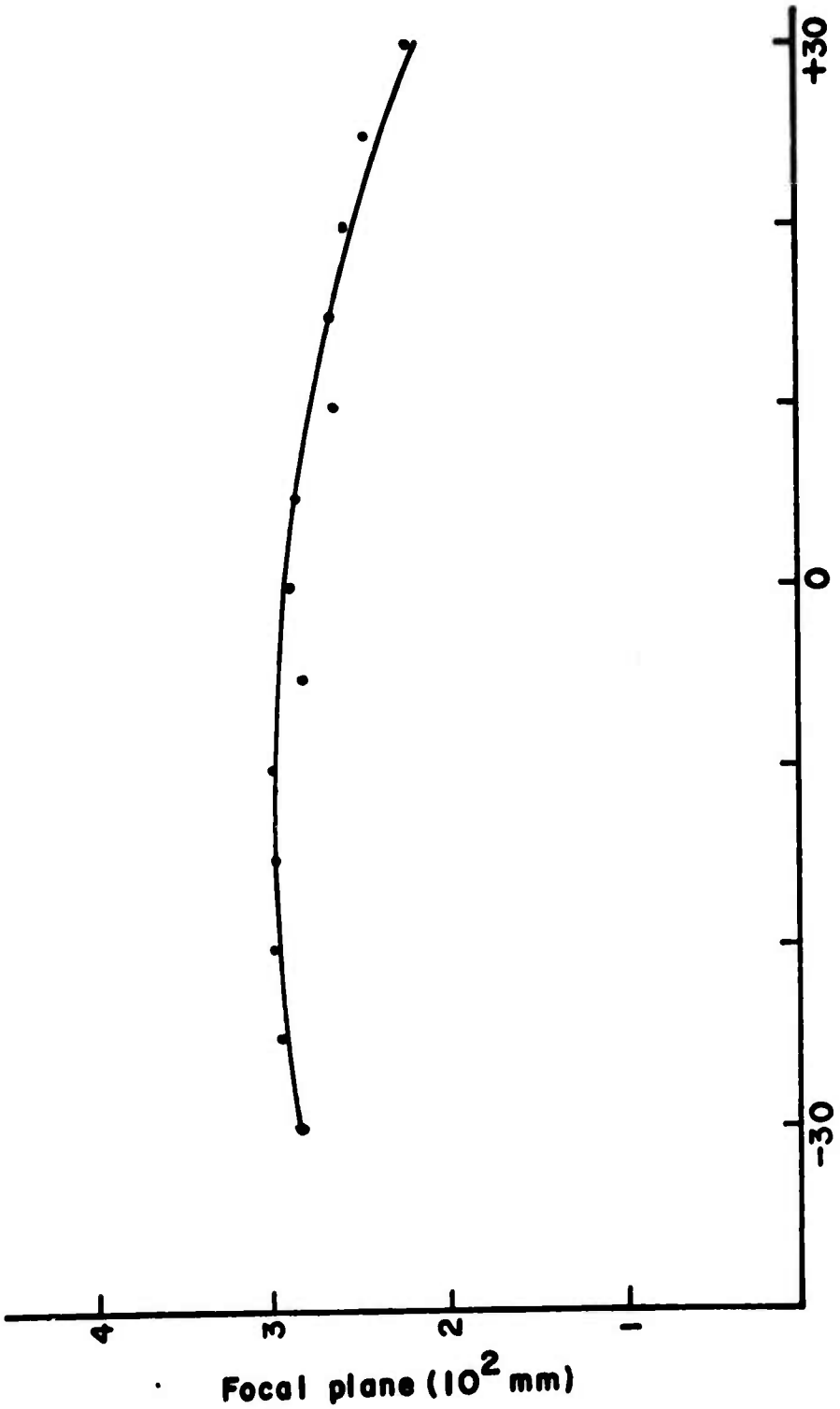

Figure 62. Plane of Best Focus vs. Object Field Angle for a Masked, Off-Axis Glass Lens Element at λ = 568.2 nm

8. DISTORTION

The distortion in the final holographic lens was determined by viewing a square matrix array through each channel. Photographs were made of the resulting images which give a fair idea of what was actually seen. The photographs are shown in figure 63 below. The distortion was found to be tolerable in the final HHUD lens.

(a)

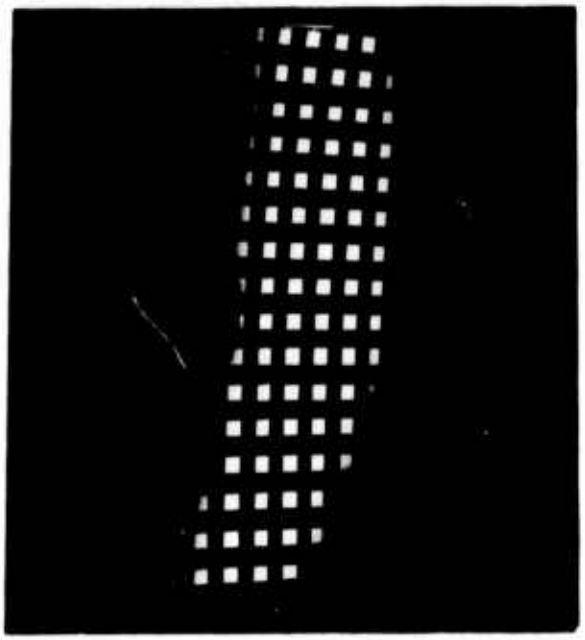

(b)

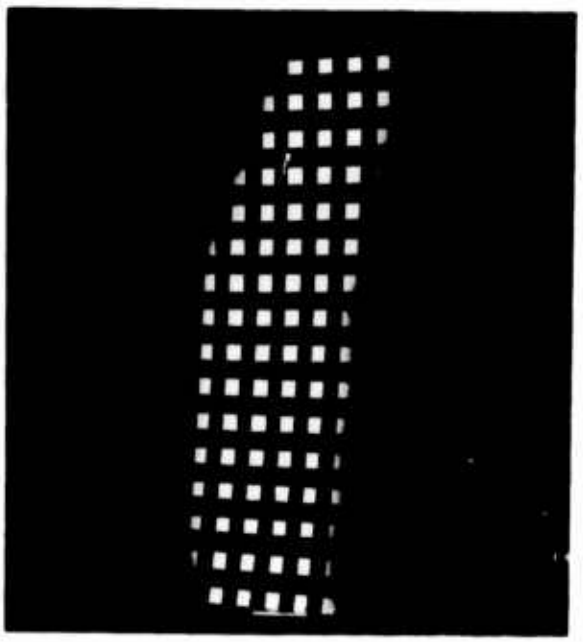

Figure 63. Images of a Square Array as Projected by the Final Lens at λ = 568.2 nm: (a) Channel 1; (b) Channel 2

9. CHROMATIC ABERRATION

The amount of chromatic aberration in the final holographic lens was determined by passing collimated light of various wavelengths through the lens and measuring the distance from the center of the lens to the sagittal focus. The results for both channels are plotted in figure 64. The chromatic aberration (from 476.2 nm to 632.8 nm) in channel 1 was 126 mm, and in channel 2 was 128 mm.

A standard Air Force resolution target was illuminated with a broadband white light source and placed at the focal point of each channel of the final lens. The holographic lens projected the target to infinity in a virtual image display. The resulting image was photographed in color in order to demonstrate the chromatic aberration. The resulting photographs are shown in figure 65.

The chromatic aberration in one holographic element was found to be intolerable for the virtual image display required. Research into doublets and triplets is required to correct this aberration.

(a)

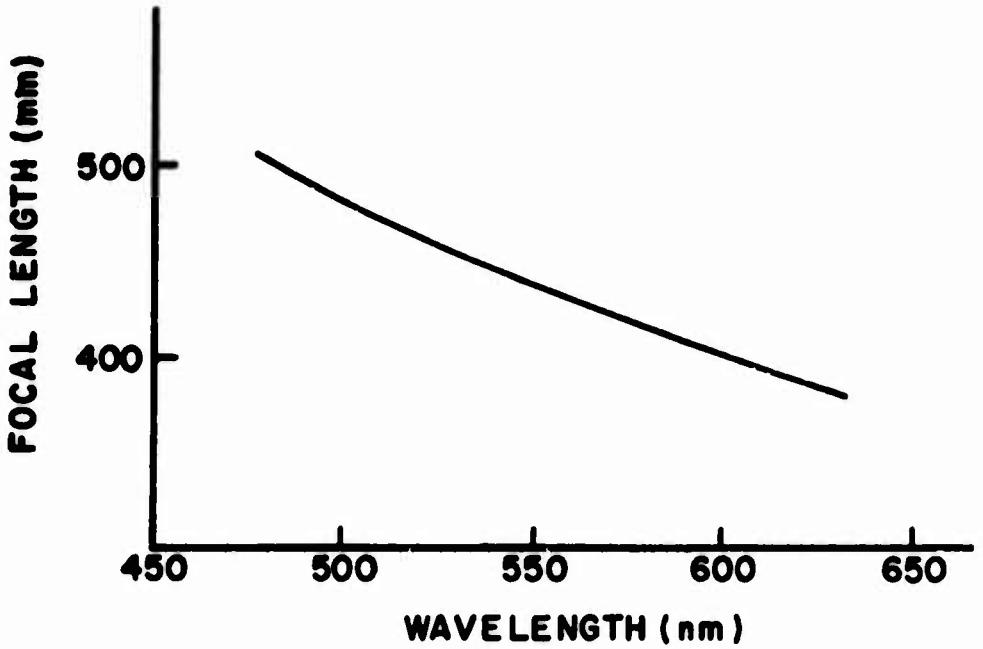

(b)

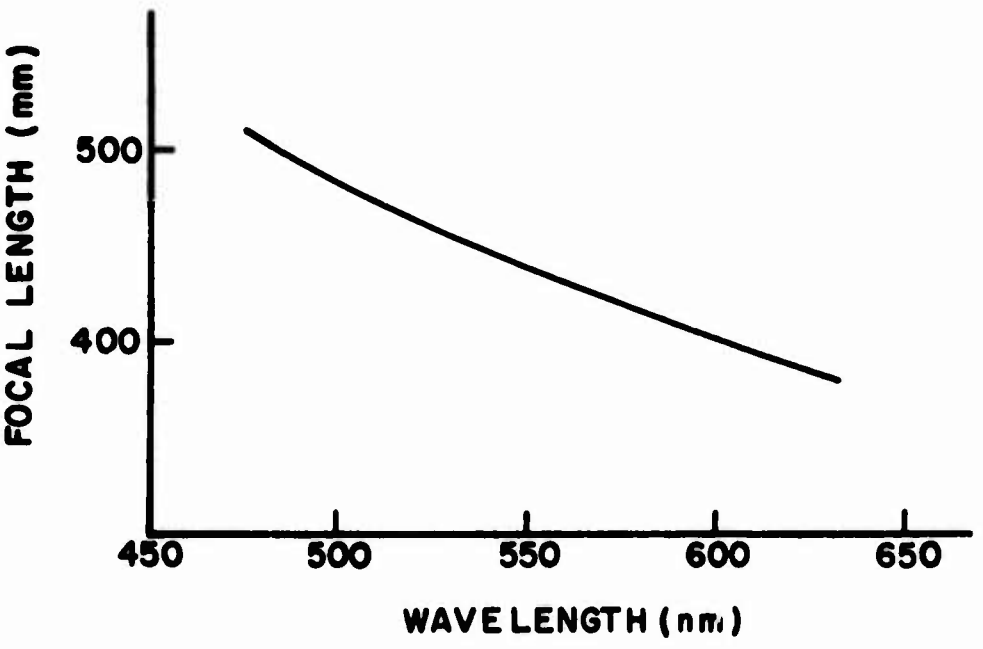

Figure 64. Chromatic Aberration in Final Holographic Lens: (a) Channel 1; (b) Channel 2

(a)

(b)

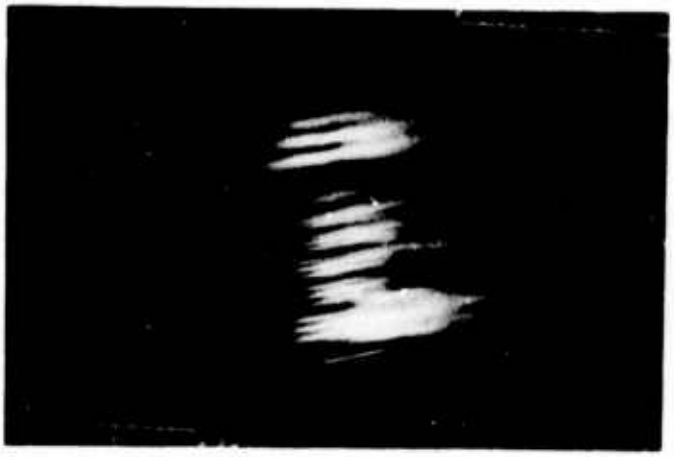

Figure 65. Photographs of Images of White Light Illuminated Resolution Targets as Projected by the Final Lens: (a) Channel 1; (b) Channel 2

10. ANGLE OF DIFFRACTION

The angle into which light was diffracted by the final holographic element was measured by passing collimated, 568.2 nm light into the lens at various object field angles and measuring the angular direction of the focal area. The results for the two channels are plotted in figures 66 and 67. The angle of focal direction is referenced to the angle of diffraction when the input light is at zero degrees. Notice that the direction of diffraction is nearly constant over 30° of the object field.

For comparison, the angle of refraction for the masked off-axis glass lens element was measured. The results of these measurements are plotted in figure 68.

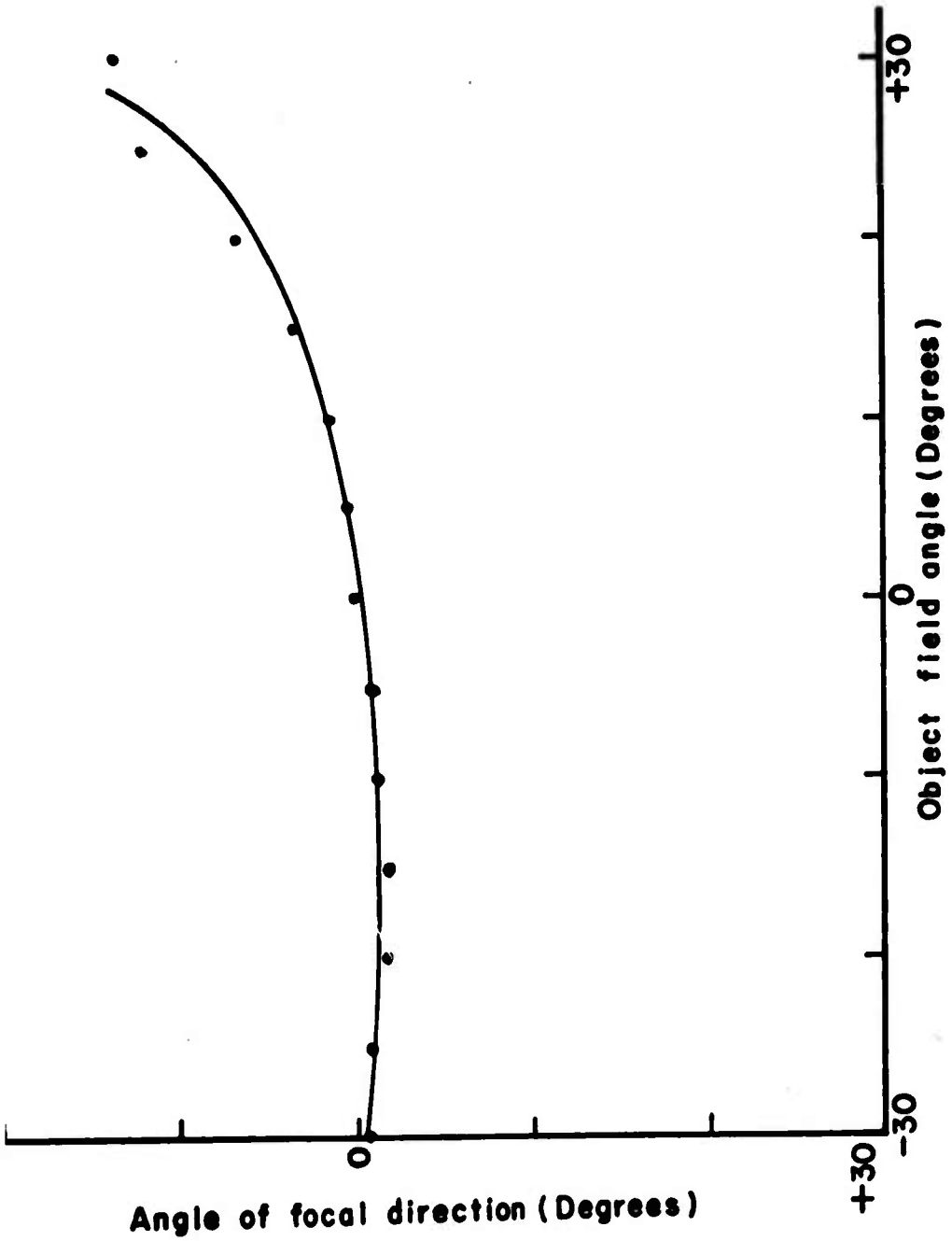

Figure 66. Angle of Diffracted Light (λ= 568.2 nm) vs. Object Field Angle for Channel 1 of Final Lens

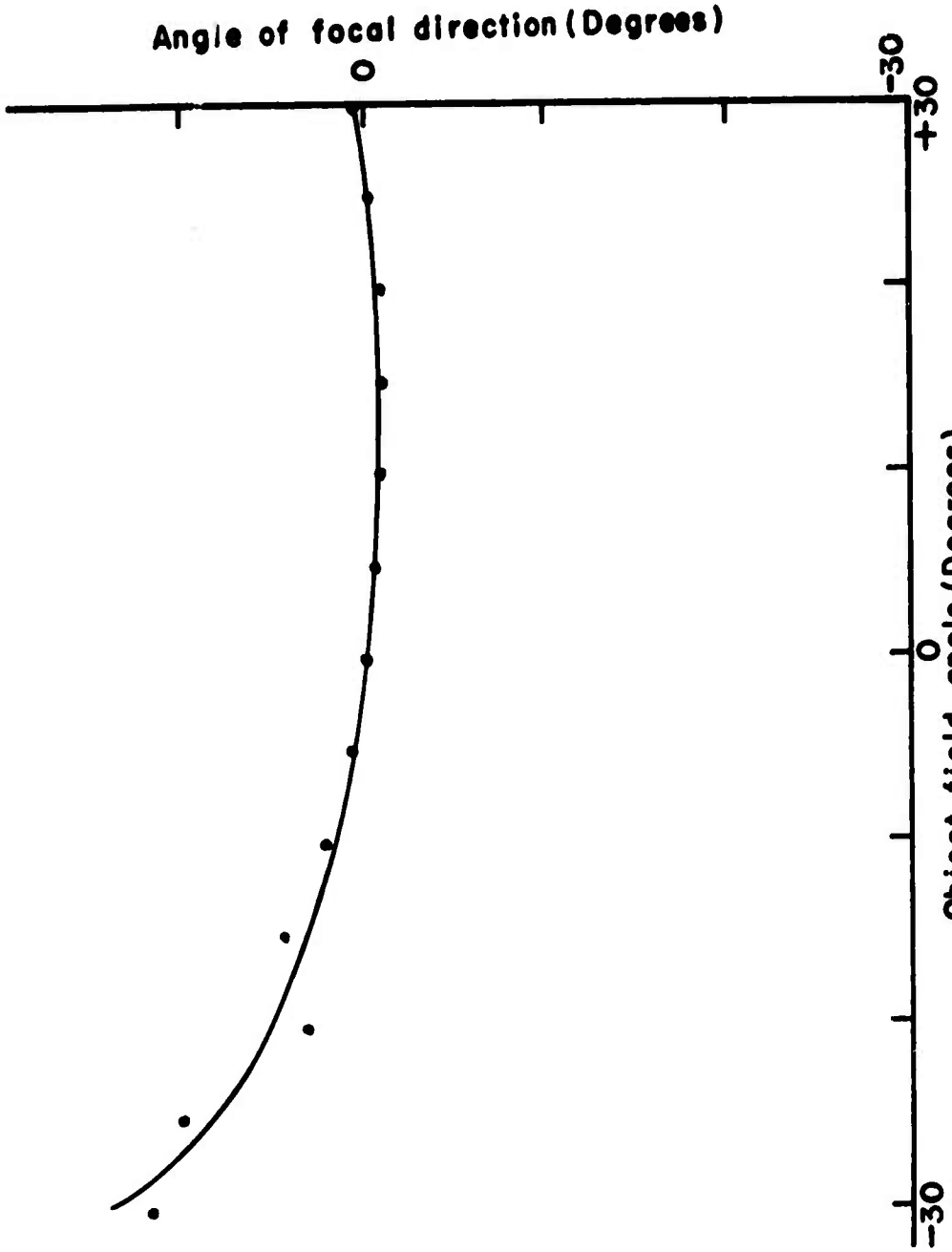

Figure 67. Angle of Diffracted Light (λ= 568.2 nm) vs. Object Field Angle for Channel 2 of Final Lens

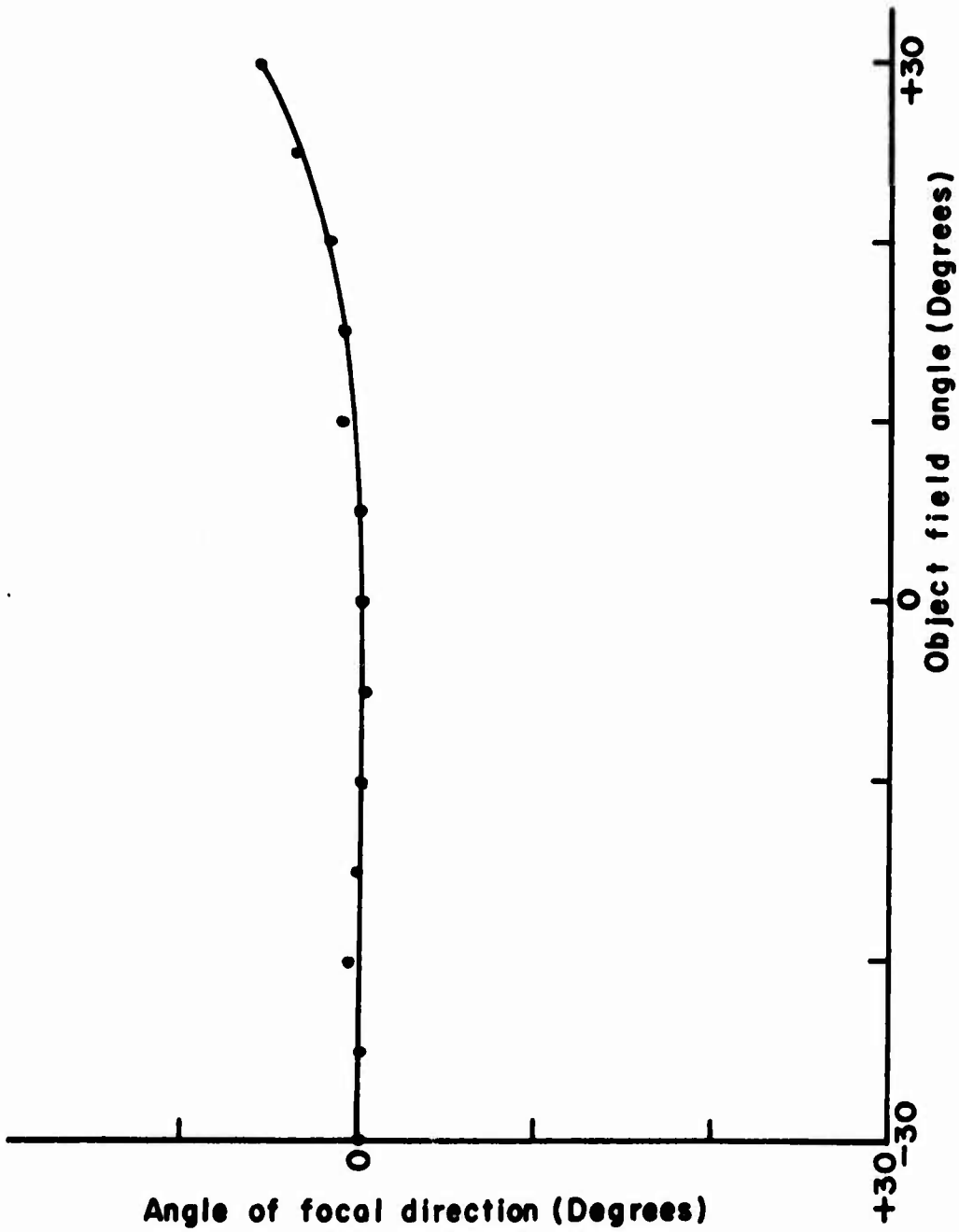

Figure 68. Angle of Diffracted Light (= 568.2 nm) vs. Object Field Angle for a Masked, Off-Axis Glass Lens

SECTION IV

CONCLUSIONS AND REMARKS

The utilization of the technology of forming lens-like holographic gratings in dichromated gelatin films has led to the fabrication of a two-channel lens system which can be incorporated in a heads-up display for training or simulation. The final display lens is capable of taking two monochromatic displays and redirecting and collimating them such that an observer sees the displays as virtual images at infinity superimposed over his direct view through the lens. The display case configuration is described in appendix C.

The design of this final display lens has been accomplished by the techniques described in this report which can also be applied to other configurations or system requirements. The dichromate processing procedures described in this report was found to be successful with the ambient conditions noted. Less involved processing may be sufficient when ambient relative humidity is 50% or less.

The evolution of the display lens, although tedious, demonstrates a useful tool for gathering hard data on image quality and aberrations and also enables some form of comparison with ordinary rotationally symmetric glass lenses.

Future efforts in this area can be directed toward incorporation of holographic optical elements in many types of optical systems used in simulators and training devices. The use of multi-channel holographic lens elements in full color displays will necessarily require much research into achromatizing such lenses.

REFERENCE:

1. McCAULEY, D.G. et al Holographic Optical Elements for Visual Display Applications Applied Optics, Feb. 1973, Vol. 12 #2 pp. 232-242
2. MEYERHOFER, D. Phase Holograms in Dichromated Gelatin, RCA Review Vol. 33 March 1972 pp. 110-130
3. BURCKHARDT, C.B. Diffraction of a Plane Wave at a Sinusoidally Stratified Dielectric Grating, Journal of the Optical Society of America, Vol. 56 #11 Nov. 1966, pp.1502-1509
4. BURCKHARDT, C.B. Efficiency of a Dielectric Grating, Journal of the Optical Society of America, Vol.57 #5 May 1967 pp.601-603
5. KOGELNIK, H. Bragg Diffraction in Hologram Grating with Multiple Internal Reflections, Journal of the Optical Society of America, Vol.57 #3 Mar 1967 pp.431-433
6. KOGELNIK,H. Reconstructing Response and Efficiency of Hologram Gratings Proceedings of the Symposium on Modern Optics, Polytechnic Institute of Brooklyn, New York, 1967 pp.605-617
7. RIGROD, W.W. Diffraction Efficiency of Nonsinusoidal, Bragg Reflection Gratings, Journal of the Optical Society of America Vol. 64 #1 Jan. 1974 pp.97-99
8. FOWLES, G.R. Introduction to Modern Optics, Holt, Rinehart, and Winston Inc. New York 1968 pp.75-78
9. BORN, M. and WOLF, E. Principles of Optics 3rd Revised Edition, Pergramon Press, New York 1965
10. GAYLORD, T.K. Optical Memories Optical Spectra, June 1974 pp.29-34
11. JAMES, T.H. and MEES, C.E. The Theory of the Photographic Process MacMillan Company Inc. New York, 1966 Chapter 3
12. STEVENS G.W.W. Microphotography John Wiley & Sons Inc. New York, 1968 Chapter 2
13. LAMBERTS, R.L. Characterization of a Bleached Photographic Material Applied Optics Vol. 11 #1 Jan. 1972 pp.33-41
14. UPATNIEKS, J. et al Diffraction Efficiency of Bleached Photographically Recorded Interference Patterns, Applied Optics Vol. 8 #1 Jan 1969 pp.85-89
15. McMAHON, D.H. et al Measurements of the Stability of Bleached Photographic Phase Holograms, Applied Optics Vol. 9#6 June 1970 pp.1363-1368
16. LAMING, F.P. et al Lifetime Extension of Bleached Holograms, Applied Optics Vol.10#5 May 1971 pp.1181-1182
17. PENNINGTON, K.S. et al New Photo Technology Suitable for Recording Phase Holograms and Similar Information in Hardened Gelatin, Applied Physics Letters Vol.18 #3 Feb. 1971 pp.80-84
18. NORMAN, S. Dye Induced Stabilization of Bleached Holograms, Applied Optics Vol. 11#5 May 1972 pp.1234-1239
19. RIGHINI, G.C. et al Low Noise and Good Efficiency Volume Holograms Applied Optics Vol. 11 #4 April 1972 pp.951-953
20. PENNINGTON, K.S. et al Techniques for Producing Low-Noise Improved Efficiency Holograms, Applied Optics Vol. 9 #7 July 1970 pp.1643-1650
21. LEHMAN, M. et al High Efficiencies, Low Noise, and Suppression of Photochromic Effects in Bleached Silver Halide Holography, Applied Optics Vol. 9 #8 Aug 1970 pp.1948
22. THIRY, H. New Techniques of Bleaching Photographic Emulsions and its Application to Holography, Applied Optics Vol.11 #7 July 1972 pp.1652-1653

REFERENCE:

23. CHENOWETH, A.J. Humidity Testing of Bleached Holograms, Applied Optics Vol. 10#4 April 1971 pp.913-915
24. UPATNIEKS, J. Efficiency and Image Contrast of Dielectric Holograms Journal of the Optical Society of America, Vol. 60#3 March 1970 pp.297-305
25. LAMBERTS, R.L. et al Reversal Bleaching for Low Flare Light in Holograms Applied Optics Vol. 10#6 June 1971 pp.1342-1347
26. COLBURN, W.S. et al Volume Hologram Formation in Photopolymer Materials Applied Optics Vol. 10#7 July 1971 pp.1636-1641
27. JENNEY, J.A. Nonlinearities of Photopolymer Holographic Recording Materials, Applied Optics Vol. 11#6 June 1972 pp.1371-1381
28. WOPSCHALL, R.H. et al Dry Photopolymer Film for Recording Holograms Applied Optics Vol. 11#9 Sept 1972 pp.2096-2097
29. BOOTH, B.L. Photopolymer Material for Holography, Applied Optics Vol.11 #12 Dec 1972 pp.2994-2995
30. BOOTH, B.L. Exposure Instructions and Characteristics of Dupont Holographic Photopolymer Materials,Engineering Physics Laboratory E.I. Dupont De Nemours & Company
31. SHANKOFF, T.A. et al Efficient, High Resolution Phase Diffraction Gratings Applied Physics Letters Vol. 13 #7 Oct 1968 pp.239-241
32. SHANKOFF, T.A. Phase Holograms in Dichromated Gelatin, Applied Optics Vol. 7 #10 Oct. 1968 pp.2101-2105
33. LIN, L.H. Hologram Formation in Hardened Dichromated Gelatin, Applied Optics Vol. 8 #5 May 1969 pp.963-966
34. BRANDES, R.G. et al Preparation of Dichromated Gelatin Films for Holography,Applied Optics Vol. 8 #11 Nov. 1969 pp.2346-2348
35. CURRAN, R.K. et al The Mechanism for Hologram Formation in Dichromated Gelatin, Applied Optics Vol. 9 #7 July 1970 pp.1651-1657
36. SOSNOWSKI, T.P. et al Ultraviolet Hologram Recorded in Dichromated Gelatin, Applied Optics Vol. 9 #9 Sept. 1970 pp.2186-2187
37. MEYERHOFER, D. Spatial Resolution of Relief Holograms in Dichromated Gelatin, Applied Optics Vol.10 #2 Feb 1971 pp.416-421
38. CHANG, M. Dichromated Gelatin of Improved Optical Quality, Applied Optics Vol. 10 #11 Nov. 1971 pp.2550-2551
39. VILKOMERSON, D. et al Some Effects of Emulsion Shrinkage on a Hologram's Image Space, Applied Optics Vol. 6 #7 July 1967 pp.1270-1272
40. MEIER,W. REINHARD Magnification and Third-Order Aberrations in Holography Journal of the Optical Society of America, Vol.55 #8 Aug 1965 pp.987
41. ROSE, W. HAROLD Holographic Lens Systems,Air Force Avionics Laboratory, Wright-Patterson Air Force Base, Ohio, Technical Report AFAL-TR-73-101, March 1973
42. ROSENDAHL, R. GOTTFRIED A New Derivation of Third-Order Aberration Coefficients, Applied Optics Vol.6 #4 April 1967 pp.765
43. CHAMPAGNE, EDWIN BERNARD A Qualitative and Quantitative Study of Holographic Imaging, Air Force Avionics Laboratory, Wright-Patterson Air Force Base Ohio, Technical Report AFAL-TR-67-107, July 1967
44. TATIAN, BERGE Aberration Balancing in Rotationally Symmetric Lenses Itek Corporation, Lexington, Massachusetts 1973
45. MOHON, NEIL Aberrations in Holographic Lenses, Technical Note TN-40, Naval Training Equipment Center, Orlando, Florida July 1973

REFERENCE:

46. MEIER, W. REINHARD Cardinal Points and the Novel Imaging Properties of a Holographic System, Journal of the Optical Society of America, Vol.56 #2 Feb. 1966 pp.219
47. UPATNIEKS, JURIS, et al Correction of Lens Aberrations by Means of Holograms, Applied Optics, Vol.5 #4 April 1966 pp.589
48. JOBIN, YVON OPTICAL SYSTEMS, Diffraction Gratings Ruled and Holographic-Handbook, Metuchen, New Jersey, 1973
49. ASAKURA, TOSHIMITSU Diffraction of Partially Coherent Light By High Numerical Aperture Systems With Sperical Aberration and Defocusing (II) Optik, Vol.38 #4 1973 pp.325
50. JENKINS, A. FRANCIS et al Fundamentals of Optics, McGraw-Hill Book Company, New York, 1957
51. CHAMPAGNE, B. EDWIN Nonparaxial Imaging, Magnification, and Aberration Properties in Holography, Journal of the Optical Society of America, Vol 57 #1 Jan 1967 pp.51
52. YU, F.T.S. Observation, Information, and Optical Synthetic Aperture of Spherical Lenses, Optik, Vol.38 #4 1973 pp.425
53. OELFKE, C.WILLIAM Heads Up Display System Using Nonparaxial Holographic Lenses, Naval Training Equipment Center, Orlando, Florida, Technical Note TN-38, Sept. 1973
54. Optical Design, Military Handbook 141, Defense Supply Agency, Washington, DC. October 1962
55. COLLIER, ROBERT J. et al Optical Holography, Academic Press, New York, 1971
56. SMITH, HOWARD M. Principles of Holography, Wiley Interscience, New York, 1969
57. FORSHAW, M.R.B. The Imaging Properties and Aberrations of thick Transmission Holograms, Optica Acta, Vol.20 #9 1973, pp.669
58. BARAKAT, RICHARD The Aberrations of Non-Rotationally Symmetric Systems and Their Diffraction Effects, Optica Acta, Vol.13 #1 1966 pp.1-30
59. KINGSLAKE, RUDOLF Applied Optics and Optical Engineering, Academic Press New York, 1969
60. DELANO, ERWIN Primary Aberrations of Fresnel Lenses, Journal of the Optical Society of America, Vol.64 #4 April 1974 pp.459
61. CAGNET, MICHEL et al Atlas of Optical Phenomena, Prentice Hall, Englewood Cliffs, New Jersey, 1962
62. GALPERN, YU D. et al Chromatic Aberrations of Real Rays, Opt. Spektrosk, Vol.34 Feb 1973 pp.375
63. LATTA, JOHN N. Computer Based Analysis of Hologram Imagery and Aberrations I,Applied Optics, Vol.10 #3 March 1971 pp.599
64. LATTA,JOHN N. Computer Based Analysis of Hologram Imagery and Aberrations II, Applied Optics, Vol.10 #3 March 1971 pp.609
65. BURCKHARDT, C.B. et al A Bleach Process for High Efficiency Low Noise Holograms, Applied Optics, Vol.8 #12 Dec. 1969 pp.2479-2482
66. CHAMPAGNE, EDWIN B. Resolution in Holography, Applied Optics, Vol.8 #9 Sept. 1969 pp.1879

APPENDIX A

Processing Procedures

BLEACH PROCESS[21]

1. Expose for silver density of 2.5 to 3.0
2. Preharden - SH-5 - 3 minutes
3. Develop - HRP developer
4. Stop - Acid stop bath - 15 seconds
5. Fix - Fixol - 3 minutes
6. Rinse - distilled water - 10 minutes
7. Bleach - 5% cupric bromide - bleach - 7 minutes
8. Rinse - distilled water - 30 seconds
9. Clear - 1 part (a) to 10 parts (b)

   (a) Potassium Permanganate - 5g.

   Distilled water - 1 liter

   (b) Sulfuric acid - 10 cm^3

   Potassium Bromide - 40 cm^3

   Distilled water - 1 liter
10. Wash - distilled water - 10 minutes
11. Dry slowly at room temperature.

BLEACH PROCESS[20]

1. Stress relieve
2. Dry and store
3. Expose
4. Preharden - SH-5 - 10 minutes
5. Wash - deionized water - 3 minutes
6. Develop - D-19 - 5 minutes
7. Short-stop - 1 minute

8. Fix - fixer - 4 minutes
9. Wash - deionized water - 10 minutes
10. Bleach - EB-2 - Clear + 2 minutes
11. Wash - deionized water - 5 minutes
12. 50% ethyl alcohol - 2 minutes
    50% deionized water
13. 75% ethyl alcohol - 2 minutes
    25% deionized water
14. 90% ethyl alcohol - 2 minutes
    10% deionized water
15. Dry - normal atmosphere.

BLEACH PROCESS[65]

1. Expose
2. Develop - D76
3. Fix - rapidfixer - 5 minutes
4. Wash - water - 10 minutes
5. Bleach - 20g Potassium Ferricyanide - 5 minutes
    10g Sodium Cabonate
    1ℓ Distilled water
6. Wash - water - 10 minutes
7. Soak - Formula 30 Ethyl Alcohol - 3 minutes
8. Soak - 200 proof Ethyl Alcohol - 5 minutes
9. Dry - Dry Nitrogen - 15 minutes.

BLEACH-DICHROMATE PROCESS[17]

1. Stress relieve - suspend plates overnight, high humidity
2. Dry and store
3. Expose
4. Preharden - SH-5 - 2 minutes
5. Wash - deionized water - 3 minutes
6. Develop - D-19 w/Nitrogen Burst - 5 minutes

7. Short-stop - 30-60 seconds
8. Fix - Fixer (no hardener) - 2-5 minutes
9. Wash - Deionized water - 10 minutes
10. Bleach - Cupric Halide - Clear + 2 minutes
    OR R-10
    OR Ferricyanide
11. Wash - deionized water - 5 minutes
12. Sensitize - Ammonium Dichromate 4 - 16% - 4-5 minutes
13. Dry - Room temperature + humidity
14. Expose - 488.0nm at Bragg angle
15. Wash & Clear - 20% sodium bisulfite - to clear
16. Wash - deionized water - 3 minutes
17. Fix - fixer - 1-2 minutes
18. Wash - deionized water - 3 minutes
19. Wash - water 64°C - 15-45 minutes
20. Soak - Boiling Isopropanol - 30-60 seconds
21. Dry - Dry Nitrogen

DICHROMATE PROCESS[38]

649F Plates

1. Fix - Part A Rapid Fixer - 10 minutes
2. Wash - Water - 15 minutes
   Start 21°C
   Raise at 1.5°C/minute to 35°C
3. Dry - Air - 1 minute
4. Rinse - Distilled water - 30 seconds
   2 drops/liter Photo-Flo 600
5. Dry - Air - Complete
6. Soak - Water - room temperature - 2 minutes
7. Fix - Rapid Fixer - 10 minutes
8. Wash - Water - 21°C - 15 minutes

9. Rinse - Same as (4.) - 30 seconds

10. Dry - Air 21-22°C - Overnight

11. Sensitize - 5-10% Ammonium Dichromate - 5 minutes
w/2 drops/liter Photo-Flo 600

12. Dry - Air - Room temperature

13. Clean - remove crystals from back of plate

14. Expose

15. Wash - water 21°C - 5 minutes

16. Dry - Isopropanol - 2 minutes

DICHROMATE PROCESS[2]

649F Plates

A. PREPARATION

1.	Fix	Fixer w/Hardener	15 minutes
2.	Wash	Water	10 minutes
3.	Soak	Methanol	10 minutes
4.	Soak	Fresh Methanol	10 minutes
5.	Dry	Air vertical	

B. PREPARE SENSITIZER

1.	Mix	50g/liter Ammonium Dichromate Fine crystals w/distilled water	
2.	Filter		

C. SENSITIZE

1.	Soak	Dichromate solution	5 minutes
2.	Dry	Tilt Plate 10°	
3.	Store	Same tilt as (2.)	
4.	Expose	Between 15 and 40 hours after sensitizing	

D. PROCESS

1.	Wash	Water	10 minutes

2.	Soak	50/50 Isopropanol/water	2 minutes
3.	Soak	90/10 Isopropanol/water	2 minutes
4.	Soak	Isopropanol	10-20 minutes
5.	Dry	Pull plate @ 1cm/min w/warm air	

DICHROMATE PROCESS[1]

649-F Plates

1.	Fix	Rapid Fixer w/Hardener	5 minutes
2.	Wash	Running water 16-20°C	25 minutes
3.	Wash	Methanol Fresh methanol	5 minutes 3 minutes
4.	Sensitize	Ammonium Dichromate 0.5 to 10.0%	10 minutes
5.	Wash	5 drops/liter Photo-Flo 200	1 second
6.	Dry	21°C 24% R.H.	Overnight
7.	Expose		
8.	Wash	Running water 16-20°C	15 minutes
9.	Soak	Isopropanol	2 minutes
10.	Dry	21°C 20-24% R.H.	

Appendix B

The Computer Program

1. OPERATION INSTRUCTIONS

a. Enter the program into the Wang 720 programmable electronic desk calculator. Verify #8474.

b. Enter the required data into the registers listed below:

Register	Symbol	Name
00 00	X_o	X coordinate of object point
00 01	Y_o	Y coordinate of object point
00 02	Z_o	Z coordinate of object point
00 03	X_R	X coordinate of reference point
00 04	Y_R	Y coordinate of reference point
00 05	Z_R	Z coordinate of reference point
00 06	X_c	X coordinate of readout point
00 07	Y_c	Y coordinate of readout point
00 08	Z_c	Z coordinate of readout point
00 09	μ	Wavelength ratio
00 10	m	hologram scaling
00 11	1	constant
00 12	1	constant
00 13	cos θ	aperture angle
00 14	sin θ	aperture angle
00 15	ρ	aperture height
20 05	Z_i	focal plane

c. Key in "Search 3" to calculate:

(1) The X_i coordinate of the light ray in the Z_i focal plane, when $\theta = 0°$

(2) The Y_i coordinate of the light ray in the Z_i focal plane, when $\theta = 90°$.

d. Key in "Search 6" to calculate the total wavefront error in the diffracted wavefront.

e. The following data concerning the diffracted ray may be recalled from the respective registers:

Register	Symbol	Name
10 06	S'	Third order spherical aberration
10 07	C'_x	Third order coma, X
10 08	C'_y	Third order coma, Y
10 09	A'_x	Third order astigmatism, X
20 00	A'_y	Third order astigmatism, Y
20 01	F'	Third order field curvature
20 02	D'_x	Third order distortion, X
20 03	D'_y	Third order distortion, Y
20 04	$\partial W/\partial \rho$	Third order ray slope
20 05	Z_i	Focal plane
20 06	$X_i(Y_i)$	Ray height in Z_i
20 07	Z_{ref}	Focal Plane of reference sphere
20 08	a_{ref}	X coordinate of reference sphere
20 09	b_{ref}	Y coordinate of reference sphere
30 00	S	Total spherical aberration
30 01	C_x	Total coma, X
30 02	C_y	Total Coma, Y
30 03	A_x	Total astigmatism, X
30 04	A_y	Total astigmatism, Y
30 05	F	Total field curvature
30 06	D_x	Total distortion, X
30 07	D_y	Total distortion, Y
40 01	$(\partial W/\partial \rho)'$	First order ray slope
40 02	ΔW	Total wavefront error.

2. PROGRAM STEPS.

(See listing next page)

I. Calculation of the third order portion of the ray slope

A. Calculation of the spherical aberration component

0000	04 08	mark
0001	07 03	"3"
0002	04 15	recall into Y
0003	00 09	register ØØ Ø9
0004	04 05	Recall into X
0005	00 12	Register ØØ 12
0006	06 03	Divide Y by X
0007	06 03	Divide Y by X
0008	06 03	Divide Y by X
0009	04 05	Recall in X
0010	00 10	Register ØØ 1Ø
0011	07 13	Square X
0012	07 13	Square X
0013	06 03	Divide Y by X
0014	04 05	Recall into X
0015	00 02	Register ØØ Ø2
0016	06 03	Divide Y by X
0017	06 03	Divide Y by X
0018	07 11	Change sign of X
0019	06 03	Divide Y by X
0020	04 14	Store Y in
0021	01 06	Register 1Ø Ø6

B. Calculation of the coma component in the x-direction

0022	04 15	Recall into Y
0023	00 09	Register ØØ Ø9
0024	04 05	Recall into X
0025	00 12	Register ØØ 12
0026	06 03	Divide Y by X
0027	06 03	Divide Y by X
0028	06 03	Divide Y by X
0029	04 05	Recall into X
0030	00 11	Register ØØ 11
0031	06 03	Divide Y by X

0032	04 05	Recall into X
0033	00 10	Register ØØ 1Ø
0034	06 03	Divide Y by X
0035	06 03	Divide Y by X
0036	06 03	Divide Y by X
0037	04 05	Recall into X
0038	00 02	Register ØØ Ø2
0039	06 03	Divide Y by X
0040	06 03	Divide Y by X
0041	07 11	Change sign of X
0042	06 03	Divide Y by X
0043	04 14	Store Y in
0044	04 00	Register 4Ø ØØ
0045	04 05	Recall into X
0046	00 00	Register ØØ ØØ
0047	06 02	Multiply Y by X
0048	04 14	Store Y in
0049	01 07	Register 1Ø Ø7

C. Calculation of the coma component in the y-direction

0050	04 15	Recall into Y
0051	04 00	Register 4Ø ØØ
0052	04 05	Recall into X
0053	00 01	Register ØØ Ø1
0054	06 02	Multiply Y by X
0055	04 14	Store Y in
0056	01 08	Register 1Ø Ø8

D. Calculation of the astigmatism component in the x-direction

0057	04 15	Recall into Y
0058	00 09	Register ØØ Ø9
0059	04 05	Recall into X
0060	00 12	Register ØØ 12
0061	06 03	Divide Y by X
0062	06 03	Divide Y by X
0063	06 03	Divide Y by X
0064	04 05	Recall into X

0065	00 11	Register ØØ 11
0066	06 03	Divide Y by X
0067	06 03	Divide Y by X
0068	04 05	Recall into X
0069	00 10	Register ØØ 1Ø
0070	06 03	Divide Y by X
0071	06 03	Divide Y by X
0072	04 05	Recall into X
0073	00 02	Register ØØ Ø2
0074	06 03	Divide Y by X
0075	06 03	Divide Y by X
0076	07 11	Change sign of X
0077	06 03	Divide Y by X
0078	04 14	Store Y in
0079	04 00	Register 4Ø ØØ
0080	04 05	Recall into X
0081	00 00	Register ØØ ØØ
0082	06 02	Multiply Y by X
0083	06 02	Multiply Y by X
0084	04 14	Store Y in
0085	01 09	Register 1Ø Ø9

E. Calculation of the astigmatism component in the y-direction

0086	04 15	Recall into X
0087	04 00	Register 4Ø ØØ
0088	04 05	Recall into X
0089	00 01	Register ØØ Ø1
0090	06 02	Multiply Y by X
0091	06 02	Multiply Y by X
0092	04 14	Store Y in
0093	02 00	Register 2Ø ØØ

F. Calculation of the field curvature component

0094	04 05	Recall into X
0095	00 00	Register ØØ ØØ
0096	07 13	Square X
0097	06 04	Move X up to Y

0098	04 05	Recall into X
0099	00 01	Register ØØ Ø1
0100	07 13	Square X
0101	06 00	Add X to Y
0102	04 05	Recall into X
0103	00 09	Register ØØ Ø9
0104	06 02	Multiply Y by X
0105	04 05	Recall into X
0106	00 12	Register ØØ 12
0107	06 03	Divide Y by X
0108	06 03	Divide Y by X
0109	06 03	Divide Y by X
0110	04 05	Recall into X
0111	00 11	Register ØØ 11
0112	06 03	Divide Y by X
0113	06 03	Divide Y by X
0114	04 05	Recall into X
0115	00 10	Register ØØ 1Ø
0116	06 03	Divide Y by X
0117	06 03	Divide Y by X
0118	04 05	Recall into X
0119	00 02	Register ØØ Ø2
0120	06 03	Divide Y by X
0121	06 03	Divide Y by X
0122	07 11	Change sign of X
0123	06 03	Divide Y by X
0124	04 14	Store Y in
0125	02 01	Register 2Ø Ø1

G. Calculation of the distortion component in the x-direction

0126	04 05	Recall into X
0127	00 06	Register ØØ Ø6
0128	06 04	Move X to Y
0129	06 02	Multiply Y by X
0130	06 02	Multiply Y by X
0131	04 14	Store Y in

0132	04 00	Register 4Ø ØØ
0133	06 04	Move X to Y
0134	04 05	Recall into X
0135	00 07	Register ØØ Ø7
0136	06 02	Multiply Y by X
0137	06 02	Multiply Y by X
0138	04 05	Recall into X
0139	04 00	Register 4Ø ØØ
0140	06 00	Add X to Y
0141	04 05	Recall into X
0142	00 08	Register ØØ Ø8
0143	06 03	Divide Y by X
0144	06 03	Divide Y by X
0145	06 03	Divide Y by X
0146	04 14	Store Y into
0147	02 02	Register 2Ø Ø2
0148	04 05	Recall into X
0149	00 00	Register ØØ ØØ
0150	06 04	Move X to Y
0151	06 02	Multiply Y by X
0152	06 02	Multiply Y by X
0153	04 14	Store Y into
0154	04 00	Register 4Ø ØØ
0155	06 04	Move X to Y
0156	04 05	Recall into X
0157	00 01	Register ØØ Ø1
0158	06 02	Multiply Y by X
0159	06 02	Multiply Y by X
0160	04 05	Recall into X
0161	04 00	Register 4Ø ØØ
0162	06 00	Add X to Y
0163	04 05	Recall into X
0164	00 09	Register ØØ Ø9
0165	06 02	Multiply Y by X
0166	04 05	Recall into X

0167	00 12	Register ØØ 12
0168	06 03	Divide Y by X
0169	06 03	Divide Y by X
0170	06 03	Divide Y by X
0171	04 05	Recall in X
0172	00 11	Register ØØ 11
0173	06 03	Divide Y by X
0174	06 03	Divide Y by X
0175	06 03	Divide Y by X
0176	04 05	Recall into X
0177	00 10	Register ØØ 1Ø
0178	06 03	Divide Y by X
0179	04 05	Recall into X
0180	00 02	Register ØØ Ø2
0181	06 03	Divide Y by X
0182	06 03	Divide Y by X
0183	06 03	Divide Y by X
0184	06 05	Move Y into X
0185	04 01	Divide X into
0186	02 02	Register 2Ø Ø2
0187	04 05	Recall into X
0188	00 03	Register ØØ Ø3
0189	06 04	Move X to Y
0190	06 02	Multiply Y by X
0191	06 02	Multiply Y by X
0192	04 14	Store Y in
0193	04 00	Register 4Ø ØØ
0194	06 04	Move X to Y
0195	04 05	Recall in X
0196	00 04	Register ØØ Ø4
0197	06 02	Multiply Y by X
0198	06 02	Multiply Y by X
0199	04 05	Recall into X
0200	04 00	Register 4Ø ØØ
0201	06 00	Add X to Y

0202	04 05	Recall into X
0203	00 09	Register ØØ Ø9
0204	06 02	Multiply Y by X
0205	04 05	Recall into X
0206	00 12	Register ØØ 12
0207	06 03	Divide Y by X
0208	06 03	Divide Y by X
0209	06 03	Divide Y by X
0210	04 05	Recall into X
0211	00 11	Register ØØ 11
0212	06 03	Divide Y by X
0213	06 03	Divide Y by X
0214	06 03	Divide Y by X
0215	04 05	Recall into X
0216	00 10	Register ØØ 1Ø
0217	06 03	Divide Y by X
0218	04 05	Recall into X
0219	00 05	Register ØØ Ø5
0220	06 03	Divide Y by X
0221	06 03	Divide Y by X
0222	06 03	Divide Y by X
0223	06 05	Move Y into X
0224	04 00	Add X to
0225	02 02	Register 2Ø Ø2

H. Calculation of the distortion component in the y-direction

0226	04 05	Recall into X
0227	00 07	Register ØØ Ø7
0228	06 04	Move X to Y
0229	06 02	Multiply Y by X
0230	06 02	Multiply Y by X
0231	04 14	Store Y in
0232	04 00	Register 4Ø ØØ
0233	06 04	Move X to Y
0234	04 05	Recall into X
0235	00 06	Register ØØ Ø6

0236	06 02	Multiply Y by X
0237	06 02	Multiply Y by X
0238	04 05	Recall into X
0239	04 00	Register 4Ø ØØ
0240	06 00	Add X to Y
0241	04 05	Recall into X
0242	00 08	Register ØØ Ø8
0243	06 03	Divide Y by X
0244	06 03	Divide Y by X
0245	06 03	Divide Y by X
0246	04 14	Store Y in
0247	02 03	Register 2Ø Ø3
0248	04 05	Recall into X
0249	00 01	Register ØØ Ø1
0250	06 04	Move X to Y
0251	06 02	Multiply Y by X
0252	06 02	Multiply Y by X
0253	04 14	Store Y in
0254	04 00	Register 4Ø ØØ
0255	06 04	Move X into Y
0256	04 05	Recall into X
0257	00 00	Register ØØ ØØ
0258	06 02	Multiply Y by X
0259	06 02	Multiply Y by X
0260	04 05	Recall into X
0261	04 00	Register 4Ø ØØ
0262	06 00	Add X to Y
0263	04 05	Recall into X
0264	00 09	Register ØØ Ø9
0265	06 02	Multiply Y by X
0266	04 05	Recall into X
0267	00 12	Register ØØ 12
0268	06 03	Divide Y by X
0269	06 03	Divide Y by X
0270	06 03	Divide Y by X

0271	04 05	Recall into X
0272	00 11	Register ØØ 11
0273	06 03	Divide Y by X
0274	06 03	Divide Y by X
0275	06 03	Divide Y by X
0276	04 05	Recall into X
0277	00 10	Register ØØ 1Ø
0278	06 03	Divide Y by X
0279	04 05	Recall into X
0280	00 02	Register ØØ Ø2
0281	06 03	Divide Y by X
0282	06 03	Divide Y by X
0283	06 03	Divide Y by X
0284	06 05	Move Y into X
0285	04 01	Subtract X from
0286	02 03	Register 2Ø Ø3
0287	04 05	Recall into X
0288	00 04	Register ØØ Ø4
0289	06 04	Move X into Y
0290	06 02	Multiply Y by X
0291	06 02	Multiply Y by X
0292	04 14	Store Y into
0293	04 00	Register 4Ø ØØ
0294	06 04	Move X into Y
0295	04 05	Recall into X
0296	00 03	Register ØØ Ø3
0297	06 02	Multiply Y by X
0298	06 02	Multiply Y by X
0299	04 05	Recall into X
0300	04 00	Register 4Ø ØØ
0301	06 00	Add X to Y
0302	04 05	Recall into X
0303	00 09	Register ØØ Ø9
0304	06 02	Multiply Y by X
0305	04 05	Recall into X

0306	00 12	Register ØØ 12
0307	06 03	Divide Y by X
0308	06 03	Divide Y by X
0309	06 03	Divide Y by X
0310	04 05	Recall into X
0311	00 11	Register ØØ 11
0312	06 03	Divide Y by X
0313	06 03	Divide Y by X
0314	06 03	Divide Y by X
0315	04 05	Recall into X
0316	00 10	Register ØØ 1Ø
0317	06 03	Divide Y by X
0318	04 05	Recall into X
0319	00 05	Register ØØ Ø5
0320	06 03	Divide Y by X
0321	06 03	Divide Y by X
0322	06 03	Divide Y by X
0323	06 05	Move Y into X
0324	04 00	Add X to
0325	02 03	Register 2Ø Ø3

II. Calculation of the ray slope using first and third order portions

A. Finding the ray slope

0326	04 15	Recall into Y
0327	01 06	Register 1Ø Ø6
0328	04 05	Recall into X
0329	00 15	Register ØØ 15
0330	06 02	Multiply Y by X
0331	06 02	Multiply Y by X
0332	06 02	Multiply Y by X
0333	07 02	Put a 2 into X
0334	07 11	Change sign of X
0335	06 03	Divide Y by X
0336	04 14	Store Y into
0337	02 04	Register 2Ø Ø4
0338	04 15	Recall into Y

0339	01 07	Register 1Ø Ø7
0340	04 05	Recall into X
0341	00 13	Register ØØ 13
0342	06 02	Multiply Y by X
0343	04 14	Store Y into
0344	04 00	Register 4Ø ØØ
0345	04 15	Recall into Y
0346	01 08	Register 1Ø Ø8
0347	04 05	Recall into X
0348	00 14	Register ØØ 14
0349	06 02	Multiply Y by X
0350	04 05	Recall into X
0351	04 00	Register 4Ø ØØ
0352	06 00	Add X into Y
0353	04 05	Recall into X
0354	00 15	Register ØØ 15
0355	06 02	Multiply Y by X
0356	06 02	Multiply Y by X
0357	07 03	Enter a 3 into X
0358	06 02	Multiply Y by X
0359	07 02	Enter a 2 into X
0360	06 03	Divide Y by X
0361	06 05	Move Y into X
0362	04 00	Add X to
0363	02 04	Register 2Ø Ø4
0364	04 15	Recall into Y
0365	01 09	Register 1Ø Ø9
0366	04 05	Recall into X
0367	00 13	Register ØØ 13
0368	07 13	Square X
0369	06 02	Multiply Y by X
0370	04 14	Store Y into
0371	04 00	Register 4Ø ØØ
0372	04 15	Recall into Y
0373	02 00	Register 2Ø ØØ

0374	04 05	Recall into X
0375	00 14	Register ØØ 14
0376	07 13	Square X
0377	06 02	Multiply Y by X
0378	06 05	Move Y into X
0379	04 00	Add X to
0380	04 00	Register 4Ø ØØ
0381	04 15	Recall into Y
0382	01 09	Register 1Ø Ø9
0383	04 05	Recall into X
0384	02 00	Register 2Ø ØØ
0385	06 02	Multiply Y by X
0386	04 05	Recall in X
0387	00 14	Register ØØ 14
0388	06 02	Multiply Y by X
0389	04 05	Recall into X
0390	00 13	Register ØØ 13
0391	06 02	Multiply Y by X
0392	07 02	Enter a 2 into X
0393	06 02	Multiply Y by X
0394	04 05	Recall into X
0395	04 00	Register 4Ø ØØ
0396	06 00	Add X to Y
0397	04 05	Recall into X
0398	00 15	Register ØØ 15
0399	06 02	Multiply Y by X
0400	06 05	Move Y into X
0401	04 01	Subtract X from
0402	02 04	Register 2Ø Ø4
0403	04 15	Recall into Y
0404	02 01	Register 2Ø Ø1
0405	04 05	Recall into X
0406	00 15	Register ØØ 15
0407	06 02	Multiply Y by X
0408	07 02	Enter a 2 into X

0409	06 03	Divide Y by X
0410	06 05	Move Y into X
0411	04 01	Subtract X from
0412	02 04	Register 2Ø Ø4
0413	04 15	Recall into Y
0414	02 02	Register 2Ø Ø2
0415	04 05	Recall into X
0416	00 13	Register ØØ 13
0417	06 02	Multiply Y by X
0418	04 14	Store Y into
0419	04 00	Register 4Ø ØØ
0420	04 15	Recall into Y
0421	02 03	Register 2Ø Ø3
0422	04 05	Recall in X
0423	00 14	Register ØØ 14
0424	06 02	Multiply Y by X
0425	04 05	Recall in X
0426	04 00	Register 4Ø ØØ
0427	06 00	Add X to Y
0428	07 02	Enter a 2 into X
0429	06 03	Divide Y by X
0430	06 05	Move Y into X
0431	04 00	Add X to
0432	02 04	Register 2Ø Ø4

B. Finding the position of the ray in the x-plane

0433	04 07	Search
0434	07 04	"4"
0435	04 08	Mark
0436	07 05	"5"
0437	04 05	Recall into X
0438	02 05	Register 2Ø Ø5
0439	07 11	Change sign of X
0440	06 02	Multiply Y by X
0441	04 05	Recall into X
0442	00 15	Register ØØ 15

0443	06 00	Add X to Y
0444	06 05	Move Y into X
0445	04 04	Store X into
0446	02 06	Register 2Ø Ø6
0447	05 15	Stop

III. Calculation of the first order portion of the ray slope

0448	04 08	Mark
0449	07 04	"4"
0450	04 15	Recall into Y
0451	00 06	Register ØØ Ø6
0452	04 05	Recall in X
0453	00 13	Register ØØ 13
0454	07 11	Change sign of X
0455	06 02	Multiply Y by X
0456	04 05	Recall in X
0457	00 08	Register ØØ Ø8
0458	06 03	Divide Y by X
0459	04 14	Store Y into
0460	04 01	Register 4Ø Ø1
0461	04 15	Recall into Y
0462	00 07	Register ØØ Ø7
0463	04 05	Recall into X
0464	00 14	Register ØØ 14
0465	06 02	Multiply Y by X
0466	04 05	Recall into X
0467	00 08	Register ØØ Ø8
0468	06 03	Divide Y by X
0469	06 05	Move Y into X
0470	04 01	Subtract X from
0471	04 01	Register 4Ø Ø1
0472	04 15	Recall into Y
0473	00 15	Register ØØ 15
0474	04 05	Recall into X
0475	00 02	Register ØØ Ø2
0476	06 03	Divide Y by X

0477	06 05	Move Y into X
0478	04 00	Add X to
0479	04 01	Register 4Ø Ø1
0480	04 15	Recall into Y
0481	00 00	Register ØØ ØØ
0482	04 05	Recall in X
0483	00 13	Register ØØ 13
0484	06 02	Multiply Y by X
0485	04 05	Recall into X
0486	00 02	Register ØØ Ø2
0487	06 03	Divide Y by X
0488	06 05	Move Y into X
0489	04 01	Subtract X from
0490	04 01	Register 4Ø Ø1
0491	04 15	Recall into Y
0492	00 01	Register ØØ Ø1
0493	04 05	Recall into X
0494	00 14	Register ØØ 14
0495	06 02	Multiply Y by X
0496	04 05	Recall in X
0497	00 02	Register ØØ Ø2
0498	06 03	Divide Y by X
0499	06 05	Move Y into X
0500	04 01	Subtract X from
0501	04 01	Register 4Ø Ø1
0502	04 15	Recall into Y
0503	00 03	Register ØØ Ø3
0504	04 05	Recall into X
0505	00 13	Register ØØ 13
0506	06 02	Multiply Y by X
0507	04 05	Recall into X
0508	00 05	Register ØØ Ø5
0509	06 03	Divide Y by X
0510	06 05	Move Y into X
0511	04 00	Add X to

0512	04 01	Register 4Ø Ø1
0513	04 15	Recall into Y
0514	00 04	Register ØØ Ø4
0515	04 05	Recall into X
0516	00 14	Register ØØ 14
0517	06 02	Multiply Y by X
0518	04 05	Recall into X
0519	00 05	Register ØØ Ø5
0520	06 03	Divide Y by X
0521	06 05	Move Y into X
0522	04 00	Add X to
0523	04 01	Register 4Ø Ø1
0524	04 15	Recall into Y
0525	04 01	Register 4Ø Ø1
0526	04 05	Recall in X
0527	02 04	Register 2Ø Ø4
0528	06 00	Add X to Y
0529	04 07	Search
0530	07 05	"5"
0531	05 15	Stop

IV. Calculation of the wavefront error based on a reference sphere

A. Finding the radius Z_r

0532	04 08	Mark
0533	07 06	"6"
0534	04 15	Recall into Y
0535	00 02	Register ØØ Ø2
0536	04 05	Recall in X
0537	00 10	Register ØØ 1Ø
0538	06 02	Multiply Y by X
0539	06 02	Multiply Y by X
0540	04 05	Recall into X
0541	00 09	Register ØØ Ø9
0542	07 11	Change sign fo X
0543	06 03	Divide Y by X
0544	06 05	Move Y into X

0545	04 04	Store X into
0546	02 07	Register 2Ø Ø7

B. Finding the x-coordinate a_r

0547	04 15	Recall into Y
0548	00 02	Register ØØ Ø2
0549	04 05	Recall into X
0550	00 03	Register ØØ Ø3
0551	06 02	Multiply Y by X
0552	04 05	Recall into X
0553	00 10	Register ØØ 1Ø
0554	06 02	Multiply Y by X
0555	04 05	Recall in X
0556	00 05	Register ØØ Ø5
0557	07 11	Change sign of X
0558	06 03	Divide Y by X
0559	04 14	Store Y in
0560	02 08	Register 2Ø Ø8
0561	04 15	Recall into Y
0562	00 00	Register ØØ ØØ
0563	04 05	Recall in X
0564	00 10	Register ØØ 1Ø
0565	06 02	Multiply Y by X
0566	06 05	Move Y into X
0567	04 00	Add X to
0568	02 08	Register 2Ø Ø8
0569	04 15	Recall into Y
0570	00 02	Register ØØ Ø2
0571	04 05	Recall into X
0572	00 06	Register ØØ Ø6
0573	06 02	Multiply Y by X
0574	04 05	Recall into X
0575	00 10	Register ØØ 1Ø
0576	06 02	Multiply Y by X
0577	06 02	Multiply Y by X
0578	04 05	Recall into X

0579	00 08	Register ØØ Ø8
0580	06 03	Divide Y by X
0581	04 05	Recall into X
0582	00 09	Register ØØ Ø9
0583	06 03	Divide Y by X
0584	06 05	Move Y into X
0585	04 01	Subtract X from
0586	02 08	Register 2Ø Ø8

C. Finding the y-coordinate b_r

0587	04 15	Recall into Y
0588	00 02	Register ØØ Ø2
0589	04 05	Recall into X
0590	00 04	Register ØØ Ø4
0591	06 02	Multiply Y by X
0592	04 05	Recall into X
0593	00 10	Register ØØ 1Ø
0594	06 02	Multiply Y by X
0595	04 05	Recall into X
0596	00 05	Register ØØ Ø5
0597	07 11	Change sign of X
0598	06 03	Divide Y by X
0599	04 14	Store Y into
0600	02 09	Register 2Ø Ø9
0601	04 15	Recall into Y
0602	00 01	Register ØØ Ø1
0603	04 05	Recall into X
0604	00 10	Register ØØ 1Ø
0605	06 02	Multiply Y by X
0606	06 05	Move Y into X
0607	04 00	Add X to
0608	02 09	Register 2Ø Ø9
0609	04 15	Recall into Y
0610	00 02	Register ØØ Ø2
0611	04 05	Recall into X
0612	00 07	Register ØØ Ø7

0613	06 02	Multiply Y by X
0614	04 05	Recall into X
0615	00 10	Register ØØ 1Ø
0616	06 02	Multiply Y by X
0617	06 02	Multiply Y by X
0618	04 05	Recall into, X
0619	00 08	Register ØØ Ø8
0620	06 03	Divide Y by X
0621	04 05	Recall into Y
0622	00 09	Register ØØ Ø9
0623	06 03	Divide Y by X
0624	06 05	Move Y into X
0625	04 01	Subtract X from
0626	02 09	Register 2Ø Ø9

D. Finding the spherical aberration component

0627	07 01	Enter a 1 into X
0628	06 04	Move X into Y
0629	04 05	Recall into X
0630	02 07	Register 2Ø Ø7
0631	06 03	Divide Y by X
0632	06 03	Divide Y by X
0633	07 11	Change sign of X
0634	06 03	Divide Y by X
0635	04 14	Store Y into
0636	03 00	Register 3Ø,ØØ
0637	04 05	Recall into X
0638	01 06	Register 1Ø Ø6
0639	04 00	Add X to

E. Finding the coma contribution in the x-direction

0640	03 00	Register 3Ø ØØ
0641	04 15	Recall into Y
0642	02 08	Register 2Ø Ø8
0643	04 05	Recall into X
0644	02 07	Register 2Ø Ø7
0645	06 03	Divide Y by X

0646	06 03	Divide Y by X
0647	07 11	Change sign of X
0648	06 03	Divide Y by X
0649	04 14	Store Y into
0650	03 01	Register 3Ø Ø1
0651	04 05	Recall in X
0652	01 07	Register 1Ø Ø7
0653	04 00	Add X to

F. Finding the coma contribution in the y-direction

0654	03 01	Register 3Ø Ø1
0655	04 15	Recall into Y
0656	02 09	Register 2Ø Ø9
0657	04 05	Recall into X
0658	02 07	Register 2Ø Ø7
0659	06 03	Divide Y by X
0660	06 03	Divide Y by X
0661	07 11	Change sign of
0662	06 03	Divide Y by X
0663	04 14	Store Y into
0664	03 02	Register 3Ø Ø2
0665	04 05	Recall into X
0666	01 08	Register 1Ø Ø8
0667	04 00	Add X to

G. Finding the astigmatism contribution in the x-direction

0668	03 02	Register 3Ø Ø2
0669	04 05	Recall into X
0670	02 08	Register 2Ø Ø8
0671	07 13	Square X
0672	06 04	Move X into Y
0673	04 05	Recall into X
0674	02 07	Register 2Ø Ø7
0675	06 03	Divide Y by X
0676	06 03	Divide Y by X
0677	07 11	Change sign of X
0678	06 03	Divide Y by X

```
0679   04 14      Store Y in
0680   03 03      Register 3Ø Ø3
0681   04 05      Recall into X
0682   01 09      Register 1Ø Ø9
0683   04 00      Add X to
```

H. Finding the astigmatism contribution in the y-direction

```
0684   03 03      Register 3Ø Ø3
0685   04 05      Recall into X
0686   02 09      Register 2Ø Ø9
0687   07 13      Square X
0688   06 04      Move X into Y
0689   04 05      Recall into X
0690   02 07      Register 2Ø Ø7
0691   06 03      Divide Y by X
0692   06 03      Divide Y by X
0693   07 11      Change sign of X
0694   06 03      Divide Y by X
0695   04 14      Store Y in
0696   03 04      Register 3Ø Ø4
0697   04 05      Recall into X
0698   02 00      Register 2Ø ØØ
0699   04 00      Add X to
```

I. Finding the field curvature contribution

```
0700   03 04      Register 3Ø Ø4
0701   04 05      Recall into X
0702   02 08      Register 2Ø Ø8
0703   07 13      Square X
0704   06 04      Move X into Y
0705   04 05      Recall into X
0706   02 09      Register 2Ø Ø9
0707   07 13      Square X
0708   06 00      Add X to Y
0709   04 05      Recall into X
0710   02 07      Register 2Ø Ø7
0711   06 03      Divide Y by X
```

0712	06 03	Divide Y by X
0713	07 11	Change sign of X
0714	06 03	Divide Y by X
0715	04 14	Store Y into
0716	03 05	Register 3Ø Ø5
0717	04 05	Recall into X
0718	02 01	Register 2Ø Ø1
0719	04 00	Add X to

J. Finding the distortion contribution in the x-direction

0720	03 05	Register 3Ø Ø5
0721	04 15	Recall into Y
0722	02 08	Register 2Ø Ø8
0723	04 05	Recall into X
0724	02 09	Register 2Ø Ø9
0725	07 13	Square X
0726	06 02	Multiply Y by X
0727	04 15	Store Y into
0728	04 00	Register 4Ø ØØ
0729	04 05	Recall into X
0730	02 08	Register 2Ø Ø8
0731	06 04	Move X into Y
0732	06 02	Multiply Y by X
0733	06 02	Multiply Y by X
0734	04 05	Recall into X
0735	04 00	Register 4Ø ØØ
0736	06 00	Add X to Y
0737	04 05	Recall into X
0738	02 07	Register 2Ø Ø7
0739	06 03	Divide Y by X
0740	06 03	Divide Y by X
0741	07 11	Change sign
0742	06 03	Divide Y by X
0743	04 14	Store Y in
0744	03 06	Register 3Ø Ø6
0745	04 05	Recall into Y

0746	02 02	Register 2Ø Ø2
0747	04 00	Add X to

K. Finding the distortion contribution in the y-direction

0748	03 06	Register 3Ø Ø6
0749	04 15	Recall into Y
0750	02 09	Register 2Ø Ø9
0751	04 05	Recall into X
0752	02 08	Register 2Ø Ø8
0753	07 13	Square X
0754	06 02	Multiply Y by X
0755	04 14	Store Y in
0756	04 00	Register 4Ø ØØ
0757	04 05	Recall into X
0758	02 09	Register 2Ø Ø9
0759	06 04	Move X into Y
0760	06 02	Multiply Y by X
0761	06 02	Multiply Y by X
0762	04 05	Recall into X
0763	04 00	Register 4Ø ØØ
0764	06 00	Add X to Y
0765	04 05	Recall into X
0766	02 07	Register 2Ø Ø7
0767	06 03	Divide Y by X
0768	06 03	Divide Y by X
0769	07 11	Change sign of X
0770	06 03	Divide Y by X
0771	04 14	Store Y in
0772	03 07	Register 3Ø Ø7
0773	04 05	Recall into X
0774	02 03	Register 2Ø Ø3
0775	04 00	Add X to

L. Finding the wavefront error

0776	03 07	Register 3Ø Ø7
0777	04 08	Mark
0778	07 07	"7"

0779	04 15	Recall into Y
0780	03 07	Register 3Ø Ø7
0781	04 05	Recall into X
0782	00 14	Register ØØ 14
0783	06 02	Multiply Y by X
0784	04 14	Store Y in
0785	04 00	Register 4Ø ØØ
0786	04 15	Recall into Y
0787	03 06	Register 3Ø Ø6
0788	04 05	Recall into X
0789	00 13	Register ØØ 13
0790	06 02	Multiply Y by X
0791	04 05	Recall into X
0792	04 00	Register 4Ø ØØ
0793	06 00	Add X to Y
0794	04 05	Recall into X
0795	00 15	Register ØØ 15
0796	06 02	Multiply Y by X
0797	07 02	Enter a 2 in X
0798	06 03	Divide Y by X
0799	04 14	Store Y into
0800	04 02	Register 4Ø Ø2
0801	04 15	Recall in Y
0802	03 05	Register 3Ø Ø5
0803	04 05	Recall into X
0804	00 15	Register ØØ 15
0805	06 02	Multiply Y by X
0806	06 02	Multiply Y by X
0807	07 04	Enter a 4 in X
0808	06 03	Divide Y by X
0809	06 05	Move Y into X
0810	04 01	Subtract X from
0811	04 02	Register 4Ø Ø2
0812	04 15	Recall into Y
0813	03 04	Register 3Ø Ø4

0814	04 05	Recall into X
0815	03 03	Register 3Ø Ø3
0816	06 02	Multiply Y by X
0817	04 05	Recall into X
0818	00 14	Register ØØ 14
0819	06 02	Multiply Y by X
0820	04 05	Recall into X
0821	00 13	Register ØØ 13
0822	06 02	Multiply Y by X
0823	07 02	Enter a 2 in X
0824	06 02	Multiply Y by X
0825	04 14	Store Y into
0826	04 00	Register 4Ø ØØ
0827	04 15	Recall into Y
0828	03 04	Register 3Ø Ø4
0829	04 05	Recall into X
0830	00 14	Register ØØ 14
0831	06 02	Multiply Y by X
0832	06 02	Multiply Y by X
0833	06 05	Move Y into X
0834	04 00	Add X to
0835	04 00	Register 4Ø ØØ
0836	04 15	Recall into Y
0837	03 03	Register 3Ø Ø3
0838	04 05	Recall into X
0839	00 13	Register ØØ 13
0840	06 02	Multiply Y by X
0841	06 02	Multiply Y by X
0842	04 05	Recall into X
0843	04 00	Register 4Ø ØØ
0844	06 00	Add X to Y
0845	04 05	Recall into X
0846	00 15	Register ØØ 15
0847	06 02	Multiply Y by X
0848	06 02	Multiply Y by X

0849	07 02	Enter a 2 into X
0850	06 03	Divide Y by X
0851	06 05	Move Y into X
0852	04 01	Subtract X from
0853	04 02	Register 4Ø Ø2
0854	04 15	Recall into Y
0855	03 02	Register 3Ø Ø2
0856	04 05	Recall into X
0857	00 14	Register ØØ 14
0858	06 02	Multiply Y by X
0859	04 14	Store Y into
0860	04 00	Register 4Ø ØØ
0861	04 05	Recall into X
0862	03 01	Register 3Ø Ø1
0863	04 05	Recall into Y
0864	00 13	Register ØØ 13
0865	06 02	Multiply Y by X
0866	04 05	Recall into X
0867	04 00	Register 4Ø ØØ
0868	06 00	Add X to Y
0869	04 05	Recall into X
0870	00 15	Register ØØ 15
0871	06 02	Multiply Y by X
0872	06 02	Multiply Y by X
0873	06 02	Multiply Y by X
0874	07 02	Enter a 2 in X
0875	06 03	Divide Y by X
0876	06 05	Move Y into X
0877	04 00	Add X to
0878	04 02	Register 4Ø Ø2
0879	04 15	Recall into Y
0880	03 00	Register 3Ø ØØ
0881	04 05	Recall into X
0882	00 15	Register ØØ 15
0883	07 13	Square X

0884	06 02	Multiply Y by X
0885	07 08	Enter an 8 in X
0886	06 03	Divide Y by X
0887	06 05	Move Y into X
0888	04 01	Subtract X from
0889	04 02	Register 4Ø Ø2
0890	04 05	Recall into X
0891	04 02	Register 4Ø Ø2
0892	06 04	Move X into Y
0893	05 15	Stop